DEVELOPMENT OF *IN VITRO* POINT OF CARE DIAGNOSTICS (IVPCD) BASED ON APTAMERS INTEGRATED BIOSENSORS

by

NILESHI SARAF
Integrated B.Tech.-M.Tech. in Nanotechnology, Center for Converging Technology,
University of Rajasthan, Jaipur, India, 2014

A dissertation submitted in partial fulfillment of the requirements
for the degree of Doctor of Philosophy in Materials Science and Engineering
in the Department of Materials Science and Engineering
in the College of Engineering and Computer Science
at University of Central Florida
Orlando, Florida

Fall Term
2018

Major Professor: Sudipta Seal

ABSTRACT

The global market for the medical diagnostic industry is worth 25 billion dollars in the United States and is expected to grow exponentially each year. Presently available methods for biodetection, such as immunoassays, chemiluminescence and fluorescent based assays are expensive, time consuming and require skilled labor with high-end instruments. Therefore, development of novel, passive colorimetric sensors and diagnostic technologies for detection and surveillance is of utmost importance especially in resource constrained communities.

The present work focusses on developing novel and advanced in vitro biodiagnostic tools based on aptamer integrated biosensors for an early detection of specific viral proteins or small biomolecules used as potential markers for deadly diseases. Aptamers are short single stranded deoxyribonucleic acid (DNA) which are designed to bind to a specific target biomolecule. These are readily synthesized in laboratory and offers several advantages over antibodies/enzymes such as stable in harsh environment, easily functionalized for immobilization, reproducibility etc. These undergo conformational changes upon target binding and produces physical or chemical changes in the system which are measured as colorimetric or electrochemical signals. Here, we have explored the aptamer-analyte interaction on different platforms such as microfluidic channel, paper based substrate as well as organic electrochemical transistor to develop multiple compact, robust and self-contained diagnostic tools. These testing tools exhibit high sensitivity (detection limit in picomolar) and selectivity against the target molecule, require no sophisticated instruments or skilled labor to implement and execute, leading a way to cheaper and more consumer driver health care. These innovative

platforms provide flexibility to incorporate additional or alternative targets by simply designing aptamers to bind to the specific biomolecule.

Keywords: Aptamers, point-of-care diagnostics, Organic electrochemical transistor, microfluidics, epinephrine, Zika, Chikungunya, Gold nanoparticles, PDMS.

I dedicate this work to my late grandfather, Mr. Purushottam D. Saraf.

ACKNOWLEDGMENTS

First of all, I would like to thank my advisor Dr. Sudipta Seal for his constant motivation, guidance and support throughout my research work. He has set an example of being an excellent mentor, researcher and a human being. I hope I could be as enthusiastic, and energetic and command an audience as well as he can. I am grateful to him for giving me the opportunity to work on multiple projects and freedom to pursue my own ideas at every step.

I would also like to extend my gratitude towards my committee members Dr. William Self, Dr. Jiyu Fang, Dr. Stephen J. Florczyk and Dr. Yajie Dong for their invaluable time and constructive discussions for shaping up the present work. I would like to thank Dr. Bradley Willenberg, Dr. Alicia Willenberg and Alex Bosak for all the discussions, ideas and feedback during the course of the work.

It was pleasure working with my fellow lab mates Aadithya Jayaranjan, Dr. Ankur Gupta and Craig J. Neal for the innumerable stimulating discussions and arguments that have helped me learn a lot. Special thanks for working with me before the deadlines, spending sleepless nights in the lab and for all the fun we had in last three years. I would like to acknowledge Dr. Tamil Selvan Sakthival, Dr. Swetha Barkam, Dr. Sushant Singh and Dr. Shashank Saraf for their help during the program.

I would also like to thank Madison Peppler, Eric R. Woods, Michael Villegas and Rasha Bara for their hard work and important contributions to this work. A special thanks to Dr. Abraham Vazquez-Guardado, NSTC and Dr. Soumen Das for their support and guidance through out the reseach work.

I would like to express my gratitude towards Materials Characterization Facility (MCF) at UCF and MCF engineer Kirk Scammon for his help during characterization and sample preparation. I would like to convey my special thanks to the administrative support provided by Sandra, Pamela, Karen, Angie, Chyrel and Kari from AMPAC, MSE.

I would like to acknowledge Florida Department of Agriculture and Consumer Services (FDACS), National Science Foundation (NSF), GATES and College of Medicine for the financial support during this research. I also owe my thanks to the Graduate student association and Student Government association at University of Central Florida, for providing me multiple scholarships and travel grants to present my work at different conferences. I would also like to thank Materials Research Society, Material Science and Technology, The Mineral, Metals and Materials Society and Electrochemical Society for providing me a platform to present my work to the scientific community.

Most of all, I would like to convey my greatest gratitude to my parents (Mr. Raman Saraf and Mrs. Anuradha Saraf) who have always been my backbone and who have made it possible for me to pursue this career. Special thanks to my younger siblings (Palak and Rishik) who have supported me throughout my life. I am grateful to my family members and friends (Noopur Jain and Deepti Jain) for their moral and emotional support throughout the years. A special mention to my grandparents without whom nothing would have been possible!

TABLE OF CONTENTS

LIST OF FIGURES

LIST OF TABLES

LIST OF ABBREVIATIONS

ΔV_G^{eff}	Change in effective Gate voltage
ALD	Atomic layer deposition
CHIKV	Chikungunya
DLS	Dynamic light scattering
EPI	Epinephrine
FTIR	Fourier transform infrared spectroscopy
HRTEM	High resolution transmission electron microscope
I_D	Drain current/Channel current
OECT	Organic electrochemical transistors
PDMS	Polydimethylsiloxane
PEDOT:PSS	poly(3,4-ethylenedioxythiophene) polystyrene sulfonate)
SEM	Scanning electron microscope
UV-Vis	Ultraviolet visible spectroscopy
V_D	Drain Voltage
V_G	Gate Voltage
V_{Offset}	Offset Voltage

CHAPTER 1: INTRODUCTION

1.1 Introduction to Biosensors

In the recent decade, the development of Point of care (POC) diagnostics has garnered tremendous amount of attention due to its applications in the early diagnosis of diseases which can be extremely helpful in the health care industry. The factors such as lack of trained personnel, well-equipped centers and cost of biosensors are the some of the obstacles which limit the use of diagnostic tools in the third world countries. WHO has defined an idealistic biosensor to an ASSURED device which stands for **A**ffordable, **S**ensitive, **S**pecific, **U**ser-friendly, **R**apid and Robust, **E**quipment-free and **D**eliverable [1-3].

In vitro point of care testing refers to the examination of reagents such as bodily fluids, tissues, cells etc using a combination of techniques, reagents or instruments with the goal of detecting an analyte in a controlled environment outside living organism (**Figure 1**). These devices offer the opportunity to perform the assay at the patient's site and obtain results rapidly and accurately with a limited infrastructure. The rapid testing results in better patient management, reduces multiple visits, enable timely treatment and more importantly, contain infectious disease. It has been reported that the successful implementation of a 90% sensitive malaria POC testing device has the ability to prevent unnecessary treatment worth of 450 million and save over 2.2 million lives. Testing techniques with higher sensitivity but with minimal laboratory requirements will prevent only 400 million unnecessary treatments. The potential of POCs to provide clinically

relevant information without the need for a laboratory setting or trained personal has fueled the demand to generate new tools to diagnose broad spectrum of biomolecules. From the research point of view, more than 73000 search items are displayed, when the keywords “point of care” are searched in PubMed [4].

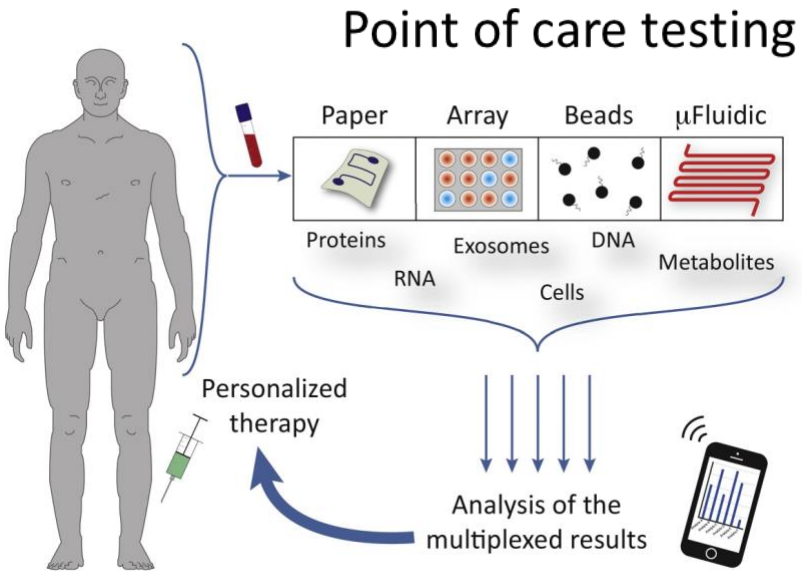

Figure 1: Multiplexed Point of Care Testing [5]

The demand for POC diagnostics has skyrocketed in recent years. The global *in vitro* diagnostic market share has been estimated to exceed USD 70 billion by 2022 according to Market search engine [6]. The major challenge is to bring the techniques to patient’s site without compromising the sensitivity or accuracy of the approach. **Figure 1** shows a schematic of a general multiplex POC testing where the blood is taken from an individual, run and analyzed on a platform and the output signal is displayed on a smart phone device. The platforms range from microfluidic channel, paper based sensors, use of nanosized beads and plate based assays. The current available biosensors are

categorized on the basis of processes that translates the binding event into an output readable signal. The next section explains different types of biosensor based on the output signal that are available today.

1.2 Types of sensors

1.2.1 Colorimetric sensor

Metal nanoparticles exhibit unique size and shape dependent optical properties [7-12]. A strong absorption band is observed in the UV-Visible spectra of the gold and silver metallic nanoparticles when light is incident on them. This band is due to the interaction of light with metal nanoparticles which results in collective oscillation of the electrons in the conduction band and gives rise to strong surface plasmon resonance (SPR) signal [13-15]. The SPR signal is highly dependent on the surface morphology of the material, therefore any change in size, shape or the dielectric properties of the surrounding medium will cause a shift in the electron density. This results in a change in the oscillation frequency, generating different absorption and scattering spectrum. Typically for gold nanoparticles smaller than 20 nm, the SPR band is seen at 520 nm which is in the range of visible range as shown in **Figure 2**. Therefore, any shift in the absorption plasmon band due to change in the morphology is visible through naked eyes without any external excitation or emission source.[16] **Figure 2B** represents different colors of gold nanoparticles which can be synthesized by varying the size. The UV-Visible spectra shows the red shift with increasing size of gold nanoparticles. It can be seen that varying the size of AuNPs from 10-100 nm causes red shift in the absorption spectrum from 520 to 580 nm (**Figure 2A**). These unique size-dependent optical properties of AuNPs along

with high extinction coefficient and high surface-to-volume has made them ideal candidate in sensing applications.

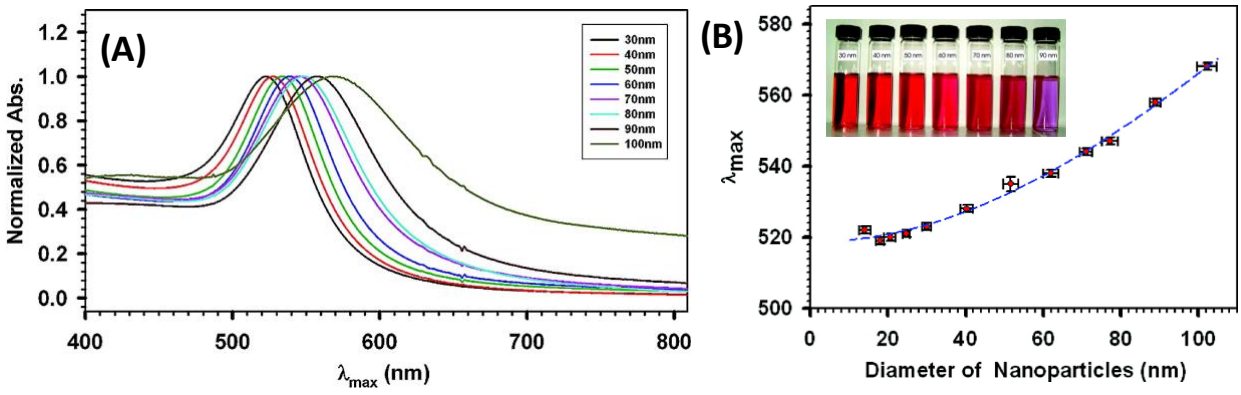

Figure 2: (A) Normalized absorbance of Gold nanoaprticles (AuNPs) with different sizes. (B) Red-shift in the SPR peak with increasing diameter of AuNPs. Inset shows different colored AuNPs with different sizes [16]

Target induced specific aggregation of the AuNPs has gained much attention in recent decades in the detection and imaging world of biological targets. The surface of the AuNPs can be easily functionalized with an acceptor molecule which shows high affinity towards a specific target. For example, AuNPs functionalized with biotin shows high affinity towards streptavidin. Exposure of these functionalized AuNPs to streptavidin will induce agglomeration in the solution changing the color of the solution from red to blue. This color change is due to the shifting of maximum SPR peak to longer wavelengths (red shift). Antibodies and DNA strands have been widely used as biorecognition elements to detect the presence of small molecules, proteins or other nucleic acid. The role of these elements is two fold- first is to specifically bind to the molecule and second

is to provide stability to the AuNPs and protect them against salt aggregation. The detection of DNA strand is done by functionalizing the surface with a single stranded (ss) DNA. In the presence of the complimentary strand, the ssDNA strand is released leaving the AuNPs surface exposed eventually leading to aggregation [17]. The similar approach has been used for the detection of dopamine, thrombin and cocaine [18, 19] in which the surface of AuNPs is functionalized with DNA designed for the specific target molecule.

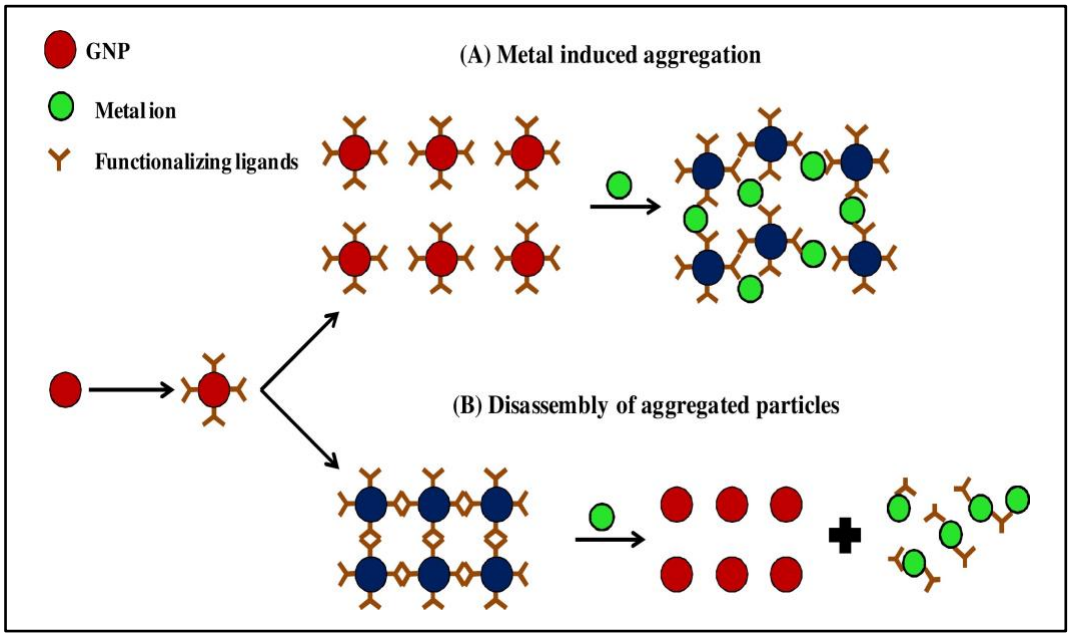

Figure 3: Schematic showing mechanism behind colorimetric detection of metal ions using AuNPs. (A) The presence of metal ions causes AuNPs to aggregate and change the color from red to blue. (B) Presence of metal ions causes disassembly of AuNPs changing color from blue to red. [20]

The schematic of the working of a basic AuNPs based colorimetric sensor has been shown in **Figure 3** [20]. The presence of analyte can lead to (a) aggregation of AuNPs or (b) disassembly of aggregated AuNPs. The aggregation of AuNPs is followed by broadening of the SPR band and change in visual color from red to blue due to the size dependent optical property. However, the disassembly causes a change from blue to red and blue shift in the SPR absorption band.

1.2.2 Enzyme-linked immunosorbent Assay

The basic principle of ELISA was pioneered in 1971 by two Swiss scientists: Engvall and Perlmann [21-23]. They modified Radioimmunoassay (RIA) method by replacing radioactive iodine with enzymes. Because of the hazardous effect of using radioactive iodine, RIA assays were modified, thus creating modern day ELISA technique. The initial research work were focused on determining the level of IgG in rabit serum and quantifying human chorionic gonadotropin in urine using horseradish enzyme [21, 23]. After the invention of ELISA, a lot of work was done in the field of diagnostic microbiology, parasitology and to detect viral proteins such as influenza, parainfluenza, mumps etc in the year 1973-1981 [24-29].

The working of ELISA is based on interaction of antigen to its specific antibody, which makes it possible for the detection of very small amount of antigen such as proteins, peptides or antibodies in a fluid sample. ELISA utilizes enzyme labelled antigens/antibodies to achieve an amplified output signal in the presence of very small of antigen. The common enzymes used are glucose oxidase, alkaline phosphatase, horseradish peroxide etc which yields a change in color or a fluorescence signal in the

presence of the molecule of interest. Quantitative analysis is done by measuring the intensity of fluorescent signal or color change which is further analyzed by a reader. Various modifications in the process of ELISA has been done in the recent decade as shown in **Figure 4**. These are as follows:

(a) **Direct ELISA-** The direct type of ELISA involves the immobilization of antibody/antigen on the surface of the plate. The enzyme tagged antibody/antigen is introduced and incubated for a particular amount of time, after which the plate is washed off to remove unbound material from the wells. An appropriate substrate is added to the well which produces an output signal through development of color.

(b) **Indirect ELISA-** The process includes the involvement of an enzyme tagged secondary antibody which attaches to the primary antibody-antigen complex and helps in the development and quantification of a signal. This type of method was first developed by Lindström and Wager in 1971 to measure porcine IgG antibody [30].

(c) **Sandwich assay-** The sandwich assay includes capturing an antigen between two different types of antibodies- capture and detection antibody. The capture antibody is immobilized on the surface of plate which attaches to the antigen and then detection antibody tagged with an enzyme is added which gives the output signal in the presence of a substrate. The signal is directly proportional to the concentration of the antigen [31].

(d) **Competitive assay-** The surface of the wells is immobilized with antibodies specific to the antigen. The sample containing antigen is added in the wells along with another tagged antibody. The immobilized antibody competes with the tagged antibody to bind to the antigen present in the well. The excess antibody is washed off and substrate is added to produce the signal. The signal is inversely proportional to the concentration of the antigen in the serum [22].

(e) **Nanoparticle based immunoassay-** Recently, nanoparticles have been utilized to develop novel immunoassays due to their unique physical, chemical and biological properties.

These materials have been adapted to improve the degree of sensitivity of a biosensor due to their potential for operating without enzymes or replacing enzymes overall [32]. The surface of the nanoparticles can be easily modified with target binding molecules and due to their existence in different colours, the need of substrate is entirely unnecessary. The application of nanoparticles in the detection of heavy metal ions, proteins, peptides, DNA and even cells have shown great potential attributing to their enhanced stability and cost effectiveness of the developed sensors.

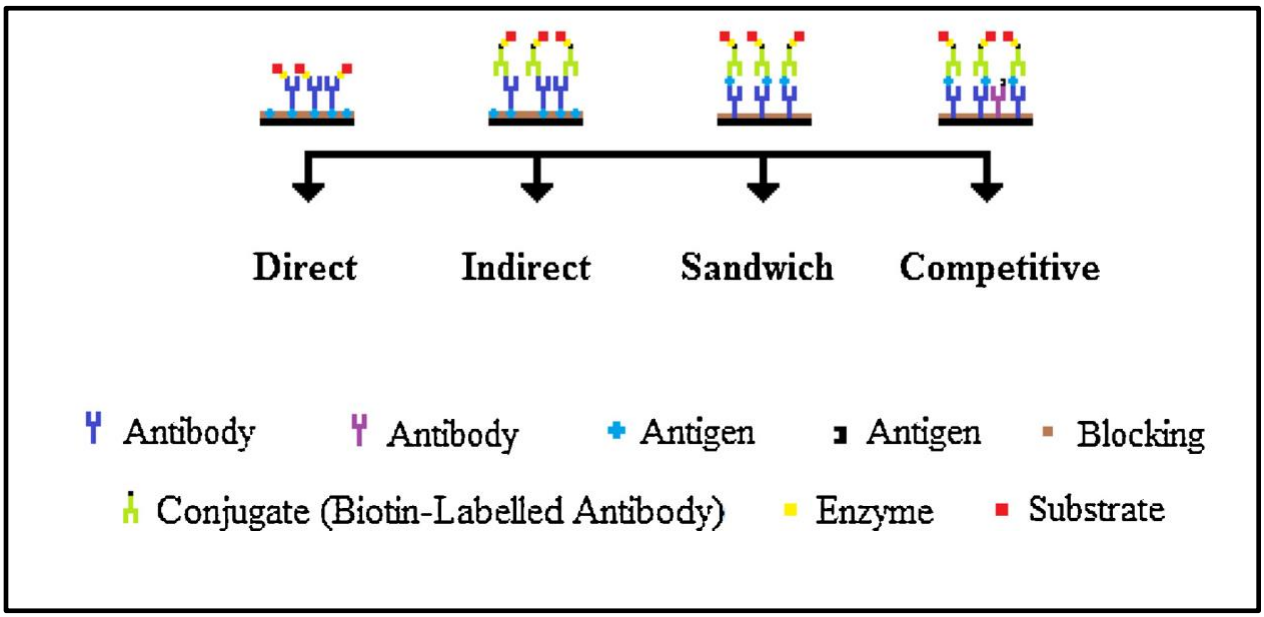

Figure 4: Different types of ELISA techniques [22].

1.2.3 Organic Electrochemical transistors

The field of organic transistors provide an attractive means for the detection and quantification of biomolecules for the applications in medical and health care industry [33-36]. The miniaturization, easy electrical read out signals, signal amplification as well as robustness are the key advantages of these devices which have given them an edge over

other approaches. A wide range of sensors such as pressure, humidity, pH, mechanical deformation and ion concentrations etc have been successfully developed using the organic transistors[37-39].

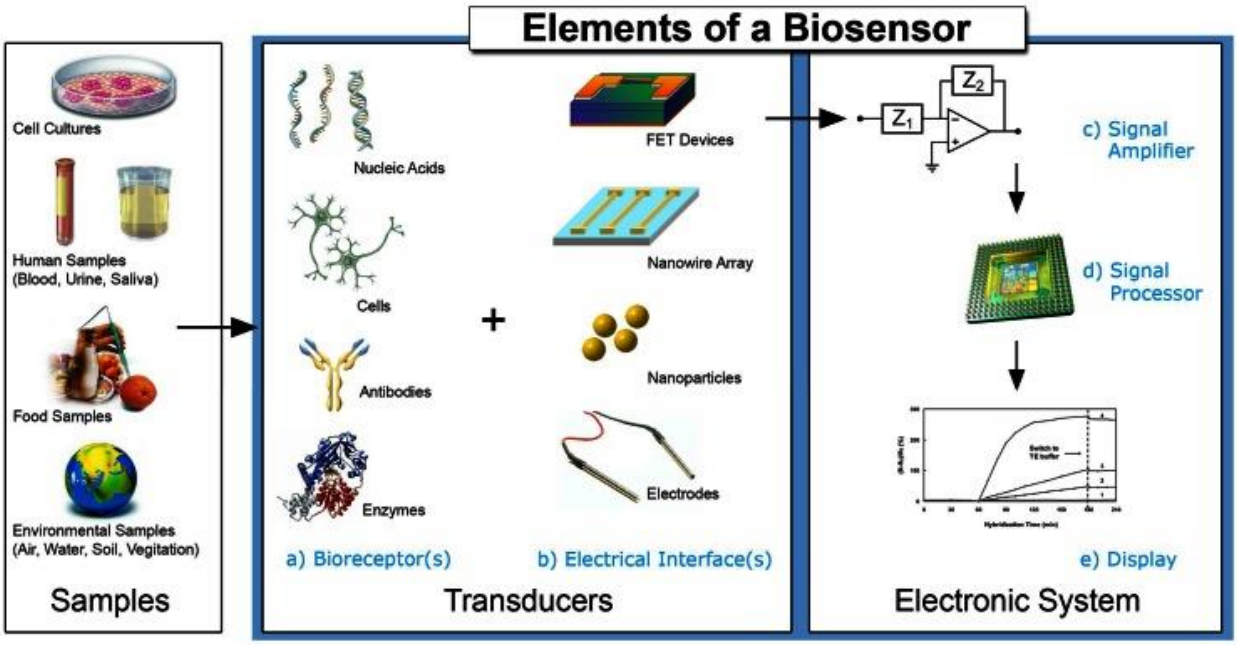

Figure 5: A flowchart showing different components of a biosensor [34].

All these sensors have different functions; however, the basic schematic comprises of the following entities (**Figure 5**):

(a) Bioreceptors (enzyme, antibodies, aptamers etc) which is specifically designed to bind the analyte molecule.

(b) Electrical interface- where the specific biological event such as binding, redox reaction etc takes place.

(c) Signal amplifier- The transduction and amplification of the biological event into an output electrical signal.

(d) Signal processor- The computer software which converts the change in electrical signal in some form of physical parameter which is read though display.

(e) Display-an interface between the computer and the human operator which displays the detection and quantification parameters in readable form.

Different operating modes of a transistor include amperometric (change in current), conductimetric (change in conductivity of the medium) and potentiometric (change in potential) sensors [37, 40-42]. The major class of electrochemical detection techniques utilizes field-effect transistor in which the change in current is measured due to the change in potential at the gate electrode. Within the family of FETs, an organic electrochemical transistor (OECT) consists of two electrodes- source and drain connected by an active layer of semiconductive material and a third electrode called gate which controls the conductivity of the channel. A typical OECT based biosensor involves the modification of metal gate electrode with a biologically active component (bioreceptors such as enzyme, antibodies, aptamers etc) which transduces an electrochemical signal in the presence of specific analyte [43]. The working of the device depends on the doping/de-doping of the semiconducting layer bridging the channel. The transistor is a combination of sensor as well as amplifier where a small change in the potential causes significant change in the current. This occurs in low operating voltages which is suitable for biological and chemical sensing in aqueous environment [44].

Researchers have been emphasizing on the use of nanotechnology to shrink the dimensions of the device which will ensure high signal to noise ratio, small sample usage and ultimately a more compact device. Research has also been focused on the advent of

new bioreceptors molecules which offers high specificity and affinity towards the molecule of interest. Most of the electrochemical sensors depend on the use of some electroactive label molecule (Fluorescent, chemiluminescent or radioactive labels) which facilitates the transfer of electron in the presence of analyte resulting in a change in the potential. The major drawback of using labels is to immobilize the label molecule over the analyte and the limited stability of the label in harsh environmental conditions. Therefore, lot of research has been done towards exploring label free biosensors to develop more reliable biosensors for practical applications [45-47]. An ideal biosensor is stable at a wide range of temperature, pH and humidity and does not show variations between different assays. It is cheap, portable, compact, user-friendly and provides real-time analysis in a timely fashion.

1.3 Introduction to Aptamer

The word aptamer is taken from Latin word ‘aptus’ which means to fit [48, 49]. Therefore, the word aptamer denotes a kind of polymer which fits to its target. Aptamers are short synthetic strands of oligonucleotides either, DNA or RNA which specifically binds to a target molecule. These are designed and selected through Systematic Evolution of Ligands by Exponential Enrichment (SELEX) procedure. First a combinatorial library of random oligonucleotide sequences is formed. A target molecule is incubated with the random sequences in an appropriate buffer and at particular temperature and pH. Then, the free nucleotides are washed away and bound nucleotides are eluted. This process consists of repetitive steps alternating between selection and amplification by using PCR

(polymerase chain reaction). The strands showing highest affinity towards the target molecule with K_d value in the nanomolar to picomolar range are extracted. It can be noted that the process of SELEX does not necessarily favor the production of aptamer for a single epitope on the given target. Till now, a wide range of aptamers has been designed for targets such as nucleic acid [50], proteins [51, 52] small organic molecule [53], metal ions [54], viruses [55], bacteria [56] and antibiotics. Aptamer can bind to the target molecule by a lock and key mechanism through conformational change (**Figure 6**) and other forces such as van der Waals interactions, hydrogen bonding and electrostatic interactions also play a major role [49].

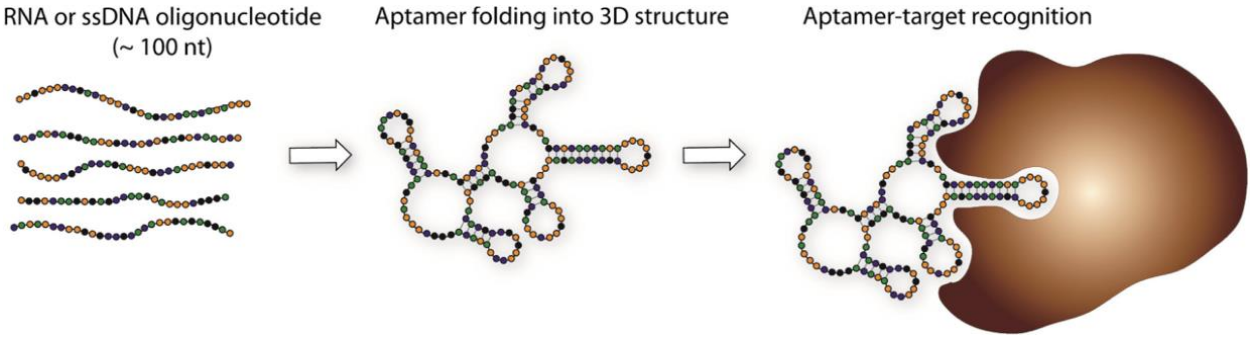

Figure 6: Schematic diagram showing the conformational change in the presence of a target molecule [57]

1.3.1 Aptamer vs Antibodies

When compared with antibodies, aptamer provide numerous advantages. Some of them are as follows:

A. Synthesis- Antibody are extracted by an in vivo process using animal's immune

response against a particular target whereas aptamers are chemically synthesized by SELEX process.

B. Reproducibility- Chemical synthesis of aptamers reduces batch-to-batch variation in aptamer and also reduces cost of production. These can be synthesized with high degree of purity, extreme accuracy and reproducibility.

C. Ease of functionalization- Aptamers ends can be functionalized easily with labels or other molecules for easier immobilization or target purification.

D. Stability- Antibodies are very sensitive to the variation in temperature or pH and can easily undergo denaturation. On the other hand, the aptamers are stable at high temperatures and can be renatured within few minutes to maintain the structure.

E. Aptamers have been a good alternative to antibodies. However, a major drawback of using aptamer is degradation by nucleases. Therefore, the entire experiment has to be done in a DNAase - RNAase free environment.

1.4 Scope of the thesis

The scope of the present thesis is to develop novel diagnostic tools for application in the point of care testing devices. The present thesis is organized in the following chapters.

Chapter 2 demonstrates the development of a colorimetric sensor based on the aggregation of gold nanoparticles in the presence of specific analyte molecule. A detailed study to investigate the role of physical morphology of AuNPs, aptamer concentration as well as the effect of salt has been performed to better understand and control the sensitivity of the approach.

Our goal in chapter 3 is to detect epinephrine in picomolar range using an electrochemical platform. The novelty in this work is the use of aptamer modified gate electrode which regulates the output current in the presence of epinephrine. The device exhibited high sensitivity (90 pM detection range) and specificity for epinephrine (no response towards common interfering agents) due to the use of aptamers.

In Chapter 4, an attempt has been made to develop a multiplex analyte detection system using a PDMS based microfluidic channel which gives an easy colorimetric readout signal. Zika and Chikungunya envelope proteins has been detected at picomolar range with naked eye detection using aptamer functionalized micro-pillars. The use of microfluidic channel offered advantages such as smaller sample volumes, lower cost, easy disposal as well as high throughput. Finally, chapter 5 discusses the conclusions and future work for the advancement of the thesis.

CHAPTER 2: COLORIMETRIC DETECTION OF EPINEPHRINE USING AN OPTIMIZED PAPER-BASED APTASENSOR

The work presented in this chapter has been published in

RSC Advances, 2017, 7, 49133-49143; DOI:10.1039/C7RA10272K

2.1 Introduction

The global market for medical diagnostic industry is worth 25 billion dollars in the United States and will continue to grow each year [58]. Presently, available methods for biodetection, such as immunoassays, [59, 60] chemiluminescence [61-63] and fluorescent based assays, [64, 65] are expensive, time consuming and require skilled labor with high-end instruments. Therefore, development of novel, passive colorimetric sensor and diagnostic technologies for detection and surveillance has garnered utmost importance. Paper-based sensors employing gold nanoparticles (AuNPs) as colorimetric probes have gained attention due to their simplicity, robustness and scalability [66-68]. These sensors are easy to fabricate and are capable of handling very small volumes of liquid (microliter) which greatly reduces reagent and sample consumption.

Gold nanoparticles (AuNPs) exhibit unique optical properties due to their bright red color in solution which is highly dependent on the interparticle distance.[7, 69] Despite being the noble metal in the bulk state, AuNPs act as catalysts in nanoscale and therefore show promising applications in electronics, [70] photonics, [71] chemical sensing and imaging [72-74]. The optical properties of AuNPs can be tuned throughout visible to near

infra-red spectra by varying AuNPs size, shape, local environment and aggregation state [14, 75-79]. When AuNPs of ~10-20 nm size are uniformly dispersed in solution, they exhibit a strong plasmon peak at ~520 nm due to the collective oscillations of the free electrons in the conduction band. Any change in physical parameters will cause a shift in the electron density, resulting in changes in oscillation frequency, absorption and scattering spectra and hence, the visible color of the AuNPs solution from red to blue. This approach can be used to design simple biosensing devices to detect various kinds of molecules.

Aptamer-functionalized gold nanoparticles (AuNPs-apt) have also attracted attention for use in detecting small proteins, [58, 80-83] oligonucleotides [19, 75, 84, 85] and metal ions [86-88] due to their low cost, simplicity and practicality [89-92]. Aptamers are short, synthetic oligonucleotide strands of either DNA or RNA which are synthesized by a procedure called Systematic Evolution of Ligands by Exponential Enrichment (SELEX) and can be functionalized onto the surface of a nanoparticle [53], [93]. These sensory molecules bind to target molecule by a lock and key mechanism driven by a conformational change as well as van der Waals forces, hydrogen bonding and electrostatic interactions [49]. This binding cause energy/charge transfer between the AuNPs-apt and the target, leading to aggregation in the solution. The target-mediated aggregation of AuNPs-apt results in the color change of the colloidal gold solution from red to blue [94, 95]. This attribute of AuNPs of transferring any biorecognition event into a color change has motivated scientists to use AuNPs as a biosensing tool for the detection of numerous biomolecules including oligonucleotides, small proteins, biomarkers and pathogens.

The catecholamine epinephrine (4-[(1R)-1-hydroxy-2-(methylamino)ethyl]benzene-1,2-diol) is a neurotransmitter and neuroendocrine hormone which acts upon α-adrenergic and β-adrenergic receptors in several organs, giving it a vast array of physiological functions [96]. Clinical uses include the treatment of anaphylactic shock, cardiac attack and asthma attacks [96]. Abnormalities in epinephrine levels may result in myocardial infarction, arrhythmias, pulmonary edema, blood pressure increase and Takotsubo cardiomyopathy [97-99]. The level of epinephrine present in the plasma is approximately 13.6 x 10^{-11} M [100]. Detection has previously been performed by electrochemical methods, [101-103] liquid chromatography, [104, 105] spectrophotometry, [106] electrophoresis, [107] flow injection analysis [108, 109] and fluorometry [48, 110]. The estimated detection limit for epinephrine obtained from all these experiments was found in the range of nanomolar to micromolar (10^{-8} to 10^{-9} M) [100]. Though these methods have high detection limits, they are time consuming and require skilled labour and expensive instrumentation. As an alternative, gold aptasensors not only provide a simple and novel testing tool but also demonstrates high sensitivity and selectivity towards epinephrine.

Despite having all the aforementioned advantages of using AuNPs-apt based colorimetric sensors, the biggest challenge which restricts the use of this sensor in real world application is the low sensitivity compared to other sensing technologies. The detection limit depends on the morphology of the AuNPs, the binding affinity of the aptamer, the ratio of the aptamer to the AuNPs and the affinity of the aptamer with respect to analyte. The shape, size and the dielectric medium surrounding the particles can be tuned such that even small amounts of analyte can trigger maximum aggregation/color

change. Along with nanospheres, various shapes such as nanorod and nanostars have been utilized for the development of colorimetric sensors [111-113]. However, there have been no systematic studies done which compare the effects of different sizes and shapes of AuNPs and aptamer-AuNPs interaction on the detection limit of a sensor. Therefore, the present work explored the effect of different parameters that govern the detection process such as the number of aptamers on the surface of AuNPs, aptamer binding, salt concentration and physical morphology of AuNPs. The aim is to optimize all these parameters such that a maximum shift in the spectra and an intense change in color can be obtained. These optimized parameters have been used to develop a sensitive and portable paper based sensor for epinephrine, which can be used as a point of care diagnostic tool.

2.2 Experimental Section

2.2.1 Materials

Both thiol-modified and unmodified aptamers were used in the present study. The 32-mer aptamers specific for epinephrine were designed and synthesized by BasePairBio Company (Pearland, TX). Chloroauric acid, trisodium citrate, L-ascorbic acid, tris (2-carboxyethyl) phosphine (TCEP), tris hydrochloride (Tris HCl), ethylenediaminetetraacetic acid (EDTA), phosphine buffered saline tablets, sodium chloride (NaCl), magnesium chloride ($MgCl_2$) and epinephrine hydrochloride were purchased from Sigma-Aldrich (St. Louis, MZ). Gold Nanospheres (15 nm, 30 nm, 50 nm) with concentration of 1 mg/ml and Gold NanoRods (660 nm resonant, 50 OD) stabilized by negatively charged citrate ions were obtained from Nanocomposix (San Diego, CA).

Experiments were performed in a DNAse - RNAse free environment using nuclease free water, tips and vials purchased from Thermofisher (Waltham, MA). Whatmann® filter paper #1 was obtained from Sigma Aldrich (St. Louis, MZ).

2.2.2 Instrumentation

Surface charge and hydrodynamic size measurements were performed using Dynamic Light Scattering (DLS) by Zetasizer, Malvern Instrument equipped with 633 nm He-Ne laser and a backscatter detector at an angle of 173 degrees. Folded capillary tubes were used for measuring Zeta potential at a controlled temperature of 25°C and a fixed voltage of 150 V. The Z-average size was calculated using the “General purpose” analysis model as provided by the Zetasizer software. For each sample, minimum of 3 measurements containing 11 runs of duration 10 seconds was performed. The results for the three readings were averaged and standard deviation was calculated to define the error bars on the DLS graphs. UV-Vis spectroscopy was performed using FLUOstar Omega plate reader to determine the absorbance spectrum in the range of 400-800 nm. UV transparent 96-well plates were used for the entire study. AuNPs based on their physical morphologies exhibit different absorbance peaks in the UV-spectrum. The size and morphology studies were also done using Philip (FEI Tecnai F30) high resolution transmission electron microscope (HRTEM) operating at 300 keV. The samples for TEM were prepared by dip-coating the carbon coated TEM grid in a diluted solution of the particles and drying it at room temperature. The steps were repeated multiple times to ensure enough AuNPs are present on the grid. The samples were stored under high

vacuum overnight to remove any moisture and protect the sample from oxidation. The average size of the particles was calculated by using Gatan Digital Micrograph software.

2.2.3 AuNPs Synthesis

AuNPs were synthesized using the standard citrate reduction procedure as reported in the literature previously [114]. Briefly, 100 mL of 1 mM $HAuCl_4$ was heated to boil under constant stirring. Next, trisodium citrate solution (2 mL, 194 mM) was added rapidly in the stirring solution resulting in a change in solution color from pale yellow to red. The solution was boiled for another 20 min and then allowed to cool at room temperature. The solution was then filtered using 0.22 µm membrane filter to ensure the monodispersivity of the AuNPs and stored at 4°C for long term stability. The concentration was calculated as 14.4 nM with the help of Beer's law by using the extinction coefficient of 2.01 x 10^8 $M^{-1}cm^{-1}$ [115]. The entire scheme is shown in **Figure 7**.

2.2.4 Preparation of AuNPs conjugated with aptamers

The aptamers were received in a dried pelleted form and were resuspended in TE buffer (10 mM Tris HCl, 0.1 mM EDTA, pH 7.5) to achieve a concentration of 100 µM. The solution was aliquoted into smaller volumes to avoid multiple freeze and thaw cycles. Before immobilization of the aptamers over the AuNPs surface, the aptamers were diluted to the required concentration using folding buffer (1 mM $MgCl_2$ and 0.01 M PBS, pH 7.5). The aptamers were brought into a folded state by incubating at 95°C for 5 min and another 15 min at room temperature. The thiolated aptamers were then reduced by using TCEP

in 1:1 v/v dilution. The addition of TECP ensures the breakage of any disulphide bonds (-S-S-) such that free –SH group is available to bind to the gold surface. The reaction was incubated for 20 min at room temperature. The unmodified aptamers did not require any reduction steps. AuNPs-aptamer complexes were prepared by mixing the AuNPs and folded aptamers in 1:1 v/v ratio and kept at room temperature for another hour. Excess aptamers were washed away by centrifugation at 14,000 rcf for 11 min and resuspending the conjugates in folding buffer.

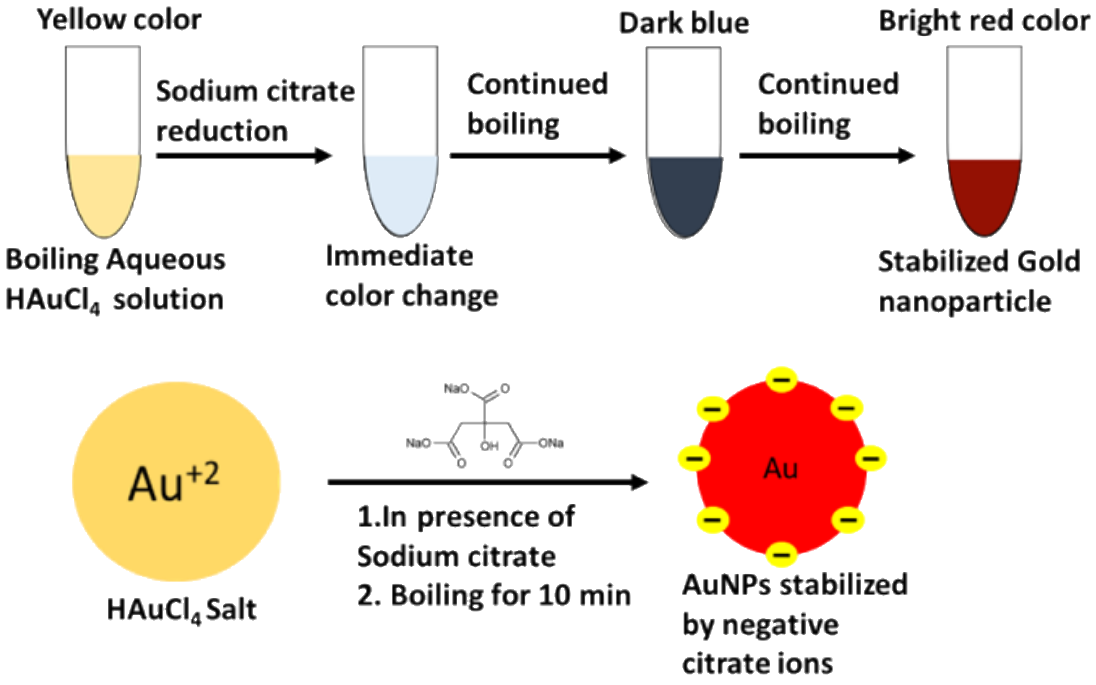

Figure 7: Schematic of AuNPs synthesis using seedless approach

2.2.5 Preparation of hydrophobic Paper substrate

Paper based substrates made up of cellulose, such as Whatman® filter paper are portable, easy to store, readily available and provide high surface area for colorimetric

bioassays. The surface and pore size of the Whatman® filter paper can be easily functionalized and controlled by various chemical treatments as per requirement [116-118]. In the present study, Whatman® filter paper was cut into strips and functionalized with wax by directly rubbing the solid wax over the paper. The paper was incubated for about an hour at 60°C such that the wax spread evenly on the paper surface and seeped through the pores of the paper. The wax provides hydrophobic nature to the paper which does not allow AuNPs to wet the surface or spread on to the surface of paper [68].

2.2.6 Colorimetric assays

25 µl of epinephrine at different concentrations was added to 50 µl of AuNPs-apt solution for each colorimetric assay in the 96 well-plate. The amounts and concentrations of epinephrine used in the study were 2 µg (360 µM), 1 µg (180 µM), 500 ng (90 µM), 350 ng (63 µM), 200 ng (36 µM), 125 ng (22 µM), 50 ng (9 µM) and so on. The AuNPs-apt and epinephrine solution was incubated for 10 min at room temperature before performing the UV-visible spectroscopy. For the different size and shape study, the concentrations of the different AuNPs were kept constant at 0.2 mg/ml for an accurate comparison of the detection limit. Each assay was performed at least in triplicate and the data is represented as mean ± standard errors.

2.3 Results and Discussions

2.3.1 AuNPs Characterization

Figure 8 shows detailed characterization of the as-synthesized (13 nm spherical particles) and purchased AuNPs. AuNPs (13 nm) were synthesized using the standard

procedure of citrate reduction of $HAuCl_4$ as shown in **Figure 7**. The hydrodynamic radii of the gold colloids are 18.15 nm, 20.10 nm, 36.48 nm, 52.47 nm and 55.91 nm as measured with DLS instrument and it can be seen that all the particles are in a very narrow range with minimum/no agglomeration (**Figure 8A).** Zeta potential results (**Figure 8B**) indicate that the citrate coated particles are negatively charged with surface charge as -21.9 mV, -28.33 mV, -37.8 mV, -52.2 mV -52.5 mV and -43.9 mV and this charge increases with respect to the size of the particles. The negative charge of AuNPs induces stability in the solution and prevents unwanted agglomeration. AuNPs of diameter 13 nm, 15 nm, 30 nm and 50 nm stabilized in water exhibited distinctive peaks (surface plasmon band, SPR) at around 518 nm, 520 nm, 524 nm and 528 nm respectively (**Figure 8C**). The SPR of the AuNPs is modified when the shape deviates from spherical geometry [119]. In the case of rods, the electrons are found to oscillate in the transverse as well as longitudinal direction. The transverse mode showed a resonance peak at approximately 520 nm whereas the longitudinal direction peak was observed at 670 nm (**Figure 8D**). Nanourchin shaped particles exhibited a broad, shifted peak at ~562 nm due to the presence of spikes which results in complex localized surface plasmon resonance (LSPR). Different absorption peaks of these particles cause changes in their visible color (**Figure 8D**).

High resolution transmission electron microscopy (HRTEM) images of the as prepared and purchased nanoparticles are shown in **Figure 9 (A-F)**. HRTEM images revealed that particles are uniformly dispersed and have spherical, spiky and rod-like morphologies. The average sizes are in order of 12.74 nm, 14.66 nm, 27.77 nm, 48.71

nm, 53.76 nm and 45.34 nm (**Table 1)**. The next section discusses the effect of aptamer concentration as well as the binding mechanism on the aggregation of the AuNPs.

Table 1: Summary of the properties of gold nanoparticles as characterized through various techniques.

Gold Nanoparticles	Zeta potential (mV)	SPR band (nm)	Hydrodynamic Size (nm)	TEM average size (nm)
Sphere-13 nm	-21.9	518	18.15 ± 2.1	12.74 ± 0.5
Sphere-15 nm	-28.33	520	20.10 ± 0.6	14.66 ± 0.3
Sphere-30 nm	-37.8	524	36.48 ± 0.3	27.77 ± 1.2
Sphere-50 nm	-52.2	528	52.47 ± 0.4	48.71 ± 2.5
Nanourchin	-52.5	562	55.91 ± 0.4	53.76 ± 6.3
Nano Rods	-43.9	520, 620	-	45.34 ± 0.4

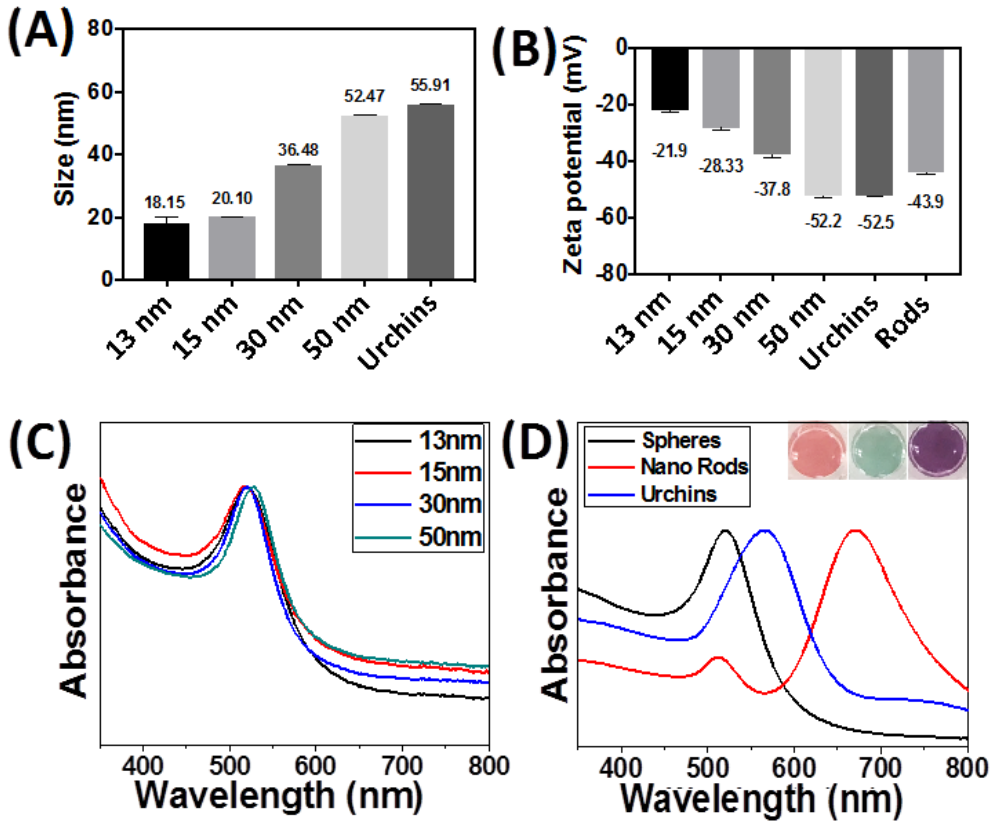

Figure 8: Thorough characterization of different kind of AuNPs. (A) Dynamic Light scattering measurements showing the diameter of the spherical particles as well as nanourchins. The mean sizes observed are 18.15 nm, 20.10 nm, 36.48 nm, 52.47 nm and 55.91 nm respectively. (B) Surface zeta potential of the given samples shows the presence of negative charge with a small error bar. (C) Normalized UV-visible spectra of the spherical particles with SPR bands at 518 nm, 520 nm, 524 nm and 528 nm. (D) UV-Visible spectra of different shapes of AuNPs. The maxima was observed at 518 nm, 562 nm for spheres and urchins where as for rods, these were 520 nm and 670 nm. The inset shows the visible color of different shapes- Spheres (red), Rods (Green) and Nanourchins (Purple).

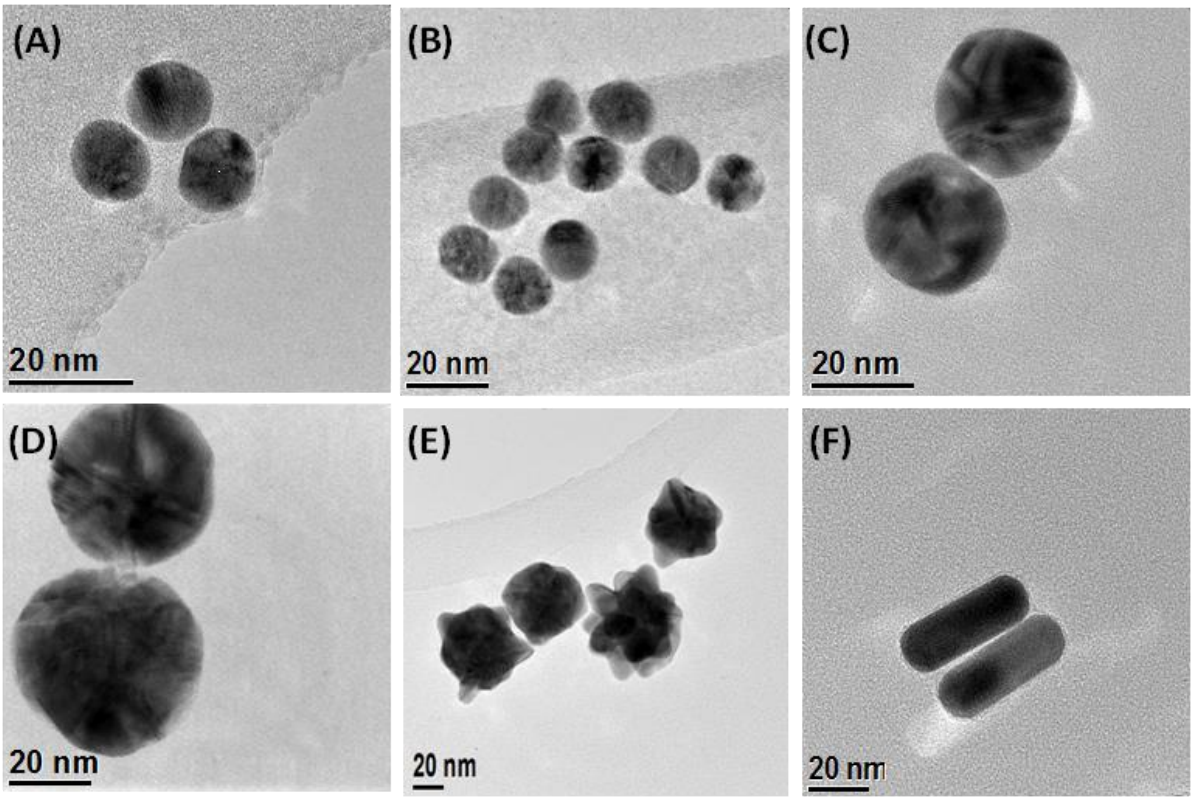

Figure 9: High Resolution Transmission Electron Microscope analysis for different sizes and shapes of gold nanoparticles. (A-F) images show the TEM for 13 nm, 15 nm, 30 nm, 50 nm, Nanourchins and Nano Rods respectively. The length is calculated using Digital Micrograph software provided by Gatan.

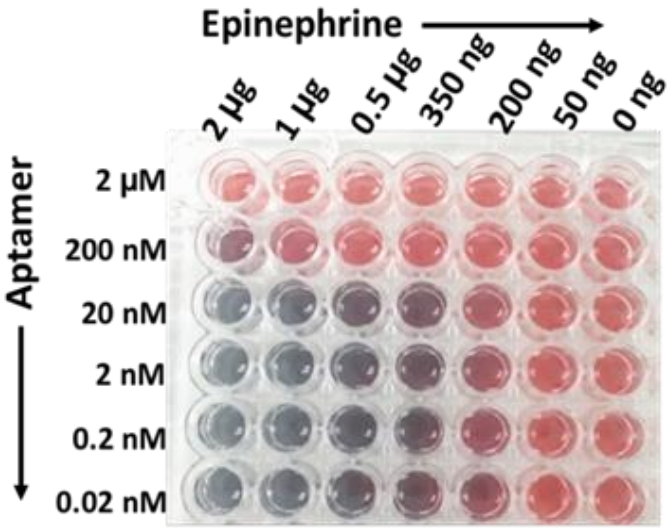

Figure 10: Visible color change in the solution of AuNPs conjugated with different concentration of thiolated aptamers (0.02 nM to 2 µM) in presence of Epinephrine. The change in color represents aggregation in the solution. The AuNPs started aggregating when the aptamer concentration was 20 nM or less and minimum concentration of epinephrine was 200 ng.

2.3.2 Effect of Aptamer Concentration

13 nm AuNPs were conjugated with different concentrations of the epinephrine-binding aptamer (2 µM, 200 nM, 20 nM, 2 nM, 0.2 nM and 0.02 nM) and tested against a range of concentrations of epinephrine (2 µg (360 µM), (1 µg (180 µM), 500 ng (90 µM), 350 ng (63 µM), 200 ng (36 µM) and 50 ng (9 µM)). **Figure 10** shows the visual color change at different aptamer concentration in the presence of epinephrine and the corresponding UV-Visible spectra of these samples is represented in **Figure 11**. The destabilization of the charge causes aggregation in the solution which can be seen from the TEM analysis as shown in **Figure 12**.

The change in color was observed in solutions starting from 200 ng of epinephrine and aptamer concentration ranging from 0.02 nM-20 nM. It was observed that the SPR of AuNPs at 520 nm broadens and shifts to a longer wavelength as a function of the epinephrine concentration. The degree of aggregation is represented in terms of A_{640}/A_{518} where A_{640} and A_{518} indicate the absorbance intensity at 640 nm and 518 nm, respectively. **Figure 13** demonstrates a comparative analysis of different samples. It can be seen that the increase in aptamer concentration (20 nM, 200 nM and 2 µM) decreases the detection limit of the AuNPs–apt system. There was no aggregation observed in the 2 µM aptamer solution at any epinephrine concentration.

This result of decreased detection with increased aptamer concentration is due to the fact that as epinephrine is introduced into the solution, the free unbound aptamer binds to it [120]. Since the epinephrine molecule is very small in size (Molecular Weight: 219.67 Da), the aptamer wraps around the molecule, making it very difficult for the molecule to interact with the other aptamers present on the gold surface, thus inhibiting aggregation of the AuNPs. Also, the conjugated aptamers add to the overall negative charge of the AuNPs, enhancing the stability of the AuNPs by increasing the electrostatic repulsion between the particles [121, 122]. It can be observed that the optimized range of aptamer for maximum detection of the analyte is below 20 nM aptamer concentration which can detect epinephrine levels as low as 200 ng. At lower concentration of aptamers, a linear increase in the ratio was observed at 50 ng , 200 ng and 350 ng of epinephrine which becomes constant at higher concentrations of epinephrine. 2 nM aptamer concentration gave the maximum A_{640}/A_{518} ratio which suggest that it is the optimum aptamer concentration at which maximum aggregation was seen in the solution at 200 ng

of epinephrine. Higher concentration of aptamer induces excess stability in the solution as discussed previously. The aptamer concentration lower than 2 nM i.e. 0.2 nM and 0.02 nM is insufficiently low in number and in the presence of low concentration of the epinephrine molecule, not enough aptamers are present to induce aggregation in the AuNPs solution. Therefore, AuNPs are conjugated with 2 nM aptamer concentration for further experiments. The aptamers can be physically adsorbed [122] on the surface of AuNPs or can bind to the surface of AuNPs via covalent bonding [123, 124]. The following experiment compares the two different types of the aptamers and studies their effect on the aggregation.

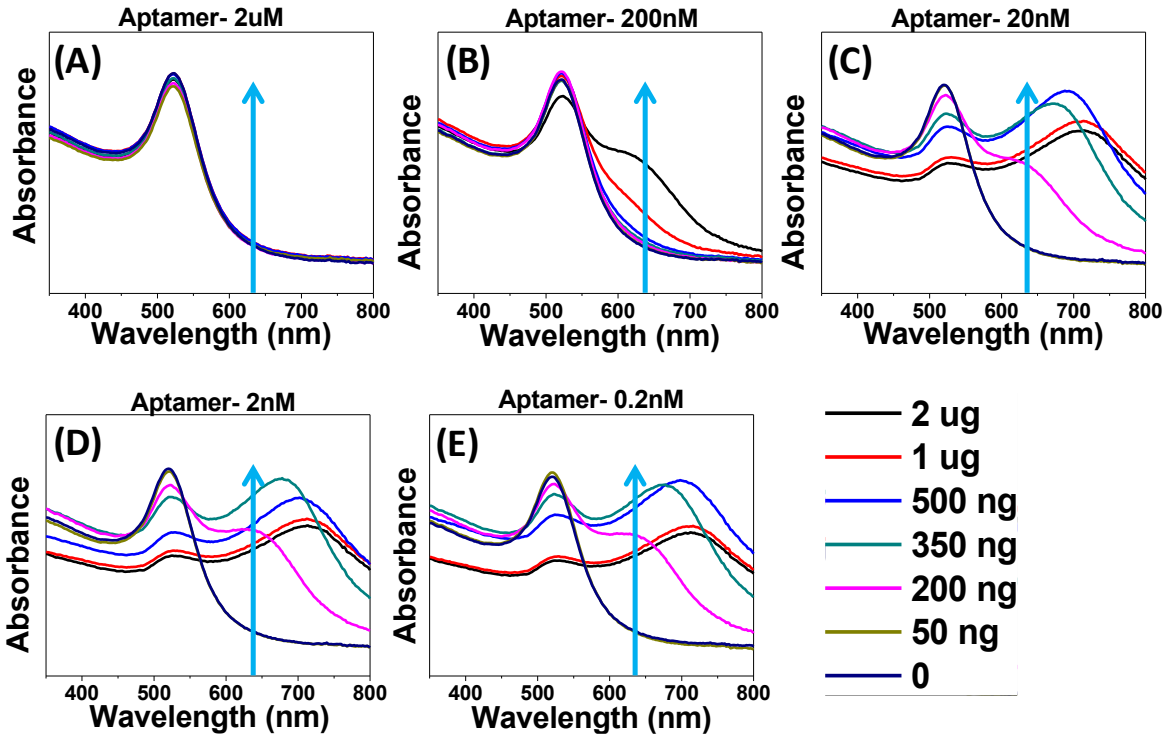

Figure 11: UV-Vis spectra of AuNPs conjugated with different concentration of thiolated aptamers (0.02 nM to 2 µM) in the presence of Epinephrine (50 ng- 2µg). The experiment demonstrates the effect of aptamer and analyte concentration on the aggregation of AuNPs. (A) 2 µM aptamer concentration causes the gold nanoparticles to be very stable and excess of aptamer in the solution binds to the Epinephrine inhinbiting aggregation in the solution. Therefore, no red shift was observed. (B) A slight shift in the peak at 640 nm was seen in the presence of 2 µg and 1 µg of Epinephrine when the aptamer is 200 nM. (C, D, E) Similar response was seen for 20 nM, 2nM and 0.2 nM aptamer concentration with an intense shift in the peak at 640 nm. Minimum amount of Epinephrine detected was 200 ng. At 50 ng, the Epinpehirne concentration is too low to induce any aggregation in the solution.

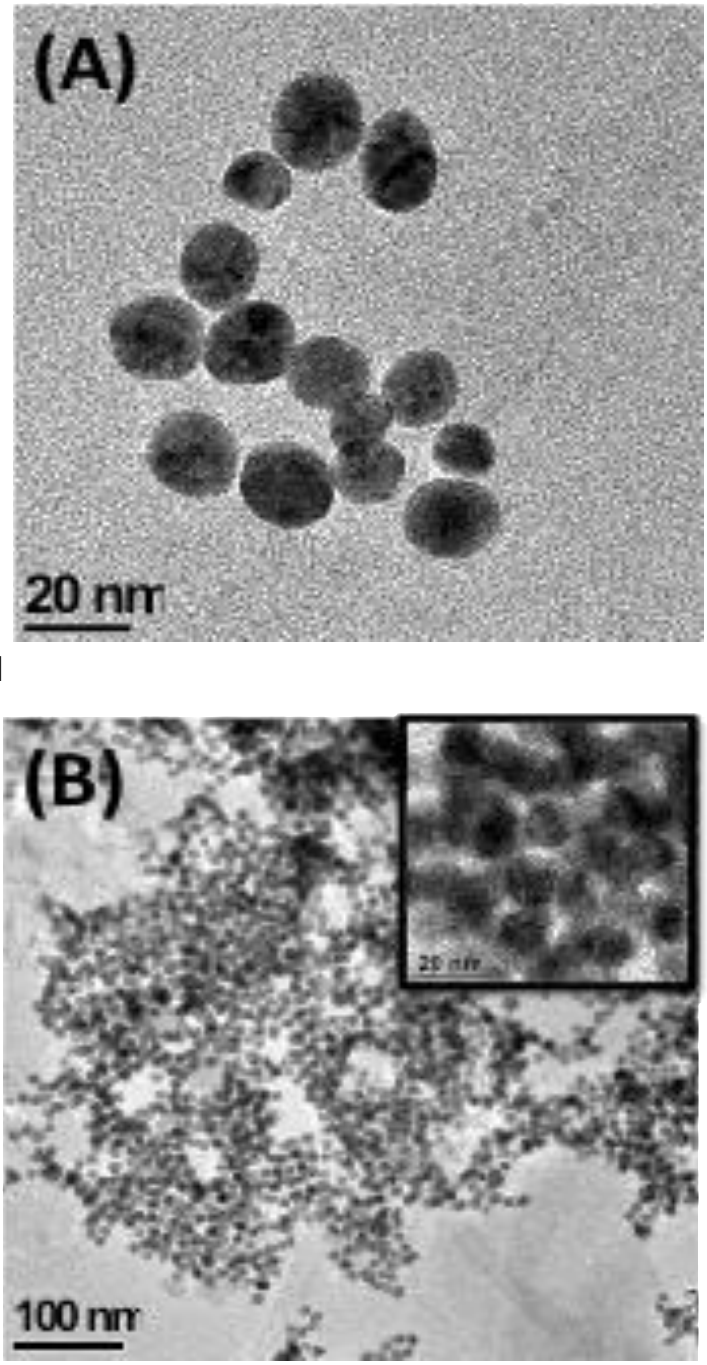

Figure 12: High Resolution Transmission Electron microscope image for (A) uniformly dispersed AuNPs and (B) aggregated AuNPs in the presence of Epinephrine. Inset showing higher magnification with a scale bar of 20 nm.

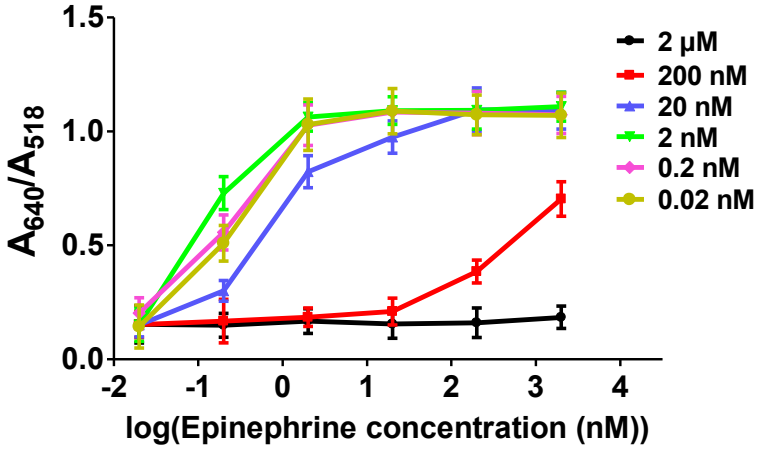

Figure 13: Comparative analysis of the A_{640}/A_{518} ratio as derived from UV-Visible spectroscopy analysis of samples containing different amount of aptamers (2 µM, 200 nM, 20 nM, 2 nM, 0.2 nM and 0.02 nM) as a function of epinephrine concentration represented in logarithmic scale (2 µg (360 µM), (1 µg (180 µM), 500 ng (90 µM), 350 ng (63 µM), 200 ng (36 µM) and 50 ng (9 µM)). The increase in the ratio is in correspondence with the color change in the solution. Solution with 2 nM concentration (green curve) shows the most significant increase in the ratio at 200 ng of Epinephrine which indicates maximum aggregation in the solution.

2.3.3 Effect of thiolated and non-thiolated aptamer conjugation

Aptamers can bind to the surface via covalent bond (Au-thiol interactions) [123, 124] or it can be adsorbed on the surface via electrostatic interactions [122]. **Figure 14** represents the comparison between the thiolated and non-thiolated epinephrine aptamer and its effect on the sensitivity of the aptasensor. As it was observed earlier that 200 ng

of epinephrine induced intense color change in the solution and red-shift in the UV spectrum, the AuNPs-aptamers were now tested against 125 ng of epinephrine. It can be seen from **Figure 15** (A, B, C), 125 ng induced slight color change in the solutions in the presence of aptamer ranging from 20 nM-0.02 nM. However, the UV-Visible data (**Figure 15**) shows the highest peak at 640 nm which belonged to 2 nM aptamer. The maximum A_{640}/A_{518} ratio was achieved for 2 nM of the thiolated aptamer as shown in **Figure 14**. The thiolated and non-thiolated produced similar results in terms of color change but UV-visible data showed that the thiolated aptamers are more efficient in detecting the analyte.

The variation in detection of analyte by thiolated versus non-thiolated aptamers is due to differences in the underlying mechanisms of these two approaches. Thiolated aptamers bind strongly to the surface of the gold and when the analyte approaches, AuNPs are pulled together strongly to form aggregates [125]. The repulsion between the citrate capped AuNPs is dominated by the affinity of aptamers towards the analyte. The presence of epinephrine bound with the aptamers causes destabilization in the charge of AuNPs which results in aggregation/color change. On the other hand, the unmodified aptamers are loosely attached to the AuNPs surface. In the presence of epinephrine, the aptamers attain a tertiary folded conformation and detach themselves from the surface, leaving the AuNPs destabilized [122, 126]. The extent of destabilization depends on the concentration of analyte and the number of aptamers detached from the surface. The lesser shift in the peak at ~640 nm in the presence of unmodified aptamers is due to aptamers remaining attached to the surface of AuNPs and screening them from aggregation. However, the difference is very minor, and therefore, it can be concluded that both thiolated and non-thiolated aptamers behave almost the same for low

epinephrine concentrations. Moving forward, thiolated aptamers were used at 2 nM concentration for testing the effect of AuNPs physical morphology on the detection of epinephrine.

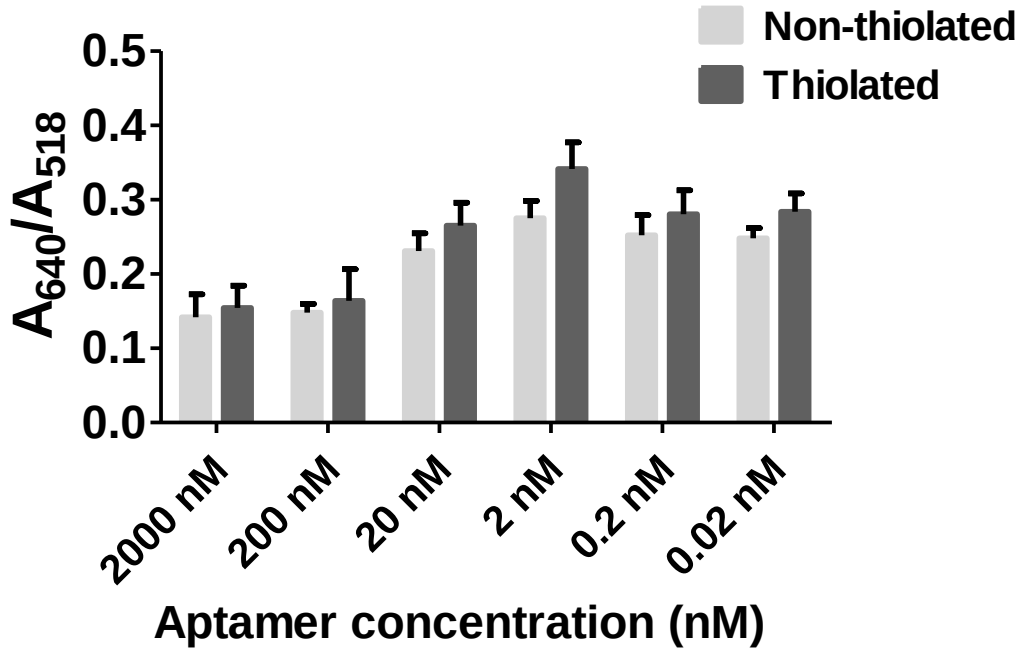

Figure 14: Comparative analysis of thiolated and non-thiolated aptamer on the surface of AuNPs in the presence of 125 ng of Epinephrine. The absorbance ratio (A_{640}/A_{518}) as calculated by UV-visible spectra represents maximum aggregation in 2nM thiolated aptamer solution. The columns represent the mean value and the error bars indicate the standard deviation in the experiments.

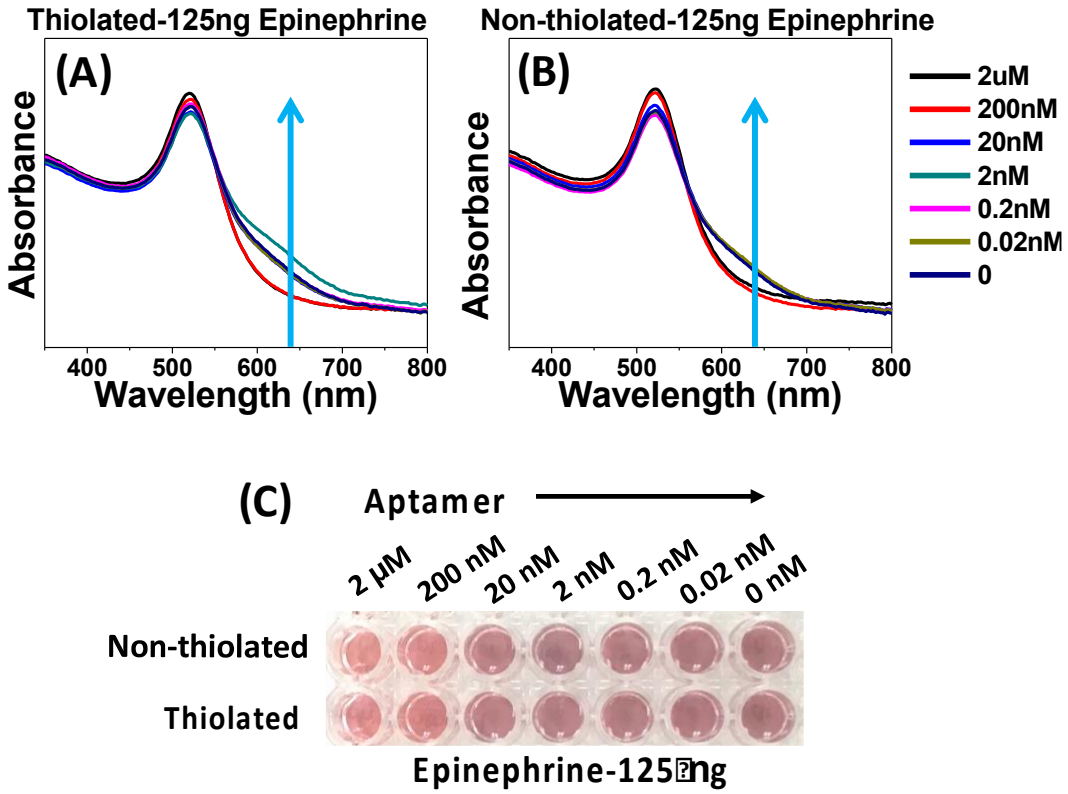

Figure 15: Comparative analysis of thiolated and non-thiolated aptamer at the surface of AuNPs on the sensitivity of the aptasensor. (A) UV-visible spectra for the AuNPs conjugated with thiolated aptamer. The peak for 2 nM aptamer has shown maximum intensity at 640 nm as compared to other concentrations of the aptamer. (B) UV-Visible spectra for the non thiolated aptamers. (C) Visible color as observed immediately after addition of Epinephrine did not show much color change as noticeable by the naked eyes.

2.3.4 Effect of Different Sizes

So far, the effect of aptamer concentration and the thiolated and non-thiolated binding of the aptamers has been discussed. 2 nM thiolated aptamer showed maximum sensitivity

and visible color change towards 125 ng of epinephrine with a maximum peak intensity at 640 nm. Different sizes of spherical gold nanoparticles (13 nm, 15 nm, 30 nm and 50 nm) have been used to test the limit of detection of the aptasensor. **Figure 16 (A, B)** shows the response of different sizes of AuNPs in the presence of 125 ng and 200 ng of epinephrine. The UV-Visible spectrum shows that the 13 nm AuNPs (black curve) exhibited a greater red shift in the presence of 125 ng and 200 ng epinephrine compared to other particles. No shift was seen for 30 nm and 50 nm AuNPs. The derived absorbance ratio (A_{640}/A_{518}) from the UV-Visible spectra (**Figure 16 C**) confirms that the maximum aggregation was observed for 13 nm particles, followed by 15 nm particles with little to no shift for 30 nm and 50 nm AuNPs. 13 nm AuNPs also exhibited the maximum color change for all tested concentration of epinephrine (**Figure 17**).

The strongly bound citrate group induces negative charge on the surface of the AuNPs which leads to repulsion between the particles [127]. Since the 50 nm AuNPs have the maximum negative surface charge (**Table 1**), very little aggregation was observed in the solution. Because larger sized particles are bulkier than smaller ones, higher concentrations of analyte are required for the aptamers to agglomerate the particles. The combined effect of the negative zeta potential as well as the interaction of aptamer and analyte is responsible for no color change in larger particles.

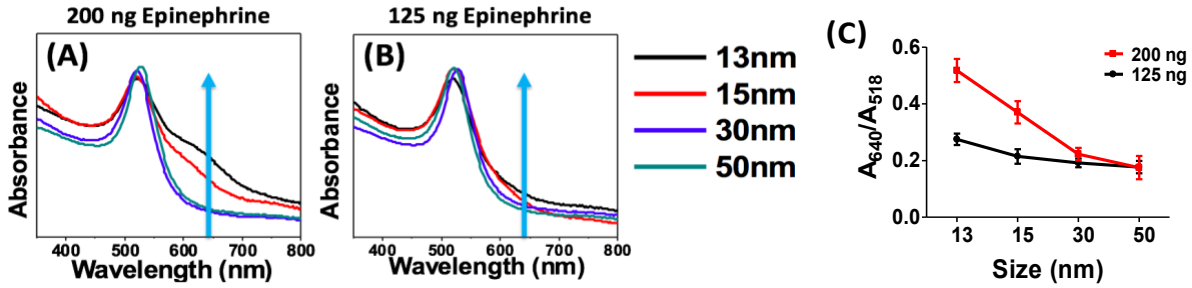

Figure 16: Size dependent study for the detection of Epinephrine. (A, B) UV-Visible spectra showing aggregation in the solution of different sizes (13 nm, 15 nm, 30 nm and 50 nm) of AuNPs at 125 ng and 200 ng of epinephrine. (C) Plot showing trend for the derived absorbance ratio (A_{640}/A_{518}) for different sized particles. 13 nm particles showed maximum aggregation in presence of 200 ng and 125 ng of Epinephrine.

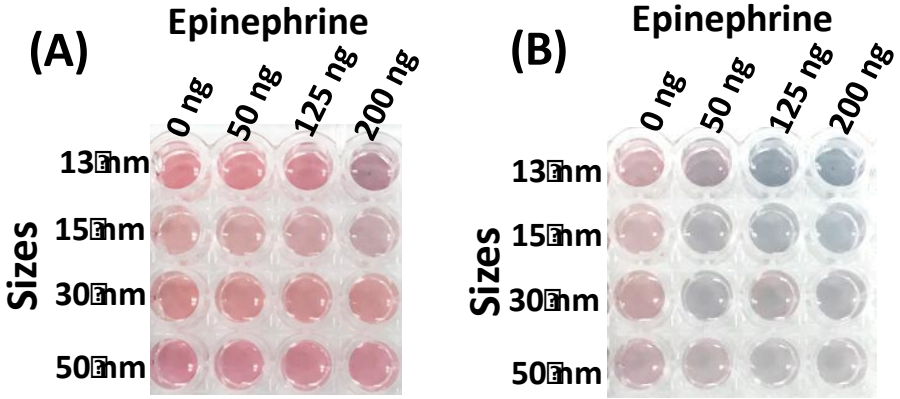

Figure 17: Visible color change in the solution of different sized AuNPs-aptamer (13 nm, 15 nm, 30 nm, 50 nm) in the presence of different concentration of Epinephrine (50 ng, 125 ng, 200 ng). (A) without salt (B) In the presence of salt (170 mM, 10 µl). Maximum color change can be observed for 200 ng for 13 nm AuNPs particles.

2.3.5 Effect of different shapes: Rods, spheres and urchins

Anisotropic nanomaterials with highly complex structures have generated wide spread interest owing to their enhanced physical and optical properties. In the present section, a comparative analysis of different shapes of AuNPs used for the detection of epinephrine has been carried out and the basic characterization is shown in **Figure 8 and 9**. The aptamer conjugation process and the concentration of all AuNPs was kept constant as used for the spherical particles. **Figure 18 (A-D)** summarizes the result of the assay. The UV-visible spectra showed an intense red shift in the peak of spherical particles (**Figure 18 A**). The maximum shift was seen by addition of 500 ng of epinephrine followed by 250 ng and 125 ng. The color change is also in line with the UV shift with maximum change caused by adding 500 ng of epinephrine. In the case of rods, there was no shift in the peaks or change in color. The intensity at peak 670 nm showed a constant decrease with respect to the epinephrine concentration and a very slight shift towards a lower wavelength. In rods, the red or blue shift is a result of change in the aspect ratio. The slight blue shift is due to the decrease in the aspect ratio which indicates that some of the rods have aggregated due to epinephrine. However, there was no change in color observed for the rods. Nanourchins on the other hand showed no change in the UV-visible spectra or visible color following the addition of epinephrine. As observed earlier, bigger size and greater negative charge leads to stability of the particles and lowers the detection limit. The rods and urchins both have sizes in the range of 50 nm and the zeta potential is also higher as compared to 13 nm spherical particles (**Table 1**). Also, the aggregation behavior of the rods and spheres are different from each other. Nanorods are more stable than the spherical particles as nanorods are known to possess steric hindrance which

causes low packing density and smaller aggregates [128-130]. The spheres and urchins both have higher curvature, thus higher packing density; however, the spiky structure disrupts aggregation of urchins. Therefore, spherical particles with size between 13-15 nm are the most suitable particles for the colorimetric sensor.

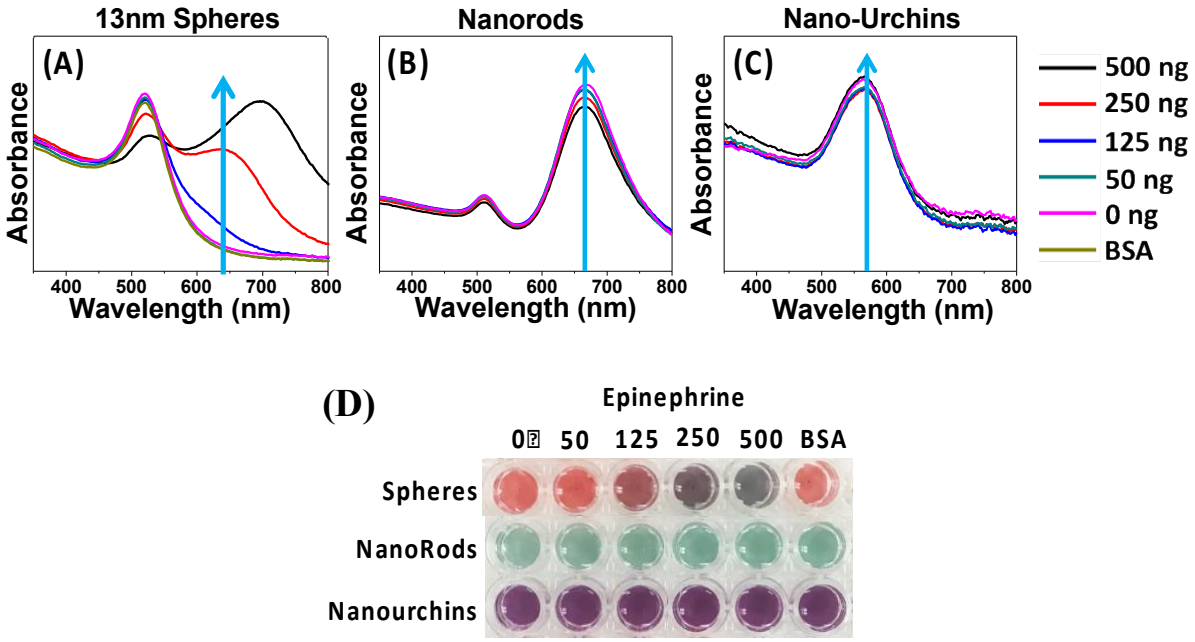

Figure 18: Detection of Epinephrine using different shapes of AuNPs. Fig. A, B and C represents the change in UV visible spectra in presence of 13 nm spherical AuNPs, Gold nanorods and 50 nm Nano urchin. Spherical particles show clear red shift at 500, 250 and 125 ng of Epinephrine whereas in case rods and nanourchin, very slight change in the intensity of the peaks can be seen. The color change as shown in Figure D is prominent for spherical particles whereas no color change was observed for Rods and Urchin.

2.3.6 Selectivity of the sensor

The specificity of the present colorimetric sensor was tested by using common interfering agents such as 3, 4-dihydroxyphenylacetic acid (DOPAC), ascorbic acid, tryptophan, homovanillic acid (HVA), tyrosine, glycine and bovine serum albumin (BSA). 900 µM of control samples were tested against 90 µM (500 ng) epinephrine to test the specificity of AuNPs-apt. Maximum shift in UV-spectroscopy is obtained by the addition of epinephrine, with very little shift being induced by dopamine and no shift by other controls (**Figure 19**). These results demonstrate the high specificity of this colorimetric biosensor against epinephrine.

2.3.7 Aggregation Study-Time based study

The aggregation kinetics was studied by examining the rate of aggregation with respect to the analyte concentration. Two different concentrations of epinephrine (200 ng and 125 ng) were used to induce aggregation in the solution and the size of the aggregates was calculated using DLS. 200 ng of epinephrine induced immediate aggregation in the solution. The change in size in the presence of 200 ng and 125 ng of epinephrine at different time intervals (0 min, 10 min, 30 min, 1 hour, 2 hours and 3 hours) is shown in **Figure 20**. It can be seen that in presence of 200 ng of epinephrine, the solution started showing an increase in size immediately with the initial size of 21.38 nm as compared to the 18.16 nm of 125 ng epinephrine. A gradual increase in size can be observed for 200 ng of epinephrine; however, no change in size of AuNPs-apt was observed in the presence of 125 ng for almost half an hour (**Figure 20**). After 1 hour, the size increased from 18.16 nm to 31.21 nm. For both samples, the size remained constant after 2 hours.

This is in compliance with the established studies in the literature which suggest that this is due to the completion of charge transfer and stabilization of the aggregates [127]. When the interparticle distance is greater than the average radius of the particles, the particles are uniformly dispersed in the solution and emits red color whereas when the interparticle distance is less than the average radius, the solution starts changing to blue color. After 24 hours, the aggregated particles precipitated in the plate and showed no further increase in size.

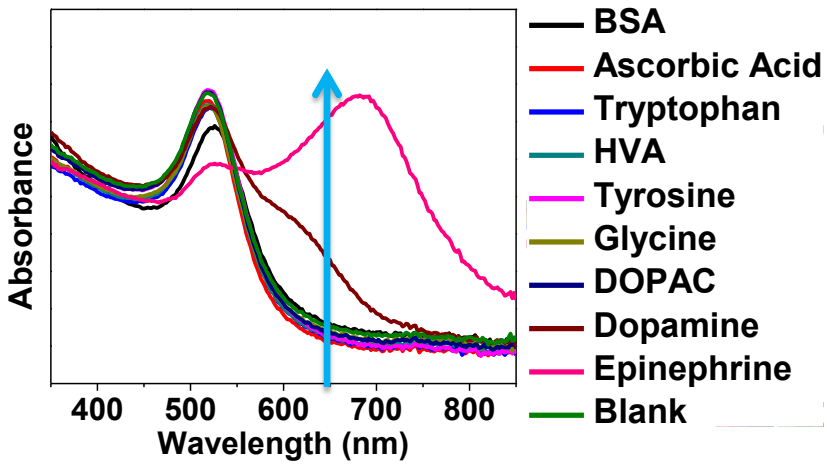

Figure 19: Specificity test: UV-Visible spectra of AuNPs conjugated with 2nM aptamer at 900 µM concentration of interfering agents such as BSA, Ascorbic acid, Tryptophan, HVA, Tyrosine, Glycine, DOPAC and Dopamine. Epinephrine (500 ng) caused maximum shift in the UV-Visible spectra. Control represents the sample without any analyte in the solution.

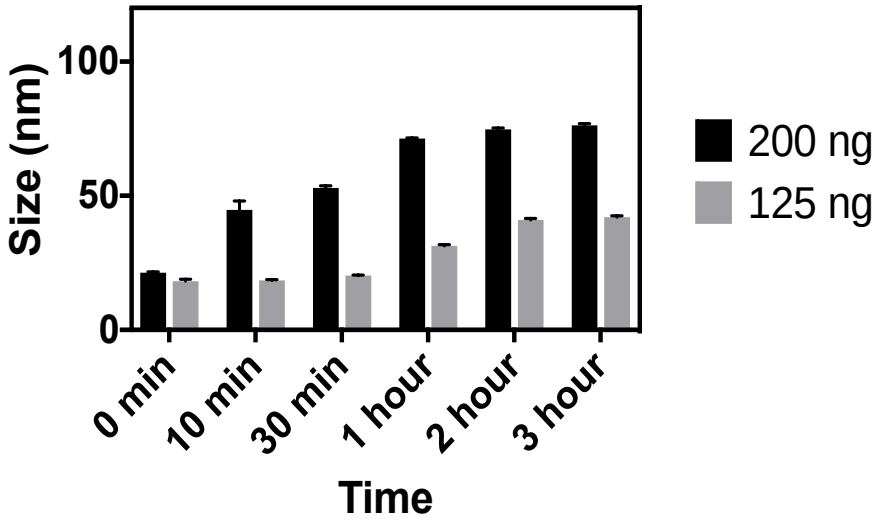

Figure 20: Comparative analysis of the change in size of AuNPs in the presence of 200 ng (black) and 125 ng (gray) of Epinephrine.

2.3.8 Effect of salt

As discussed previously, the surface of the synthesized AuNPs is derivatized with citrate ligands which provide them stability against aggregation. Increases in salt concentration increase the ionic strength of a solution which results in screening of this repulsion force and induction of aggregation/flocculation of AuNPs. When the AuNPs are conjugated with aptamers, the aptamers protect the surface of the AuNPs against salt induced aggregation. However, the presence of epinephrine bound to the aptamer decreases the overall negative charge of the AuNPs and causes destabilization of the apt-AuNPs. Addition of salt further amplifies the charge destabilization and causes aggregation in solution.

The present AuNPs-aptamer system was tested against a range of NaCl concentration and it was observed that 170 mM NaCl induced no shift in the UV spectra

and was therefore chosen for further experiments. **Figure 21A** shows the UV-Visible spectra of the AuNPs-aptamer in the presence of different concentration of epinephrine after the addition of 170 mM NaCl. There is a clear red shift in the spectra with the increase in the concentration of epinephrine. The derived absorbance ratio (A_{640}/A_{518}) increases proportionally from 0.22 to 1.15 with increase in the epinephrine concentration which corresponds to aggregation in the solution (**Figure 21B**). The lowest amount of epinephrine that induced red shift in the spectra was 0.005 ng (0.9 nM) as shown in **Figure 21**. In the absence of epinephrine, the aptamers conjugated AuNPs show high stability against NaCl and no red shift was observed in the UV-Visible spectra. The present approach with the optimized parameters was then tested on a hydrophobic paper substrate to formulate an easy-to-use device.

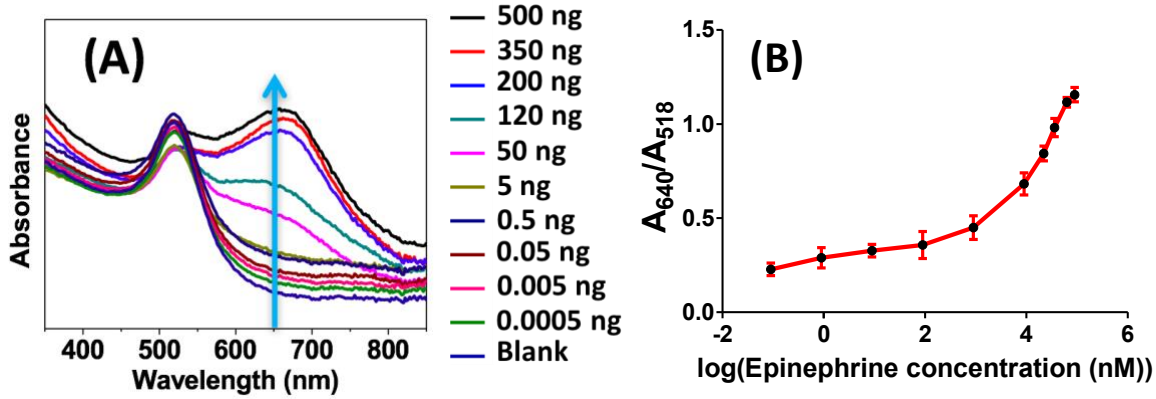

Figure 21: Effect of addition of salt on the detection limit of the sensor. (A) UV-Visible spectroscopy showing spectral shift in the presence of difference concentration of epinephrine ranging from 0.5 pg to 500 ng (0.09 nM to 90 µM) and salt (170 mM). Addition of salt causes red shift in the spectra in the presence of epinephrine whereas

no shift was seen for the blank sample (no analyte). (B) The derived absorbance ratio (A_{640}/A_{518}) increases proportionally with the increase in epinephrine concentration. Lowest concentration of epinephrine that induced red shift in the UV-Visible spectra is 0.9 nM.

2.4 Paper based sensor

So far, it has been discussed that 13 nm spherical particles when conjugated with 2 nM thiolated aptamers in the presence of salt showed high detection limit for epinephrine (0.9 nM). The increase in concentration of epinephrine leads to increase in aggregation and thus increases the intensity of color change as seen from the shift in UV-Visible spectra. The concentration of AuNPs was varied to study the effect on the detection of Epinephrine. The AuNPs conjugated with aptamer were concentrated to 2X, 3X and 4X times by centrifuging at 11500 rcf for 11 min resulting in a concentration of 14 nM, 21 nM and 28 nM. The results demonstrated that 4X concentration showed the maximum sensitivity towards epinephrine. As explained earlier, the aggregation depends on the interparticle distance as well as the radius of the particles. In 4X solution, the number of AuNPs is four times the original solution in a same volume of the solution. The distance between each particle decreases, therefore, the probability of aggregation as well as the intensity of color change also increases with increasing concentration. The AuNPs-aptamer based biosensor with all the optimized parameters were then used for the fabrication of a paper based sensor.

The color change on the paper was calculated quantitatively using the red-green-blue values of each AuNPs spot determined by image processing software (Color helper,

2013) [131]. The blue/red ratio directly correlates with the degree of aggregation in the solution and hence the concentration of epinephrine. 10 µl of AuNPs-aptamer was added on the surface of the paper and different concentrations of epinephrine (9 µM, 4.5 µM, 1.8 µM, 9 µM, 900 nM, 90 nM, 9 nM, 900 fM, 90 fM) were added onto the drop of AuNPs solution. To enhance the aggregation in the solution, 2 µl of 170 mM NaCl was also added in all the samples which resulted in immediate color change (**Figure 22**). The addition of as low as 9 nM epinephrine began inducing color change in the solution and resulted in a significant increase in the B/R ratio. The B/R value for AuNPs without aggregation in the solution was found to be around 0.58 and addition of epinephrine increases this value to more than 1 which indicates aggregation of AuNPs-apt in solution.

The developed paper based sensor can be used in conditions where plasma catecholamines reach supraphysiological levels. In patients with stress induced cardiomyopathy (Takotsubo cardiomyopathy) and Killip Class III myocardial infarction, epinephrine levels average 6.9×10^{-9} M and 2.1×10^{-9} M after 1 or 2 days, respectively [132]. Normal physiological serum epinephrine concentration is approximately 0.13×10^{-9} M, which is below the detection limit of the sensor. [100] Therefore, supraphysiological levels of epinephrine will induce a color shift on the optimized paper sensor detectable with UV-visible spectroscopy but normal physiological values will not. This supports the diagnostic use of the sensor in a real-world situation. Furthermore, since the UV-vis shift is correlated to the concentration of target analyte, this method may also be used as a quick determinant of epinephrine levels in the patient.

The use of a cellulose-based paper approach provides a simple, easy and equipment free tool for sensing biomolecules. Of note, the paper did not interfere with the

sensing mechanism but further enhanced the color variance by providing high contrast background [68, 133]. The test result was stable for up to 30 min and indicates high sensitivity for the epinephrine molecule.

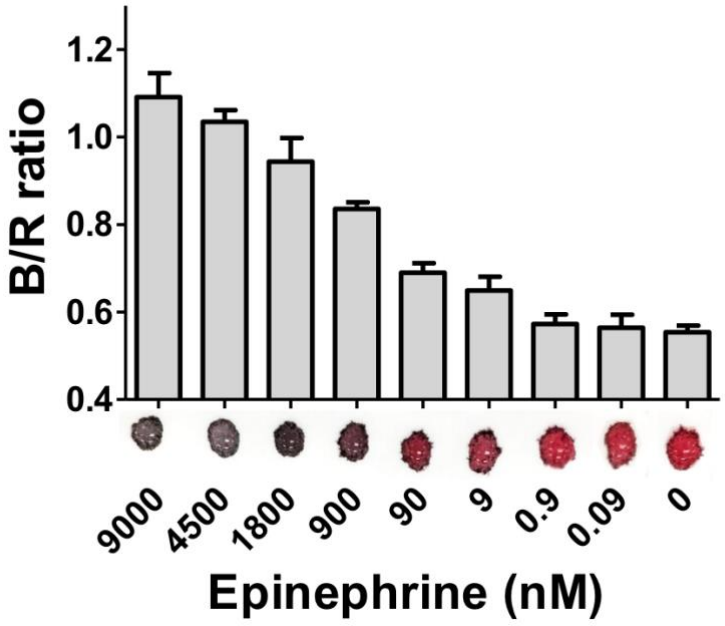

Figure 22: Colorimetric analysis of AuNPs-aptamer in the presence of different concentration of epinephrine (9 µM, 4.5 µM, 1.8 µM, 9 µM, 900 nM, 90 nM, 9 nM, 900 pM, 90 pM) on a hydrophobic paper based substrate. The corresponding ratio of blue/red colour values of the AuNPs spots are represented in the figure. The columns represent the mean values whereas the small error bars represent the standard deviation in the different set of experiments. The change in colour was observed at 9 nM with a significant increase in B/R value from 0.58 to 0.65.

2.5 Summary

To the best of our knowledge, the present work is the first established colorimetric detection of epinephrine using an aptamer based approach. The minimum amount of epinephrine detected using AuNPs-apt system was 9 x 10^{-9} M on a paper based sensor and 0.9 x 10^{-9} M using UV-Visible spectroscopy. While all the parameters tested in this current study played an important role in the functionality of the paper-based sensor, the size and morphology of the AuNPs proved most crucial in controlling the detection limit. It was observed that bigger size particles with greater negative charge are too stable and therefore not suitable for an efficient sensor. This optimized AuNPs-apt sensor approach can be used for the detection of any biomolecule so long as the bound aptamer is designed to detect the target analyte. Successful implementation of this paper-based sensor will provide easy, rapid, portable and inexpensive point-of-care testing which will revolutionize the world of bio-diagnostics and bio-imaging.

CHAPTER 3: HIGHLY SELECTIVE APTAMER BASED ORGANIC ELECTROCHEMICAL BIOSENSOR WITH PICO-LEVEL DETECTION

The work presented in this chapter has been published in

Biosensors and Bioelectronics 117 (2018) 40–46; DOI: 10.1016/j.bios.2018.05.031

Reproduced by permission of Elsevier

3.1 Introduction

Organic electrochemical transistors (OECTs) show great potential in the field of biosensors due to their low operating voltages and signal amplification. Over the past 30 years, OECTs have been utilized to detect numerous metal ions [134], small biomolecules [135, 136], proteins [137], oligonucleotides [138] and many other biological reagents [139-142]. The cost effectiveness, availability, simplicity and portability of OECTs give them an edge over other traditional optical techniques used as biosensors in diagnosis [143]. The OECT device based on PEDOT: PSS (poly(3,4-ethylenedioxythiophene) polystyrene sulfonate) has shown a higher transconductance as compared to silicon based transistor and also outperformed electrolyte-gated graphene [144, 145]. PEDOT: PSS based OECTs offer a means of developing highly efficient point-of-care testing tool which exhibit high sensitivity and selectivity for the detection of molecule of interest.

A typical OECT device consists of a source-drain channel which is connected by an organic semiconducting material such as PEDOT: PSS as an active layer. The device can be switched on or off by varying the channel current that flows through the active layer controlled by an applied voltage from the third electrode called gate [146]. The

effective gate voltage depends on the potential difference between the PEDOT: PSS/electrolyte and gate/electrolyte interface. The conductivity of the active layer can be modulated through doping/de-doping effects of the electrochemical reactions occurring in the device [147]. Therefore, any charge transfer reaction which alters the surface potential of the gate electrode causes a significant change in channel current which can be measured with high accuracy using simple instrumentation [148]. The transducing properties along with high specificity in these devices make them excellent candidate in biosensing especially in healthcare industry where detection at an early stage can be extremely helpful.

The application of OECT device as a biosensor [134-142] relies on the use of some biorecognition element such as enzymes, antibodies, oligonucleotides etc. which can transduce an electrochemical change in the presence of molecule of interest. Aptamers have been extensively used as the biorecognition molecule in the field of colorimetric [149], [122], electrochemical [150], spectrophotometry [151], [152], mass-sensitive [153], and electrophoretic sensing [154], [155]. Aptamers are short DNA or RNA chains which selectively bind to a target molecule with high affinity. As compared to antibodies and enzymes, aptamers are resilient to heat, pH variation and chemically harsh conditions which makes them more efficient for practical applications [137]. The process of SELEX (Systematic Evolution of Ligands by Exponential Enrichment) is used to design and select appropriate aptamers for the target molecules [138]. Once the aptamers are designed, these can be synthesized in large quantities with high purity and reproducibility [153]. Thus, the use of aptamers offers a method for sensitive, selective, and affordable biomolecule detection.

In this study, an ultra-sensitive label free aptamer based OECT device has been developed to detect the presence of catecholamine epinephrine. Epinephrine, commonly known as Adrenaline, is responsible to prepare the body for “fight or flight” response by accelerating the heartbeat, stimulate glucose production [156], dilate pupil [157] etc. It is generally administered in case of severe emergency situations such as cardiac attack, anaphylactic shocks or asthma attacks. The physiological level of epinephrine in a human body under normal conditions ranges form 120-200 pM [158] which shoots up in conditions like pulmonary edema [159], Takotsubo cardiomyopathy [160], myocardial infarction [161], arrhythmias [162] and other thyroid problems [158]. Therefore, detection of epineprhine has significance in a variety of applications ranging from severe allergy reactions, anti-doping regulations to treatments for cardiac attacks. The detetction of such small molecules has been done using various spectroscopic and chromatographic techniques [104, 149, 163-168] which has given impressive results, however these techniques are generally time consuming, complex and require skilled labour. The present approach introduces a highly efficient sensor providing a means for real-time detection in a timely and efficient manner and requires very small volume of the sample to run.

Figure 23A illustrates the aptamer based OECT device fabricated for the detection of epinephrine molecule in the present study. The gate, source, and drain electrodes are labelled as 1, 2, and 3 respectively. The source and drain electrodes are bridged by an organic semiconductor layer PEDOT: PSS, shown by the translucent, dark blue rectangle. The epinephrine specific aptamers are immobilized on to the gate electrode by thiol bonding. A PDMS mold is used to contain the electrolyte solution which ensures direct

flow of current between the aptamer modified part of the gate (labelled as 4) and the PEDOT: PSS layer. The working principle of the current approach is based on the interaction of aptamers with epinephrine which enables the oxidation of the molecule in the vicinity of gate electrode. The oxidation generates $2e^-$ in the solution which produces Faradaic current in the device. The screening of the negative charge of aptamers along with the production of Faradaic current results in an increase in the effective gate voltage and decrease in the overall channel current which is measured as output signal. The present approach leads to a highly sensitive and specific label-free sensor which exhibits time and cost effectiveness, easy readout signals and utilizes off-the-shelf electronics.

3.2 Methods & Materials

3.2.1 Chemical Reagents

Epinephrine binding thiolated 32-mer aptamers were synthesized and provided by BasePairBio Company (Pearland, TX). Chemicals such as epinephrine, 3,4-dihydroxyphenylacetic acid (DOPAC), tyrosine, glycine, dopamine, cysteine, L-ascorbic acid, tryptophan, PEDOT: PSS, and DMSO (dimethylsulfoxide) used during testing were purchased from Sigma-Aldrich (St. Louis, MZ). The TCEP (Tris (2-carboxyethyl) phosphine), Tris hydrochloride, phosphate buffered saline, and magnesium chloride that were utilized to make folding and resuspension buffers were also purchased from Sigma-Aldrich (St. Louis, MZ). LOR, Shipley microposit S1813, MF-CD-26 developer, and PG remover used for photolithography and pattering of the electrodes were purchased from Microchem (Westborough, MA). Gold pellets for deposition of gold electrodes were obtained from Kurt J. Lesker Company (Jefferson Hills, PA). The silicon wafers with

orientation (100) were purchased from Wafer World Inc. (West Palm Beach, FL). For all experiments in the study, DNAse – RNAse free tips, vials and water purchased from Thermofisher (Waltham, MA), were used to avoid nuclease contamination.

3.2.2 Fabrication and measurement of OECT- based sensor

The OECT device used in the present study (**Figure 23A**) was constructed on silicon wafer. First, the wafer was cleaned by rinsing with acetone, isopropanol, and water. The wafer was dried by using nitrogen followed by a 30 second bake at 120°C. To begin the fabrication process, the wafer was coated with a 10 nm thick aluminum oxide layer by using an Atomic layer deposition system. The deposition rate was kept at 0.1 nm per cycle for a total of 100 cycles at 150°C. The aluminum oxide layer ensured electrical insulation of the silicon.

The following photolithography steps were conducted in a clean room:

A. The wafer was coated with LOR by spin coating at 3000 rpm for 50 seconds followed by a 5 min bake at 175°C.

B. After cooling, the wafer was coated with Shipley S1813 by spin coating at 5000 rpm for 50 seconds followed by a 2 min bake at 120°C.

C. The wafer was then exposed to UV at a wavelength of 275 nm for 20 seconds under a mask which was used to pattern the electrode onto the wafer.

D. After another bake for 2 minutes at 120°C, the wafer was developed in MF-CD-26 developer for 1 minute with constant agitation.

E. Finally, the wafer was rinsed with deionized water, blow dried with nitrogen and baked for 30 seconds at 120°C.

F. To deposit gold, an AJA e-beam evaporator was used. First, 3 nm layer of titanium was deposited to enhance the adhesion of the gold to the silicon wafer. Then, 50 nm layer of gold was deposited. After deposition, LOR, Shipley, and unwanted sections of gold were removed by ultrasonicating the wafer in PG remover for 20 minutes.

G. The end result left gold deposited only on the sections patterned by UV exposure, creating the gold electrodes for OECT. The entire channel length and the width of the electrodes were 2.6 cm and 0.5 cm respectively. The diameter of the gate electrode was kept at 0.4 cm.

3.2.3 PEDOT: PSS deposition

The PEDOT: PSS layer was deposited using a similar protocol as gold deposition. After the transistor fabrication process, the transistor was rinsed with acetone, isopropanol, and water, and then properly dried. Shipley microposit S1813 was deposited by spin coating at 5000 rpm for 50 seconds followed by a 2 min bake at 120°C. Again, UV exposure for 20 seconds was used for patterning, but a different mask was used which only patterned the junction between the source and drain electrodes. The wafers were developed in MF-CD-26 developer for 1 minute with constant agitation. The wafer was rinsed with deionized water, blow dried with nitrogen and baked for 30 seconds at 120°C.

The active layer of PEDOT: PSS was deposited using the same photolithography protocol. The solution of PEDOT: PSS was first filtered using a 0.22 µm membrane filter and modified with the addition of 5% by volume DMSO to decrease its solubility in aqueous solutions and increase its conductivity [169]. The filtered solution was spin coated onto the patterned wafer, followed by baking at 120°C for 40 minutes. The result

was a thin, translucent layer of the active material deposited at the junction of the channel. The thickness of the layer as measured using Dektak Profilometer was around ~200 nm. The optimization of PEDOT: PSS deposition for uniform thickness, surface area and shape ensured consistent electrical and physical properties and less variability between different samples.

3.2.4 Aptamer Preparation and Immobilization

The lyophilized epinephrine binding aptamers were dissolved in suspension buffer (TE buffer, 0.1 mM EDTA, 10 mM Tris HCl, pH 7.5) to achieve a concentration of 100 µM. The aptamers were then aliquoted into smaller volumes and stored at -20°C for long term storage. To prepare the aptamers for conjugation, a standard protocol of folding and reducing steps was followed. The aptamers were diluted using the folding buffer (1 mM $MgCl_2$ and 0.01 M PBS, pH 7.5) to acquire the working concentration and incubated for 5 min at 95°C. The aptamers were then allowed to cool at room temperature for 15 min so that they can attain their folded conformation which enables binding to the analyte molecule. Before immobilization the aptamers were reduced using TCEP which cleaves the disulphide bonds and forms sulfhydryl group which is used for attachment to the gold surface. 10 µL of 10 µM reduced aptamers were applied to the gate electrode and allowed to incubate for 2 hours at room temperature. The excess aptamer solution was removed and the gate electrode was washed multiple times with PBS to remove any unbound aptamers from the surface.

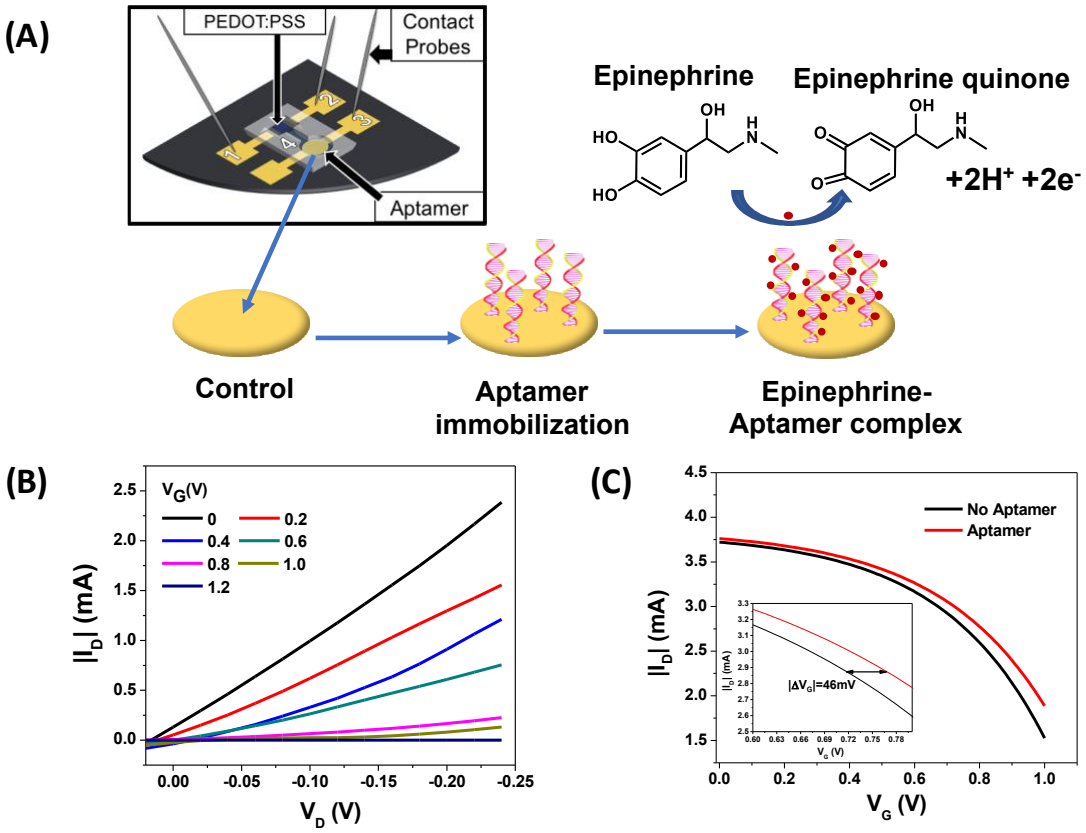

Figure 23: (A) Schematic illustration of the fabricated aptamer based OECT device on a silicon wafer. The source, drain and gate electrodes are labelled as 1, 2 and 3 respectively. Organic semiconducting layer of PEDOT: PSS is used as an active layer to bridge the channel and is represented by blue translucent rectangle. The magnified image of the gate electrode shows the immobilization of aptamers with help of thiol bonding. Further, the formation of epinephrine-aptamer complex upon addition of the epinephrine and the oxidation of epinephrine on the aptamer modified gate electrode has been shown. (B): Output characteristics (I_D vs V_D) of the aptamer based OECT device measured in pure PBS solution in the absence of epinephrine at V_G values of 0, 0.2, 0.4, 0.6, 0.8 and 1.0 V (from top to bottom). (C): Transfer characteristics (I_D vs V_G) of the OECT device measured in PBS solution before and after immobilization of the

aptamers on the gate electrode at V_D = +0.1 V. The immobilization of the aptamers caused a right shift in the V_G curve and the difference is measured out to be 46 mV.

3.2.5 Testing Apparatus

The electrical characteristics of the device were studied by a Keysight B2902A Precision Source and Measurement Unit controlled by EasyEXPERT software. The Keithley source meter was connected to the electrodes to apply and measure both voltage and current through the device simultaneously. During testing, a PDMS gel mold was used to contain the electrolyte solution between the aptamer modified part of the gate electrode and channel (**Figure 23A**, labelled as 4). The mold was shaped to ensure that the solution only contacted the PEDOT: PSS and the aptamer conjugated part of the gate electrode.

3.3 Results

3.3.1 Output characteristics

The output characteristics (Channel current, I_D vs source-drain voltage, V_D) of the present OECT device at varying V_G from 0 to +1.2 V along with a negative bias at V_D is shown in **Figure 23B**. I_D decreases with the increase in the gate voltage, V_G which is a typical response of PEDOT: PSS based OECT device operating in depletion mode (increase gate voltage decreases the channel current) [170], [171]. The positive voltage applied at the gate induces cations from the electrolyte into PEDOT: PSS and compensate for the negative sulphonate anions present on PSS. This results in de-doping of the

semiconducting layer causing a decrease in the hole density which in turn decreases the overall channel current. The de-doping in PEDOT: PSS is reversible in nature and the layer attains its original state when the gate voltage goes to zero [172].

3.3.2 Aptamer functionalization

The functionalization of gate electrode with aptamers was confirmed by measuring the absorbance intensity of the applied aptamer solution before and after incubation. A significant decrease in absorbance intensity at 260 nm (A_{260}) was observed and quantitative analysis was done by plotting the calibration curve. The packing density for the attached aptamers was calculated to be 2.2×10^{12} aptamers per cm^2. (**Figure 24 (A, B)**). The higher packing density of the aptamers hinders the binding of aptamer-analyte due to the close packing of the strands whereas the lower packing density results in low performance because of the less binding sites available. The packing density of 2.2×10^{12} lies near the optimum packing density (1.6×10^{12}) as reported in the previous studies [173, 174].

The effect of addition of aptamers over Au gate electrode was also examined through output characteristics. **Figure 23C** shows the I_D versus V_G characteristics at a V_D of +0.1 V. The measurement was done in same electrolyte solution (pure PBS) before and after functionalization with epinephrine aptamers. A significant increase in channel current was observed after functionalization of gate electrodes. As reported previously, the performance of an OECT depends extensively on the surface potential and electrolyte/gate interface capacitance of the gate electrode [171, 175, 176]. Therefore,

the immobilization of the aptamers over the gate electrode increased the overall negative charge density due to the presence of phosphate backbone which resulted in a decrease in the effective gate voltage and thus increase the overall channel current [138, 177, 178].

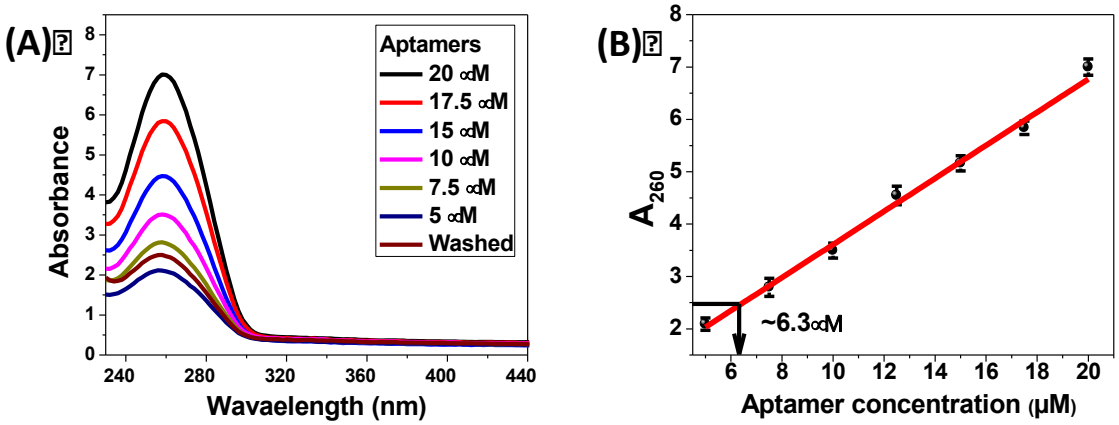

Figure 24: (A) UV-spectra of aptamers at different concentration in PBS solution. (B) The absorbance at 260 nm (A_{260}) as a function of concentration of aptamers. Washed aptamers showed an absorbance of 2.4 which corresponds to 6.3 μM concentration.

3.3.3 Transfer characteristics

The transfer characteristics (I_D vs V_G) were studied at V_D= +0.1V by using PBS as the electrolyte. The aptamers conjugated gate electrode of the device was incubated with epinephrine solution (90 pM, 900 pM, 9 nM, 90 nM, 900 nM, 9 μM, 90 μM, 900 μM) for 10 min and then washed off to remove unbound epinephrine. **Figure 25A** shows the channel

current (I_D) vs. gate voltage (V_G) transfer curve at various concentrations of epinephrine. It was found that as the concentration of epinephrine increased from 90 pM to 900 µM, the transfer curve showed a distinct trend towards lower gate voltage. The change in gate voltage (ΔV_G) as a function of concentration of epinephrine (log[Epi]) was plotted with the help of transfer characteristics (I_D vs V_G) shown in **Figure 25B**. The device shows a constant increase in $|\Delta V_G|$ with increase in the concentration of epinephrine and a linear behavior can be seen from 90 pM to 900 nM. The ΔV_G becomes constant due to saturation of aptamer binding sites at higher concentration of epinephrine (>900 nM). The detection limit of the system was found to be 90 pM which showed a change of 53 mV upon addition of epinephrine.

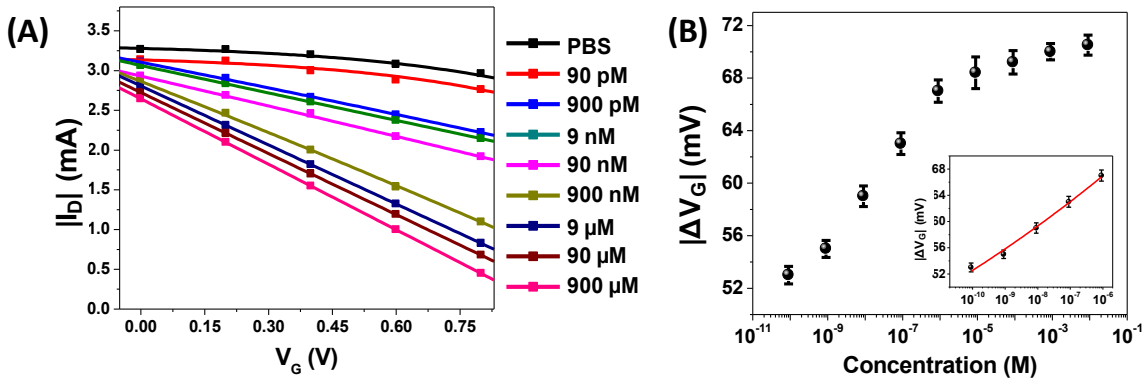

Figure 25:(A) Transfer characteristics (I_D vs V_G) of the aptamer based OECT device in the presence of different concentration of epinephrine at V_D=+0.1V in PBS solution. A constant left shift in the V_G with increasing amount of the epinephrine can be seen. (B) The change in V_G of the OECT induced by interaction of epinephrine with the aptamers as derived by the transfer characteristics. The inset shows the fitting of the linear range (90 pM to 900 nM) having an R^2 value of 0.98.

3.3.4 I_D -time characteristics

In order to monitor the real-time response of the aptamer modified OECT device, channel current, I_D vs time curve was plotted at V_D= +0.1V and V_G= +0.7V as fixed parameters. The dependence of the source-drain current on the consecutive additions of epinephrine at various concentrations (90 pM-90 µM) is shown in **Figure 26A**. It can be seen that the addition of epinephrine at consecutive time intervals caused constant drops in the current which was seen almost immediately after the addition. It was also observed that along with the drop in current, there was slight increase in the channel current before the next addition. The binding of epinephrine to the aptamer is a dynamic process. The process includes constant association and dissociation of the molecules which takes a few seconds to equilibrate so that the system can attain lowest energy state. Therefore, instead of a straight curve, slight elevations were observed at lower concentrations (90 pM, 900 pM, 9 nM and 900 nM). At higher concentrations, sharp drop in the channel current was observed after the addition. The change in channel current ($|\Delta I_D|$) gives a linear dependence on logarithmic function of concentration of epinephrine as shown in **Figure 26B**.

3.3.5 Selectivity Assay Results

To test the selectivity of the aptamer based OECT sensor, an I_D vs t test was conducted to observe the device response to biomolecules other than epinephrine. The interfering species selected were DOPAC, tryptophan, tyrosine, glycine, cysteine, dopamine, and ascorbic acid. These species were chosen either due to their structural similarity to epinephrine, or their similar biological functions. **Figure 26C** demonstrates device

response in terms of change in I_D with subsequent addition of interfering species at a time interval of 5 min. The sensor displayed a sharp decrease in I_D after the addition of epinephrine whereas for other reagents, very slight/no change in the current was seen.

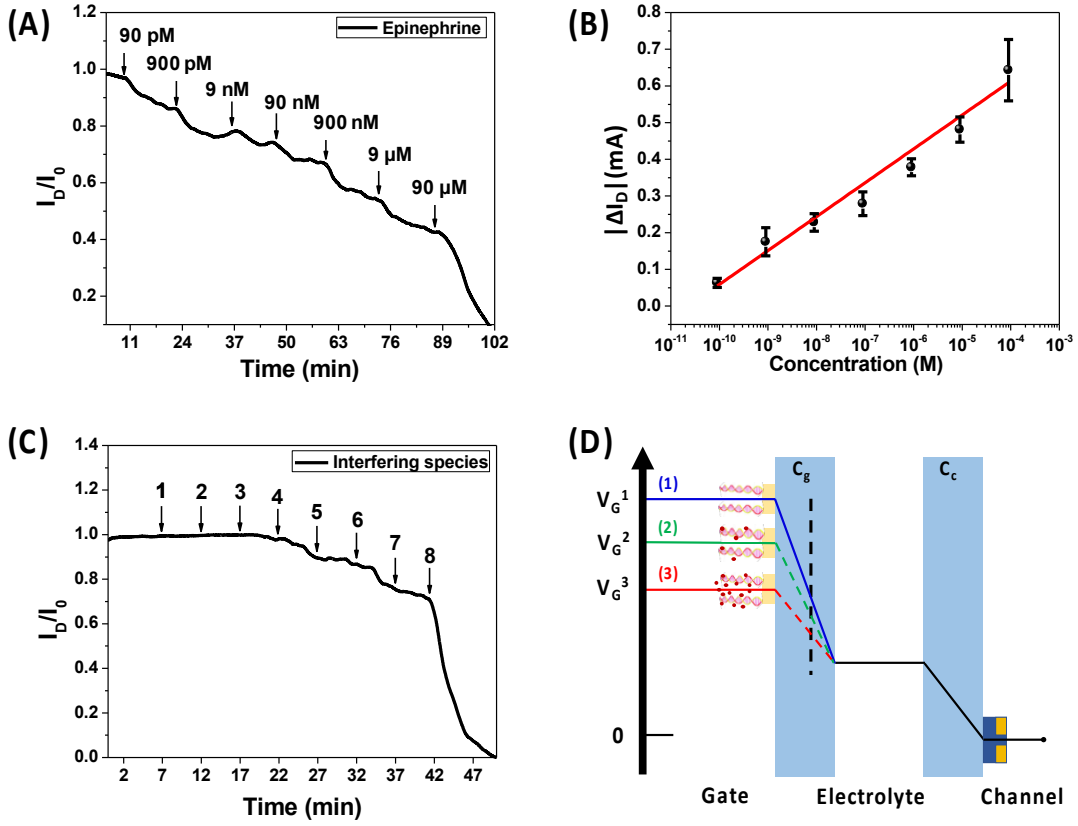

Figure 26: (A) The normalized time-current (I_D/I_0 versus t) characteristics of the present OECT device at V_D= +0.1 V and V_G= +0.7 V as fixed parameters. Addition of epinephrine was done at subsequent intervals of 13 minutes at a concentration of 90 pM, 900 pM, 9 nM, 90 nM, 900 nM, 9 µM, 90 µM - left to right. The increase in epinephrine resulted in constant drops in the channel current. (B) The change in channel current (mA) is plotted as a function of epinephrine concentration (90 pM-90 µM). A linear response was observed in the presence of epinephrine concentration with R^2 value of 0.96. Error bars represent the standard deviation from the mean value. The

large error bar at 90 μM is due to the saturation of aptamer binding sites. (C) The normalized current response as a function of time (I_D vs t) in the presence of interfering species (10 μM). The addition was done at an interval of 5 min in the order of DOPAC (1), tryptophan (2), tyrosine (3), dopamine (4), glycine (5), cysteine (6), ascorbic acid (7) and epinephrine (8). A sudden drop in the current was seen after the addition of epinephrine (1 μM). (D) A schematic illustration of the change in V_G before and after addition of epinephrine. To maintain the same effective voltage in the device, the V_G decreases to offset the Faradaic current produced due to the oxidation of epinephrine. V_G^1 represents the device with only immobilized aptamers and V_G^2, V_G^3 represents the new gate voltage with increasing concentration of epinephrine respectively. $V_G^1 > V_G^2 > V_G^3$.

The concentration of epinephrine used was 1 μM whereas 10 μM for the interfering species.The addition of cysteine and dopamine caused slight decrease in the current as can be observed at 22 min and 32 min. Interference from dopamine can be due to high structural similarity between epinephrine and dopamine. The thiol group present in the cysteine molecule could have interfered in the output signal as thiol is known to have a high affinity for the gold surface. Overall, the presence of aptamers suppressed the nonspecific binding of the interfering species at the gate electrode.

3.4 Discussions

The working of an OECT device depends largely on the change in conductance of the active layer due to the electrochemical doping/de-doping of the cations from the

electrolyte controlled by variation in the effective gate voltage (ΔV_G^{eff}) of the device. The ΔV_G^{eff} depends on the potential difference between the gate-aptamer/electrolyte and PEDOT: PSS/electrolyte. In the present study, the ΔV_G^{eff} is dependent only on the change in the potential at gate-aptamer/electrolyte interface since epinephrine-aptamers complex are formed on the gate electrode. The channel current of an OCET device at a certain V_G and V_D is given by the following equation.

$$I_D = \frac{Wq\mu tp_0}{LV_P}\left(V_P - V_G^{eff} + \frac{V_D}{2}\right)V_D, (when\ |V_D| \ll \left|V_P - V_G^{eff}\right|) \quad (1)$$

$$V_P = \frac{qtp_0}{C_i}$$

$$V_G^{eff} = V_G + V_{offset} \quad (2)$$

where W and L represents the width and length of the channel, t is the thickness of the organic semiconductor layer (PEDOT: PSS), q is the electronic charge (1.6 x 10^{19}), μ is the hole mobility, C_i is the effective gate capacitance and p_0 is the initial hole density of the channel before applying V_G. V_P is the pinch-off voltage and V_D is the source-drain voltage. The ΔV_G^{eff} represents the effective gate voltage in the device and V_{Offset} is the change in potential due to potential difference between the gate/electrolyte and PEDOT: PSS/electrolyte interface.

After the binding of epinephrine to the aptamers and application of positive voltage at the gate electrode, the electro-oxidation of epinephrine occurs. The oxidation causes release of 2*e*- in the solution which produces Faradaic current at the gate/electrolyte interface.

$$\text{Epinephrine} \rightarrow \text{Epinephrine quinone} + 2H^+ + 2e^-$$

As a result, there is a decrease in the potential drop which increases the effective gate voltage of the device. This change in effective gate voltage further decreases the overall channel current as given in Equation 1. The change in effective gate voltage due to the electro-oxidation of epinephrine is given by:

$$V_{offset} = \frac{2.3(1+\gamma)kT}{ne}\log[Epi] + constant \quad (3)$$

where γ is defined as the ratio between the capacitances of the channel (C_C) and the gate (C_G) with respect to the electrolyte, $\gamma = C_C/C_G$; n (=2) is the number of electrons released during the oxidation, k and T represent the Boltzmann constant and room temperature and log[Epi] is the logarithmic function of concentration of epinephrine. As shown in **Figure 25B**, the slope of the fitted curve was found out to be 80 mV/decade in the linear region and thus the value of γ was 1.24. The left shift in the I_D vs V_G curve with increase in the concentration of epinephrine, [Epi] is occurring due to the change in V_{Offset} value which is directly proportional to the concentration of epinephrine as given in Equation 3. At higher concentrations of epinephrine, the V_{Offset} becomes constant as the aptamer binding sites becomes saturated with epinephrine. The unbound epinephrine molecules were washed off before measuring the transfer characteristics. Therefore, the present sensor follows linear dependence on epinephrine concentration in the 90 pm-900 nM concentration regime.

Figure 26D represents the working of the present OECT device. As discussed previously, the immobilization of the aptamers introduces negative charge on the gate electrode which decreases the surface potential. To maintain the same effective voltage in the device, the V_G increases and a shift in the transfer curve to the right side is observed

(**Figure 23C**). However, upon the addition of epinephrine, the negative charge is balanced by the positively charged epinephrine (pK_a 8.02), the overall effective gate voltage increases. To balance this extra potential change, the V_G decreases and curve shifts to left side (**Figure 25A**). The change in V_G showed a linear dependence on the concentration of the epinephrine molecule in the range of 90 pM to 900 nM after which it starts saturating. The synergistic effect of the binding event of aptamers along with the oxidation of the epinephrine molecule enhances the ΔV_G^{eff} as a function of concentration of epinephrine which amplifies the change in current and therefore the sensitivity of the present OECT device.

The addition of epinephrine on the bare gate electrode (no aptamers) was also studied with the help of real time I_D response curve as shown in **Figure 27**. The plot shows no change in the current upon addition of epinephrine at 100 pM, 1 nM, 10 nM until 100 nM when a huge drop in current was observed. The decrease in the current is due to increased concentration of epinephrine in the electrolyte solution which facilitated the oxidation of epinephrine. The binding of epinephrine to the aptamers not only changes the surface potential of the gate electrode but also ensures the accumulation of epinephrine molecules in the vicinity of the gate electrode. The increased concentration of epinephrine around gate expedites the oxidation of the molecule and hence, maximizes the sensitivity of the sensor. Therefore, the presence of aptamers contributes to the high specificity of the sensor and also increases the detection limit by an order of atleast 10^3 magnitude.

So far it has been established that the detection limit of the current approach is 90 pM. The physiological level of epinephrine for a healthy individual is in the range of 120-

200 pM which increases in conditions like hyperthyroidism (359 ± 150 pM) and hypothyroidism (373 ± 150 pM) [158]. The increase in epinephrine level is also prominent in Takotsubo cardiomyopathy and Killip Class III myocardial infarction which averages the level to 6.9 nM and 2.1 nM after 1 or 2 days respectively [132]. Quantitative analysis of epinephrine can be done using the present approach in the range of 90 pM to 900 nM which can be used for the early detection of pathological conditions as described above. **Table 2** summarizes the different approaches used for the detection of epinephrine and their respective detection limits as listed in the literature. 2015 Mak *et al.* study reported a comparable detection limit of 100 pM [165] . The study is based on the electrical oxidation of epinephrine molecule using Pt based gate electrode modified with nafion and single walled carbon nanotube. The interference from ascorbic acid was seen at 100 nM whereas the present sensor showed no response to ascorbic acid even at a concentration of 10 µM. Selectivity is essential for real-world sensors to avoid the need for costly and time-consuming purification steps. Therefore, the aptamer-based OECT sensor presented in this work exhibits great potential in the real-world applications which gives fast and easy-to-read signals.

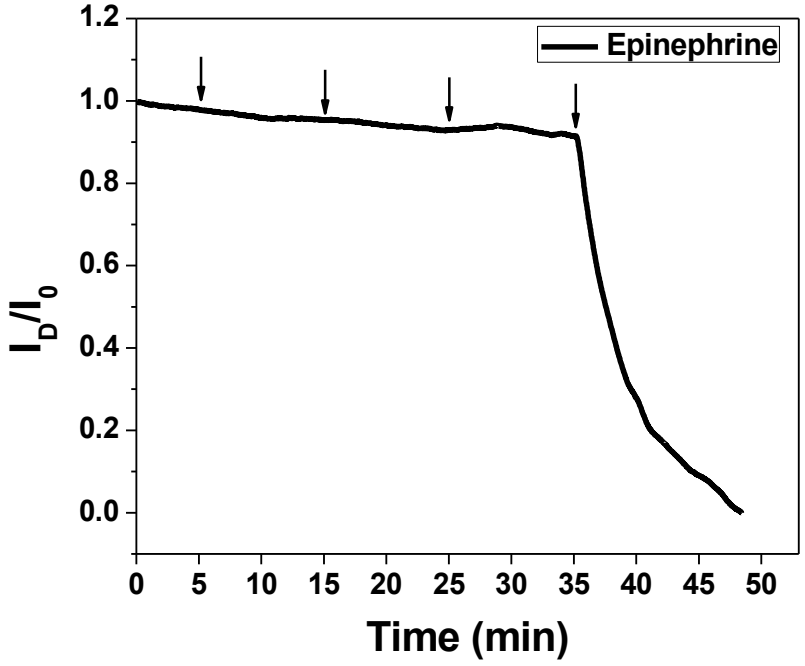

Figure 27: The normalized time-current (I_D/I_0 versus t) characteristics of the present OECT device in the presence of different concentration of epinephrine on bare Au gate electrode. The addition was done at an interval of 10 min in the order of 100 pM, 1 nM, 10 nM and 100 nM in the presence of PBS as electrolyte. The plot shows no change in the current upon addition of epinephrine at 100 pM, 1 nM, 10 nM until 100 nM when a huge drop in current was observed.

Table 2: Comparison of different techniques used for the detection of epinephrine and their respective detection limits.

Method	Detection limit	References
Colorimetric	900 pM	[149]
Capillary Electrophoresis	100 nM	[163]
Ion chromatography	5.9 nM	[167]
HPLC-MS	56 nM	[104]
Differential Pulse Voltammetry	90 nM	[168]
Chemiluminescence	1.1 µM	[164]
Differential Pulse Voltammetry	30 nM	[166]
OECT	100 pM	[165]
OECT	90 pM	Present method

3.5 Summary

A. A PEDOT: PSS based OECT sensor functionalized with aptamers was fabricated to detect the presence of epinephrine molecule. The high binding affinity of the aptamers towards epinephrine and the electro-oxidation of the molecule in the vicinity of gate electrode allow the present aptasensor with 90 pM limit of detection. The addition of epinephrine on the gate electrode resulted in a significant decrease in the channel current which was observed in both I_D vs V_G and I_D vs time characteristics. In addition, experiments were conducted against common interfering agents to determine the selectivity of the OECT sensor. The device showed an instant drop in current upon addition of epinephrine as opposed to the other interfering molecules, indicating highly selective nature of the sensor. The inclusion of aptamers resulted in an increase of sensitivity by 10^3 magnitude and high specificity towards epinephrine molecule. The present approach provides an easy, simple, rapid method for detecting epinephrine, however more work needs to be done in order to test the repeatability and reusability of the sensor. The future work will be aimed at extending the current approach to develop flexible sensor capable of detecting various biomolecules by utilizing different aptamers on a single platform. The present work lays the ground for developing a wide range of personalized point-of-care testing tools for therapeutic applications.

CHAPTER 4: MULTIPLEX VIRAL DETECTION SYSTEM BASED ON APTAMERS INTEGRATED MICROFLUIDIC CHANNEL

4.1 Introduction

Zika virus (ZIKV) is a mosquito-borne virus which is vectored by Aedes family (*aegypti* and *albopictus*) and is known to pose a serious threat to the population worldwide. Nearly 440k-1300k cases associated with microcephaly and central nervous system abnormalities were reported during Zika outbreak in Brazil in 2015[179, 180]. Besides Brazil, cases associated with Zika infection have also been reported in 66 other countries till date [181]. The world health organization declared a Public Health Emergency of International Concern (PHEIC) in 2016 due to the increase in microcephaly cases and neurological disorders that were generated by the Zika virus.[182] More than 5k cases since 2016 have been confirmed in United States alone as confirmed by Pan American Health Organization[179]. The transmission of Zika occurs through infected mosquito bite, in utero mother to fetus and sexual contact. Zika infection is usually asymptomatic, however sometimes non-specific symptoms such as rash, fever, headache, vomiting and joint pains of varying degrees can be observed [183, 184]. These symptoms overlap significantly with other flaviviruses infection such as Chikungunya (CHIKV). Due to a shared vector as well as non-specific symptoms, adequate diagnosis of Zika at an early stage poses a serious challenge specially in resource constrained communities where both the viral infection are endemic.

The current diagnostic tools for the detection of Zika virus depend mostly on RT-PCR (reverse transcription polymerase chain reaction)[183], RT-LAMP (reverse-

transcription loop-mediated isothermal amplification)[185-189] and RT-RPA (reverse transcription recombinase polymerase amplification)[190] coupled with external power source and a display unit such as smart phone for an easy readout signal.[191-197] These techniques often require expensive instrumentation, skilled labor and sometimes faces major disadvantage of false negative/positive results arising from new strains or contamination.[198] Other methods for Zika diagnosis such as IgM-capture ELISA and plaque reduction neutralization test (PRNT) face a major challenge of cross-reactivity with other flaviviruses[198] leading to ambiguous results. Therefore, there is a dire need for the development of novel, compact and passive point-of-care (POC) testing tools which can provide multiplexed diagnosis in a rapid and cost-effective manner.

To this end, we have fabricated a flexible, portable, easy-to-use aptamer based microfluidic sensor for the multiplex detection of recombinant Zika and CHIKV envelope proteins. Aptamers are short single-stranded oligonucleotides that are designed using *in vitro* SELEX (Systematic Evolution of Ligands by Exponential enrichment) process to bind to a specific target with high specificity and affinity. Aptamers offers several advantages over antibodies such as stability in harsh environment, ease of synthesis and functionalization, high batch to batch consistency and wide variety of targets.[199-202] The use of microfluidic platform allows for the manipulation of fluids at the micron-scale and are used to implement operations that require large, expensive equipment onto a micro-sized device.[203, 204] The compatibility of polydimethylsiloxane (PDMS) with microfluidic fabrication offers flexibility and optical transparency which enhances the colorimetric signal obtained in the presence of analytes produced during the test.

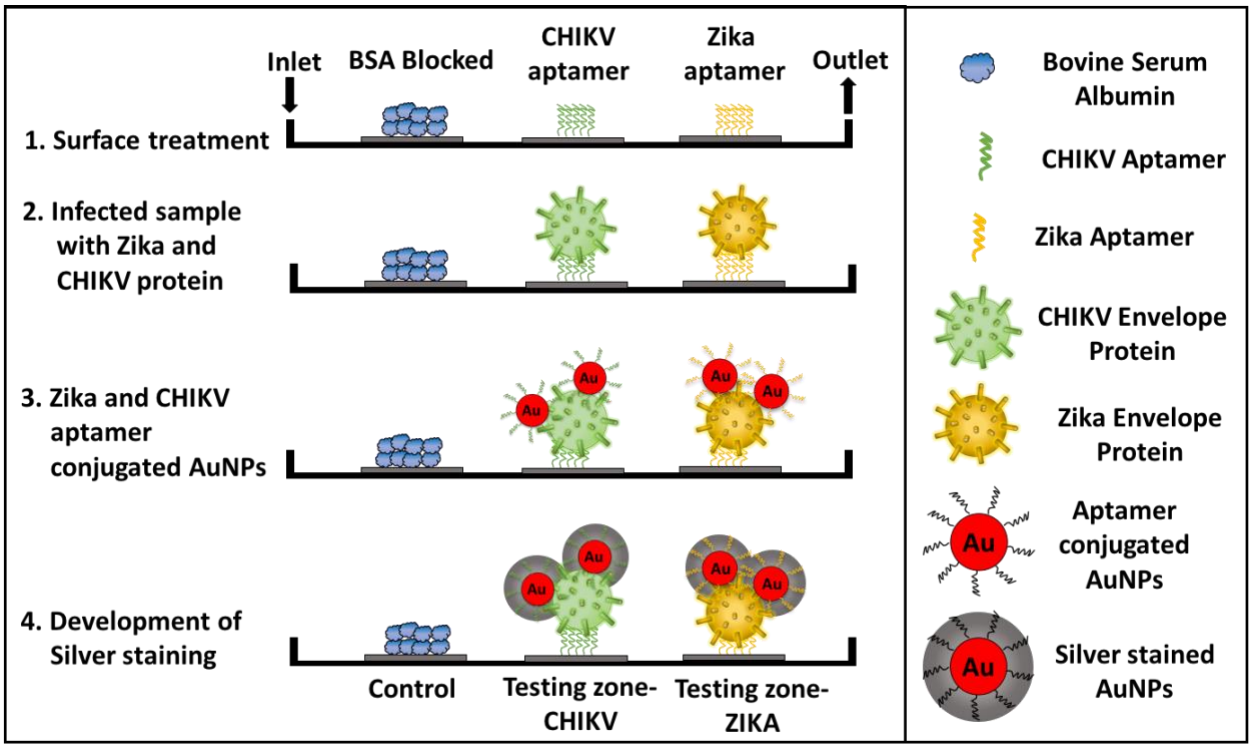

Figure 28: Schematic representation of the current approach based on sandwich assay for the detection of multiple viral proteins on a single platform. The surface is first conjugated with a linker molecule, PMPI which attaches to thiolated end of the aptamers (1). Control site is blocked with BSA molecule. The infected sample containing viral protein is introduced in the channel where the specific aptamers bind to their specific proteins (2). AuNPs conjugated with aptamers is then allowed to bind to a different epitope on the protein forming a sandwich morphology (3). If no protein is present, all the AuNPs will be washed off. In the end, silver reagents are introduced in the channel which deposits over the surface of AuNPs giving a colorimetric signal to the presence of viral protein (4).

The current sensor depends on the engineered sandwich assay with Aptamer1-Antigen-Aptamer2 for the detection of ZIKA and CHIKV antigens (**Figure 28**). The Aptamer1 is immobilized on the microfluidic channel which captures the incoming protein present in the infected samples. The Aptamer2 conjugated with gold nanoparticles (AuNPs) is used to report the presence of antigen by generating an output signal in the form of color change. Development of silver around the AuNPs results in dark gray color depending on the concentration of protein which amplifies the color change in the channel. The major advantage of using antigen-capture sandwich assay is high sensitivity and colorimetric detection capabilities with crude sample preparation.[205] The approach is similar to the ELISA technique but avoids the use of expensive plates and plate readers, and is very easy to handle. Also, the replacement of antibodies with the aptamers makes this technique more robust while maintaining the accuracy and reliability of the approach.

4.2 Materials and Methods

4.2.1 Chemical reagents

Recombinant Zika envelope protein (ZKV-005) and Chikungunya type E1 (CHI-001) were obtained from Prospecbio (Israel). The protein samples were provided to BasePair Biotechnologies (Pearland, TX) for a custom-made set of aptamers. The aptamers showing highest binding affinity were used for experimentation. Aptamer folding buffer, reducing buffer and resuspension buffer were also provided by Basepair Biotechnologies to prepare the aptamers for immobilization. Other chemicals such as Gold(III) chloride trihydrate, trisodium citrate, phosphine buffered saline tablets, sodium hydroxide,

hexamethyldisilazane (HMDS), acetonitrile and magnesium chloride ($MgCl_2$) were purchased from Sigma-Aldrich (St. Louis, MZ). PMPI (p-maleimidophenyl isocyanate) used for the functionalization of PDMS was obtained from Thermofisher (Waltham, MA). Dow Corning Sylgard 184 Silicone Encapsulant Clear Kit for the fabrication of microfluidic channels was purchased from Ellsworth (Germantown, WI). SU8 and SU8 developer used during photolithography was purchased from MicroChem (Westborough, MA). The masks were printed by CAD/Art Servies (Bandon, OR). The silver enhancement kit was purchased from Cytodiagnostics (Burlington, ON). Silicon wafers were obtained from Waferworld Inc. (West Palm Beach, FL). The entire study was done using DNAse-RNAse free water, vials and pipette tips obtained from Thermofisher.

4.2.2 Fabrication of microfluidic channel

Fabrication of Master mold: PDMS based microfluidic channels were fabricated using a soft lithography technique. [206] The silicon wafers were cleaned thoroughly by rinsing with acetone, isopropanol and water, followed by nitrogen blow. These were kept at 80^{o}C for 15 min to evaporate any residual water. After cleaning, the wafers were pretreated with HMDS overnight to improve the adhesion between the photoresist layer and wafer surface. The HMDS treated wafers were deposited with SU8 photoresist for the development of master mold. The wafer was centered on rotating stage of the spin coater and a dollop of SU8-2050 was poured in the center. SU-8 was spincoated over the wafer at 2500 rpm for 50 sec which gave an average thickness of 70 μm of the layer. After spinning, the wafer was soft baked at 65^{o}C for 3 min followed by 95^{o}C for 8 min. The wafer was allowed to cool at room temperature for atleast 5 min. The next step in the

lithography is to transfer the pattern of the mask onto the SU8 deposited Si wafer. The mask was placed over the Si wafer in the mask aligner and exposed to UV (275 nm) for 50 sec. After UV exposure, the silicon wafers were baked for 1 min at 65^{o}C followed by a 6 min bake at 95^{o}C. Upon cooling, the wafers were developed in copious amount of SU-8 developer for 5 min, followed by rinsing with Isopropanol. If white streaks were seen, the wafers were again kept in fresh developer solution for few seconds and then rinsed with IPA. The developed wafers were dried using nitrogen blow and baked at 95^{o}C for 3 min. The fabricated master molds were silanized using tricholorsilane for 2 hours under vacuum to make the peeling step easier.

Development of Microfluidic channels: The PDMS mixture was formed by adding the base and cross-linker (provided in the Dow Corning kit) in 10:1 weight ratio in a disposable plastic weigh boat. The mixture was thoroughly mixed with a plastic-stir rod until it became cloudy and suspended with air bubbles. The air bubbles were removed by placing the boat under vacuum in a desiccator and venting it periodically. Once all the air bubbles were removed, the PDMS mixture was poured slowly on to the master mold in a petri dish. The petri dish was then placed in a pre-heated oven at 65^{o}C for 1 hour to cure. After curing, the PDMS hardened over the mold and took the features of the mold as shown in **Figure 29A**. It was then peeled off carefully and individual channels were cut using a sharp blade.

Surface treatment of Microfluidic channels: The microfluidic channels were treated with 1 mM NaOH solution at room temperature for 16 hours under gentle shaking. The

samples were then washed thoroughly with DNase-RNase free water, followed by drying with nitrogen blow. After this, PMPI dissolved in acetonitrile (10 mg/ml) was applied onto the testing regions and kept for 3 hours at room temperature. The surface treatment of PDMS with PMPI offers a free maleimide group which shows high affinity towards thiol bond present at the end of aptamers. The samples were washed with acetonitrile and working buffer (1 mM $MgCl_2$, 1X PBS, pH 7.5) thrice before conjugating with aptamers.

4.2.3 Preparation of aptamers and immobilization

The obtained thiolated aptamers (both CHIKV and Zika) were dissolved in resuspension buffer to obtain a 100 μM stock concentration. The aptamers were diluted to 50 μM using folding buffer and heated at 95°C for 5 min. Then, these were cooled to room temperature for 15 min. This allows the aptamers to fold properly and attain their native conformation required for binding to the target molecule. After 15 min, the aptamer solution was mixed with the reducing buffer (TCEP) in 1:1 ratio (v/v) to obtain a final concentration of 25 μM and kept at room temperature for another 20 min. The TCEP is used to cleave the disulphide bonds (-S-S-) which allows for free –SH group. The -SH group plays a major role in binding of the aptamers to the Gold Nanoparticles as well as PDMS surface.

Immobilization on AuNPs: 13 nm citrate capped AuNPs prepared using standard Turkevich method were used in the present study. The aptamers were immobilized on AuNPs surface by incubating 1 ml of AuNPs (0.2 mg/ml) with 20 μM (10 μl) of reduced aptamers at room temperature with gentle stirring overnight. The AuNPs solution was then centrifuged down (11000 rcf, 11 min) to remove unbound aptamers and

resuspended in working buffer. The conjugation of aptamers was confirmed by performing gel electrophoresis on the bare as well as aptamer conjugated AuNPs.

Immobilization on PDMS: The prepared aptamers were added directly to the functionalized testing zone on the microfluidic channel and allowed to sit for 3 hours with gentle stirring. The final concentration of the aptamers used for each testing zone was 25 μM, 20 μl. After 3 hours of incubation, the channels were washed gently with working buffer to remove unbound aptamers. To avoid non-specific binding of the protein, the channels were then passivated using 1% BSA for 1 hour.

4.3 Results and Discussion

4.3.1 Development of microfluidic channel

The fabricated microfluidic channels were integrated with micro-sized pillars to increase the surface area in the testing region. The enhanced surface area ensured more number of aptamers in the testing zone which increased the binding sites for the protein molecules, thus enhancing the sensitivity of the approach. The SEM analysis shown in **Figure 29B** confirms the presence of pillars in the magnified view of the testing zone. The analysis of the vertical and lateral view (inset) indicates that the pillars have an average diameter and height of 50 μm and 45 μm respectively.

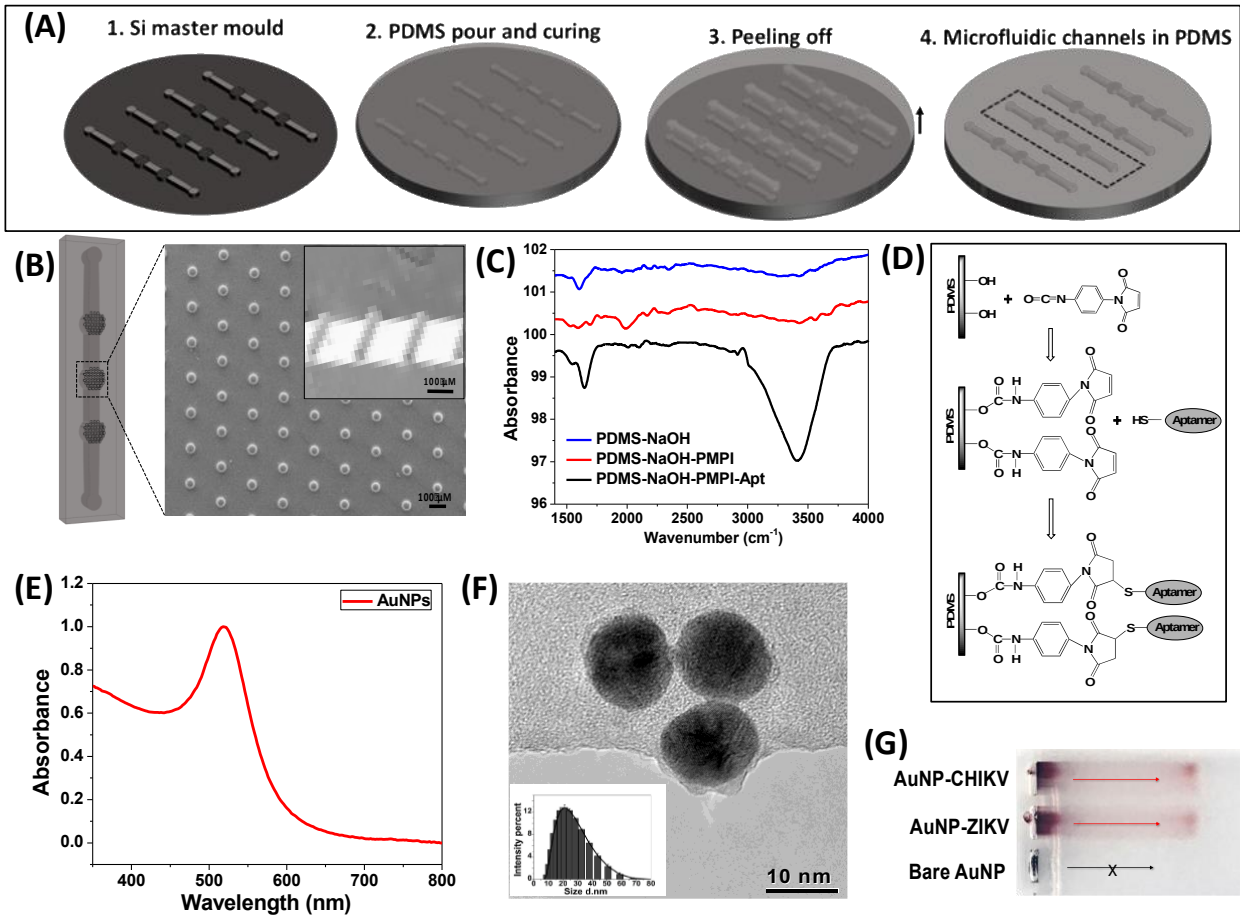

Figure 29: (A) Fabrication process of microfluidic channels using a Si master mould. PDMS is poured carefully and cured at 65°C for 1 hour. Next step shows peeling off the layer from the mould and channels being formed in the PDMS layer. (B) Image of a single microfluidic channel. SEM image representing magnified view of the testing zone showing the presence of pillars with an average diameter of 50 µm. (C) FTIR spectroscopy of the microfluidic channel at different steps of functionalization: NaOH, PMPI and aptamers treatment. Peaks at 1698 cm^{-1} and 1531 cm^{-1} represents amide I and amide II bands in PMPI which shows the presence of urethane linkage. (D) Schematic representation of the functionalization of the channel using PMPI as the linker molecule to immobilize aptamers. (E, F) UV-visible spectroscopy and TEM

analysis of the Turkevich method based Gold nanoparticles. Inset shows narrow size distribution of the particles in the range of 15-20 nm as measured by DLS. (G) Gel Electrophoresis of the bare and aptamer conjugated AuNPs. Migration is observed in the aptamer conjugated samples due to the negative charge on the particle surface.

4.3.2 Functionalization of Microfluidic channel

The microfluidic channels were first treated with aqueous solution of NaOH to make the surface hydrophilic in nature. The treatment with NaOH introduces hydroxyl group (-OH) at the surface which not only improves the flow but also facilitates functionalization of the surface with other chemicals.[207-209] The major advantage of using NaOH over traditional ozone treatment is the enhanced stability of the samples irrespective of the storage condition. In the second step, the -OH groups were allowed to react with PMPI which is used as a linker molecule between aptamers and PDMS surface. The isocyanate end (-N=C=O) of PMPI interacts with -OH and forms urethane linkage. This renders the maleimide end available for coupling with the thiol group present at the end of aptamers.[210-212] The schematic of the reaction is shown in **Figure 29D.** The FTIR spectra (**Figure 29C)** exhibit different characteristic peaks obtained during the surface treatment of PDMS with NaOH, PMPI and aptamers. The FTIR spectrum of PDMS-NaOH-PMPI showed peaks at 1698 cm^{-1} and 1531cm^{-1} which corresponds to Amide I and Amide II bands (C=O stretching and –N-H bending) respectively.[211, 213, 214] A distinct peak at 1585 cm^{-1} is also observed which points to the presence of C=C in the maleimide group. After the immobilization of the aptamers, a significant peak at ~3410 cm^{-1} is

observed which is due to large number of hydroxyl groups present at the end of aptamers. A peak at 1648 cm^{-1} is also seen which indicates the presence of the purine and pyrimidine rings in the aptamers.[215] The FTIR data confirmed the immobilization of the aptamers over PDMS using PMPI as the linker molecule.

4.3.3 Gold nanoparticles synthesis and functionalization

The Gold nanoparticles were synthesized using a standard Turkevich method in which gold chloride precursor salt is reduced using trisodium citrate at high temperature. The characterization of the synthesized AuNPs is shown in **Figure 29E** and **29F**. The TEM results indicate that the particles are uniformly distributed and spherical in nature with an average diameter of 13 nm. The UV visible spectrum (**Figure 29E**) shows a distinctive absorbance peak at 520 nm which represents the surface plasmon band of AuNPs. The particles were conjugated with Zika and CHIKV aptamers using a standard protocol at a concentration of 200 nM. The successful conjugation of the aptamers over the AuNPs was confirmed by running the particles through 0.5% agarose gel under the influence of voltage (**Figure 29G**). It was observed that the aptamer conjugated AuNPs migrated through the gel (red arrow) whereas the bare AuNPs remained in the well (black arrow). The migration of conjugated particles is due to the overall negative particle charge imparted by the conjugated aptamers, which enables these Apt-AuNPs to be driven through the gel in response to the applied voltage.

4.3.4 Testing of Microfluidic channel

The present approach was first tested on a PDMS substrate to examine the sensitivity and selectivity of aptamers for the target arboviral envelope proteins. A distinct color development was observed from 500 pM of CHIKV envelope protein, which intensified with increasing protein concentrations (**Figure 30**). The approach was then extended to the microfluidic channels with a controlled flow rate (80µL/min). The aptamer-conjugated microfluidic channels were tested against different concentration (10 fM-1 nM) of both CHIKV and ZIKV envelope proteins. **Figure 31A** shows distinct development of silver in the testing zones represented by circles. The '+' and '-' sign indicates the presence or absence of the specific arboviral envelope protein in the testing solution. For 0 nM, the PBS was spiked with BSA which was used as the negative control to test non-specific interactions of AuNPs in the channel. No color development was observed in the negative control regions in any of the channels, which indicates high specificity of the Apt-AuNPs. Also, for the last two channels, only one viral envelope protein (either ZIKV or CHIKV) was injected as per (+) or (-) symbol. It can be seen that ZIKV envelope protein at a very high concentration of 10 nM did not interfere with the CHIKV aptamers and vice versa. This clearly suggests that the current approach is not only highly sensitive with a detection limit of 1 pM but also exhibits high level of selectivity among different arboviruses such as ZIKV and CHIKV.

The color change in the channels was also measured using an image processing software to calculate the CMYK (cyan, magenta, yellow and key) values. The key value represents the black color that was used as the measure of silver development in the microfluidic channels. The more numbers of AuNPs results in increased silver deposition

in the testing zone, leading to an intense color change. **Figure 31B** shows the key value with respect to concentration of protein. It can be seen that with increasing protein concentration, K value increases. The measure of K value can be used for a quantitative estimation of the arboviral envelope protein concentration present in the sample.

The microfluidic device was also tested against sterile, mechanically-defibrinated calf blood and complete sheep se-rum spiked with the given ZIKV and CHIKV recombinant envelope proteins as surrogates for infected human blood/blood products. The results are represented as black key color (K) as a function of protein concentration (**Figure 32**). The testing showed a response to as low as 1 pM of the recombinant protein in PBS and 10 pM when tested against spiked 10% calf blood (diluted with working buffer) or sheep serum. In the case of undiluted (i.e., 100%) calf blood, a slight increase in K value was observed in the presence of 100 pM (~5 ng/ml) of the protein. Diluting the blood with the binding buffer therefore increased the sensitivity of the system by ~10 fold. A comparative analysis of different detection techniques is shown in Table S1. The present sensor gives a minimum detection limit of 1 pM (50 pg/ml) for the ZIKV envelope protein and the CHIKV envelope protein E1 in PBS which is the lowest obtained so far. The similar detection limit (in buffer) was also obtained by Zeng et. al. using an antibody-aptamer mediated sandwich assay on a 96-well ELISA plate[216]. The current approach abrogates the use of expensive plates or sophisticated plate reader making the device more adoptable in re-source constrained areas.

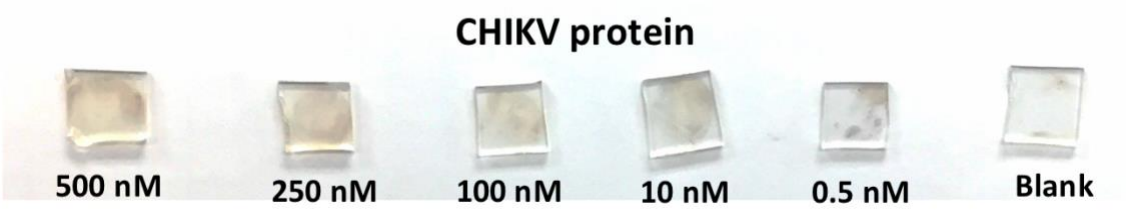

Figure 30: PDMS substrate for the detection of CHIKV protein

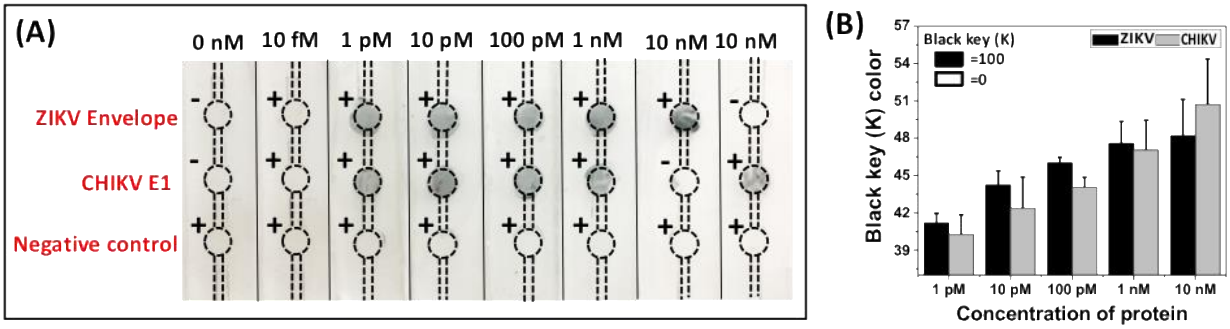

Figure 31: (A) Digital image of the microfluidic channels representing color change in the testing zones in presence of different concentration of protein (1 pM, 10 pM, 100 pM, 1 nM). The last two channels represent the specificity of the current sensor. The sample containing only ZIKV protein (10 nM) was introduced in the channel and no color change in the CHIKV region was observed and vice versa. This shows that the aptamers are highly specific in nature. (B) Graph represents the change in Key value (CMYK color model) calculated using ImageJ as a function of concentration of protein. Black and white are represented 100 and 0 respectively. It can be seen that the Key value moves towards black attributing to the increased deposition of Silver in the testing zone.

Table 3: Comparative analysis of different techniques used to detect the presence of Zika infection.

Analyte	Method	Limit of Detection	Detection Mode	Reference
Zika RNA	RT-RPA	5 PFU/mL	Mobile phone	[190]
Zika RNA	RT-LAMP	50 PFU/ml	Naked eye-Colorimetric	[186]
Zika NS1	ELISA	0.1 ng/ml (2 pM)	UV absorbance-Colorimetric	[216]
NS1 (flaviviruses)	Impedimetric	3 ng/mL, 30 ng/mL	Potentiostat	[217]
NS1 (flaviviruses)	Capacitance	0.2 ng/mL, 0.5 ng/mL	Potentiostat	[217]
E protein (ZIKV)	Chemiluminescence	10 PFU/mL	Electro-generated chemiluminescence instrument	[218]
Zika NS1 protein-	Commercially available ELISA kits	0.1 ng/ml	UV absorbance-Colorimetric	[219] [220]
Zika, Chikungunya	Nanoparticle immunoassay	50 pg/ml (1 pM)	Naked eye-Colorimetric	Current work

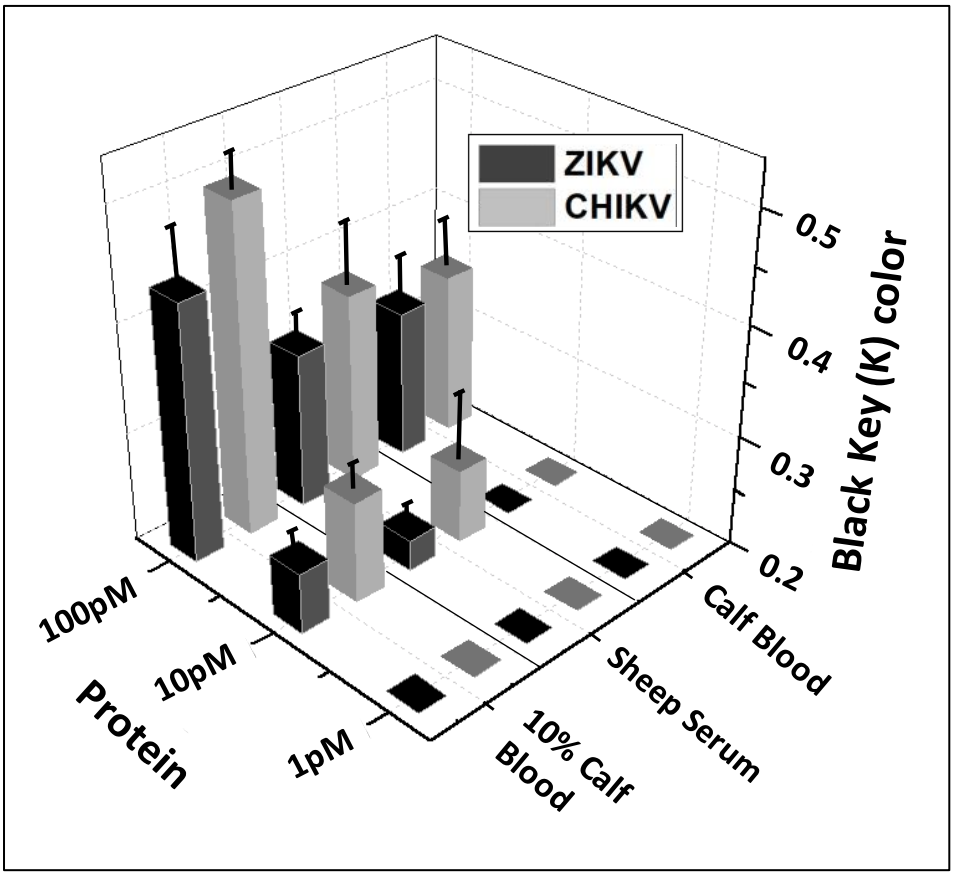

Figure 32: Development of silver in the microfluidic channels as a function of different concentration of ZIKV and CHIKV envelop proteins (1 pM, 10 pM and 100 pM) has been represented in terms of Key value (CMYK color code). No change in K values for calf blood and sheep serum was observed in the presence of 1 pM of the protein. Serum and 10% calf blood exhibited a slight color development at 10 pM of the recombinant protein. In case of 100 pM, distinct color development was observed in all the three cases.

4.4 Summary

In summary, a multiplex detection system for ZIKV and CHIKV arboviral envelope proteins has been developed using an aptamer-conjugated microfluidic channel approach. This novel method implements the immobilizing aptamers to the PDMS substrate using PMPI as the linker molecule. The channels are patterned with microsized pillars that facilitate an enhanced sensitivity of the approach down to detections of 1 pM (50 pg/ml) of viral envelope protein targets in PBS and 10 pM in dilute (10%) mechanically-defibrinated calf blood. The detection is based on a silver-enhancement technique that deposits a thick silver shell over the surface of target-bound Apt-AuNPs. This enhancement enables significant color changes on the PDMS substrate indicating the presence of target protein. The device also exhibited high specificity towards target protein with no interference from other, off-target arboviral proteins. The use of aptamers as the biorecognition molecule provides flexibility to incorporate additional or alternative targets by designing the specific aptamers and immobilizing them in the microfluidic channel. The present approach can be extended to detect other clinically important biomarkers for which there are few POC options available.

CHAPTER 5: CONCLUSIONS

The present work successfully exhibited the development of unique biosensors detecting small biomolecules as well as viral protein such as Zika. These approaches provide a real-time detection of a large range of biomolecules and viral proteins in a time and cost-effective manner and has applications in point-of-care testing tool for several diagnostics.

In the first chapter, colorimetric detection of epinephrine molecules has been demonstrated using a simple paper based substrate. Epinephrine is an excitatory neurotransmitter which plays an important role in the functioning of different biological reactions. The present sensor utilized aptamers functionalized gold nanoparticles as the colorimetric probes to induce a color change (red to blue) in the solution in the presence of epinephrine molecule. The study also investigated role of different parameters such as morphology of AuNPs (size and shape), aptamer concentration and salt destabilization to achieve a highly sensitive and selective biosensor. It was observed that the size and shape of the gold nanoparticles played most important role in controlling the detection limit of the sensor. The sensor exhibited a detection limit of 900 pM for epinephrine giving colorimetric signal which has not been achieved in any other study till date.

The second chapter emphasizes on the detection of epinephrine using a PEDOT:PSS based organic electrochemical transistor platform. The Au gate electrode was functionalized using epinephrine binding aptamers which acts as transducer. In the presence of epinephrine molecule, a significant decrease in the channel current was observed in the transfer characteristics as well as chronoamperometric measurements. This effect is attributed to the screening of the negative charge of aptamers and oxidation of epinephrine which increases the effective gate voltage resulting in a decrease in

current. The device was found to be highly sensitive towards epinephrine with a limit of detection of 90 pM which is less than the normal physiological range in humans (120 pM). Also, the device did not show any response towards common interfering agents such as dopamine, ascorbic acid, DOPAC etc. The approach provides a platform for the real-time detection of large range of biomolecules and viral proteins in a timely and efficient manner.

In the third chapter, the development of an aptamer based microfluidic sensor to detect multiple viral proteins has been shown. The working principle of the sensor is based on the formation of sandwich type morphology among aptamer-analyte-aptamer-gold which induces color change visible to naked eye. Silver reagent has been used to enhance the color change. The sensor showed high affinity towards zika and CHIKV protein and no interference was observed by control sample. The colorimetric detection limit of the sensor has been found to be 1 pM (50 pg/ml) of viral envelope protein targets in PBS and 10 pM in dilute (10%) mechanically-defibrinated calf blood which is relevant to the practical applications. The use of microfluidic channel enables multiplex detection, integrates the whole system and reduces the complexity of the assay. The current sensor provides rapid, easy and cheap sensing technique with high sensitivity and selectivity, leading to a more consumer driven health care.

The major advantage of employing aptasensors is that it can be designed for a large number of analyte molecules which offers a great potential to be applied in the fields of bioassay, biomedical diagnostic or environmental monitoring. The current work presents a set of tool box which provides a multiplex detection system for different viral proteins and show huge potential to be used in real world applications. Successful

implementation of these current sensors provides a means to a highly efficient, low cost, rapid and easy-to-use point of care diagnostic tools.

APPENDIX A: COPYRIGHT PERMISSION LETTER FOR FIGURE 1

Title: Multiplexed Point-of-Care Testing – xPOCT

Author: Can Dincer,Richard Bruch,André Kling,Petra S. Dittrich,Gerald A. Urban

Publication: Trends in Biotechnology

Publisher: Elsevier

Date: August 2017

Creative Commons Attribution-NonCommercial-No Derivatives License (CC BY NC ND)

APPENDIX B: COPYRIGHT PERMISSION LETTER FOR FIGURE 2

APPENDIX C: COPYRIGHT PERMISSION LETTER FOR FIGURE 3

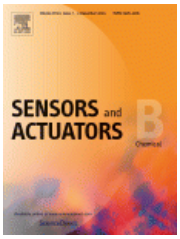

Title: Gold nanoparticles as efficient sensors in colorimetric detection of toxic metal ions: A review

Author: E. Priyadarshini,N. Pradhan

Publication: Sensors and Actuators B: Chemical

Publisher: Elsevier

Date: January 2017

Review Order

Please review the order details and the associated terms and conditions.

No royalties will be charged for this reuse request although you are required to obtain a license and comply with the license terms and conditions. To obtain the license, click the Accept button below.

Licensed Content Publisher	Elsevier
Licensed Content Publication	Sensors and Actuators B: Chemical
Licensed Content Title	Gold nanoparticles as efficient sensors in colorimetric detection of toxic metal ions: A review
Licensed Content Author	E. Priyadarshini,N. Pradhan
Licensed Content Date	January 2017
Licensed Content Volume	238
Licensed Content Issue	n/a
Licensed Content Pages	15
Type of Use	reuse in a thesis/dissertation
Portion	figures/tables/illustrations
Number of figures/tables/illustrations	1
Format	both print and electronic
Are you the author of this Elsevier article?	No
Will you be translating?	No
Original figure numbers	Figure 2
Title of your thesis/dissertation	Development of in vitro point of care diagnostics (IVPCD) based on Aptamers integrated Biosensors.
Expected completion date	Dec 2018
Estimated size (number of pages)	140
Requestor Location	Ms. Nileshi Saraf 3060, White Ash Trail Knights Landing ORLANDO, FL 32826 United States Attn: Ms. Nileshi Saraf
Publisher Tax ID	98-0397604
Total	0.00 USD

Edit Order Details
Edit Requestor Location This location may be used to determine your tax liability.

☐ I agree to these terms and conditions.

APPENDIX D: COPYRIGHT PERMISSION LETTER FOR FIGURE 4

Title: A short history, principles, and types of ELISA, and our laboratory experience with peptide/protein analyses using ELISA

Author: Suleyman Aydin

Publication: Peptides

Publisher: Elsevier

Date: October 2015

Review Order

Please review the order details and the associated terms and conditions.

No royalties will be charged for this reuse request although you are required to obtain a license and comply with the license terms and conditions. To obtain the license, click the Accept button below.

Licensed Content Publisher	Elsevier
Licensed Content Publication	Peptides
Licensed Content Title	A short history, principles, and types of ELISA, and our laboratory experience with peptide/protein analyses using ELISA
Licensed Content Author	Suleyman Aydin
Licensed Content Date	October 2015
Licensed Content Volume	72
Licensed Content Issue	n/a
Licensed Content Pages	12
Type of Use	reuse in a thesis/dissertation
Portion	figures/tables/illustrations
Number of figures/tables/illustrations	1
Format	both print and electronic
Are you the author of this Elsevier article?	No
Will you be translating?	No
Original figure numbers	figure 1
Title of your thesis/dissertation	Development of in vitro point of care diagnostics (IVPCD) based on Aptamers integrated Biosensors.
Expected completion date	Dec 2018
Estimated size (number of pages)	140
Requestor Location	Ms. Nileshi Saraf 3060, White Ash Trail Knights Landing ORLANDO, FL 32826 United States Attn: Ms. Nileshi Saraf
Publisher Tax ID	98-0397604
Total	0.00 USD

Edit Order Details

Edit Requestor Location This location may be used to determine your tax liability.

APPENDIX E: COPYRIGHT PERMISSION LETTER FOR FIGURE 5

PMC full text: Sensors (Basel). 2008 Mar; 8(3): 1400–1458.
Published online 2008 Mar 7. doi: 10.3390/s80314000
Copyright/License ▼ Request permission to reuse

<< Prev Figure 1. Next >>

Figure 1.

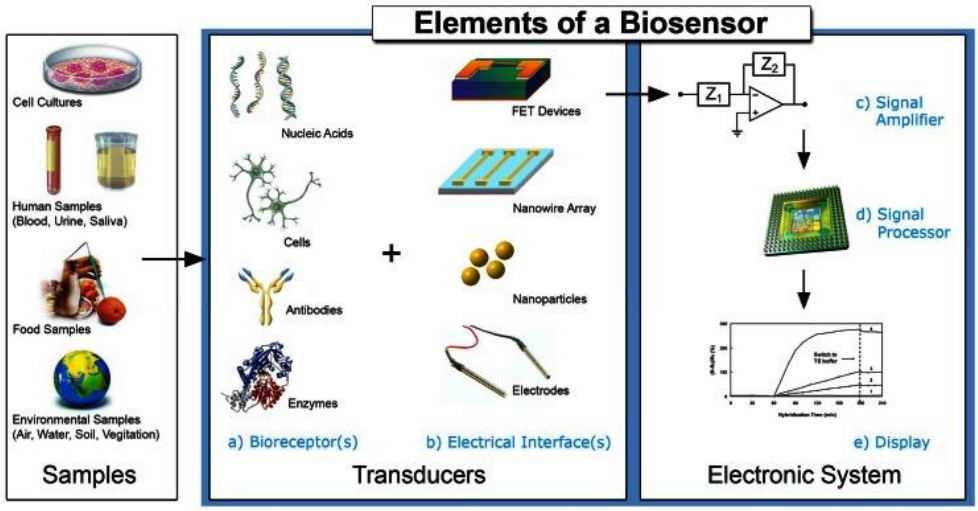

Elements and selected components of a typical biosensor [1, 2, 3].

Images in this article

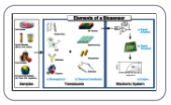
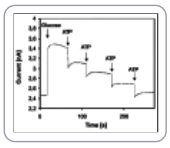
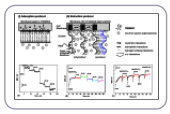
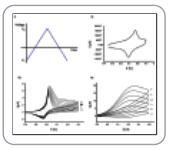
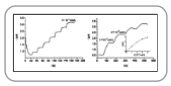
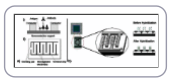
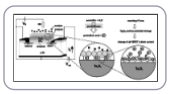
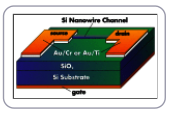

APPENDIX F: COPYRIGHT PERMISSION LETTER FOR FIGURE 6

Title: Current approaches in SELEX: An update to aptamer selection technology

Author: Mariia Darmostuk,Silvie Rimpelova,Helena Gbelcova,Tomas Ruml

Publication: Biotechnology Advances

Publisher: Elsevier

Date: 1 November 2015

Review Order

Please review the order details and the associated terms and conditions.

No royalties will be charged for this reuse request although you are required to obtain a license and comply with the license terms and conditions. To obtain the license, click the Accept button below.

Licensed Content Publisher	Elsevier
Licensed Content Publication	Biotechnology Advances
Licensed Content Title	Current approaches in SELEX: An update to aptamer selection technology
Licensed Content Author	Mariia Darmostuk,Silvie Rimpelova,Helena Gbelcova,Tomas Ruml
Licensed Content Date	1 November 2015
Licensed Content Volume	33
Licensed Content Issue	6
Licensed Content Pages	21
Type of Use	reuse in a thesis/dissertation
Portion	figures/tables/illustrations
Number of figures/tables/illustrations	1
Format	both print and electronic
Are you the author of this Elsevier article?	No
Will you be translating?	No
Original figure numbers	figure 1
Title of your thesis/dissertation	Development of in vitro point of care diagnostics (IVPCD) based on Aptamers integrated Biosensors.
Expected completion date	Dec 2018
Estimated size (number of pages)	140
Requestor Location	Ms. Nileshi Saraf 3060, White Ash Trail Knights Landing ORLANDO, FL 32826 United States Attn: Ms. Nileshi Saraf
Publisher Tax ID	98-0397604
Total	0.00 USD

Edit Order Details
Edit Requestor Location This location may be used to determine your tax liability.

☐ I agree to these terms and conditions.

APPENDIX G: LIST OF PUBLICATIONS

1. **Nileshi Saraf,** Alexander Bosak, Alicia Willenberg, Michael Kwan, Barry Alto, George W. Jackson, Robert H. Batchelor, Truong D. Nguyen, Vinoth Sankarapani, Griffith Parks, Sudipta Seal, Bradley Jay Willenberg, “Aptamer-Gold Nanoparticle Conjugates for the Colorimetric Detection of Arboviruses and Vector Mosquito Species” (Manuscript under preparation, **2018**)
2. **Nileshi Saraf,** Michael Villegas and Sudipta Seal, “Multiplex viral detection system based on aptamers integrated microfluidic channel” (under review, ACS Sensors, **2018**)
3. **Nileshi Saraf**, Madison Peppler, Swetha Barkam, Anna Metke, Abraham V. Guardado, Sushant Singh, Clarence Emile, Adrian Bico, Corey Rodas and Sudipta Seal, “Microsensor for limonin detection: an indicator of citrus greening disease” (under review, Sensors and Actuators, **2018**)
4. **Nileshi Saraf,** Eric R Woods, Madison Peppler and Sudipta Seal “Highly selective aptamer based organic electrochemical biosensor with picolevel detection”, Biosensors and Bioelectronics. 117, 40–46 **2018**.
5. **Nileshi Saraf**, Alexander Bosak, A. Willenberg, S. Das, Bradley J. Willenberg and Sudipta Seal, “Colorimetric detection of epinephrine using an optimized paper-based aptasensor”, RSC Adv. 7, 49133-49143, **2017**.
6. Sudha Joseph, **Nileshi Saraf**, Adithi Umamaheswara, Vijayaraghavan Madakasira, Navakanta Bhat, “Role of thermal annealing on SiGe thin films fabricated by PECVD”, Mater. Sci. Semicond. Process. Vol 40, 655–663, **2015**.

7. Anurag Srivastava, **Nileshi Saraf**, A.K Nagawat, “Conductance analysis of Zigzag Carbon Nanotubes under Stress: An ab-initio study”, Quantum Matter, Vol. 2, 1–7, **2013.**
8. Abhisek Mohapatra, Joydeep Dhar, **Nileshi Saraf**, Ramasamy Murugesan, Vaishakhi Mohanta, Satish Patil, “Tuning Molecular Assembly through H-Bonding: An Approach Towards Efficient Organic Photovoltaics.” (Manuscript under preparation).

REFERENCES

[1] R.W. Peeling, K.K. Holmes, D. Mabey, A. Ronald, Rapid tests for STIs: the way forward, Sexually transmitted infections (2006).

[2] G. Wu, M.H. Zaman, Low-cost tools for diagnosing and monitoring HIV infection in low-resource settings, Bulletin of the World Health Organization 90 (2012) 914-920.

[3] F. Bedin, L. Boulet, E. Voilin, G. Theillet, A. Rubens, C. Rozand, Paper-based point-of-care testing for cost-effective diagnosis of acute flavivirus infections, Journal of medical virology 89(9) (2017) 1520-1527.

[4] PubMed, PubMed, (2018).

[5] C. Dincer, R. Bruch, A. Kling, P.S. Dittrich, G.A. Urban, Multiplexed point-of-care testing–xPOCT, Trends in biotechnology 35(8) (2017) 728-742.

[6] MarketResearchEngine, MarketResearchEngine, (2018).

[7] M.A. El-Sayed, Some interesting properties of metals confined in time and nanometer space of different shapes, Accounts of Chemical Research 34(4) (2001) 257-264.

[8] C.D. Grant, A.M. Schwartzberg, T.J. Norman, J.Z. Zhang, Ultrafast electronic relaxation and coherent vibrational oscillation of strongly coupled gold nanoparticle aggregates, Journal of the American Chemical Society 125(2) (2003) 549-553.

[9] M.L. Sandrock, C.A. Foss, Synthesis and linear optical properties of nanoscopic gold particle pair structures, The Journal of Physical Chemistry B 103(51) (1999) 11398-11406.

[10] J.J. Storhoff, R. Elghanian, R.C. Mucic, C.A. Mirkin, R.L. Letsinger, One-pot colorimetric differentiation of polynucleotides with single base imperfections using gold nanoparticle probes, Journal of the American Chemical Society 120(9) (1998) 1959-1964.

[11] J.J. Storhoff, A.A. Lazarides, R.C. Mucic, C.A. Mirkin, R.L. Letsinger, G.C. Schatz, What controls the optical properties of DNA-linked gold nanoparticle assemblies?, Journal of the American Chemical Society 122(19) (2000) 4640-4650.

[12] D.A. Vanden Bout, Metal Nanoparticles: Synthesis, Characterization, and Applications Edited by Daniel L. Feldheim (North Carolina State University) and Colby A. Foss, Jr. (Georgetown University). Marcel Dekker, Inc.: New York and Basel. 2002. x+ 338 pp. $150.00. ISBN: 0-8247-0604-8, Journal of the American Chemical Society 124(26) (2002) 7874-7875.

[13] R. Jin, Y. Cao, C.A. Mirkin, K. Kelly, G.C. Schatz, J. Zheng, Photoinduced conversion of silver nanospheres to nanoprisms, Science 294(5548) (2001) 1901-1903.

[14] I.O. Sosa, C. Noguez, R.G. Barrera, Optical properties of metal nanoparticles with arbitrary shapes, The Journal of Physical Chemistry B 107(26) (2003) 6269-6275.

[15] K.L. Kelly, E. Coronado, L.L. Zhao, G.C. Schatz, The optical properties of metal nanoparticles: the influence of size, shape, and dielectric environment, ACS Publications, 2003.

[16] P.N. Njoki, I.-I.S. Lim, D. Mott, H.-Y. Park, B. Khan, S. Mishra, R. Sujakumar, J. Luo, C.-J. Zhong, Size correlation of optical and spectroscopic properties for gold nanoparticles, The Journal of Physical Chemistry C 111(40) (2007) 14664-14669.

[17] H. Li, L. Rothberg, Colorimetric detection of DNA sequences based on electrostatic interactions with unmodified gold nanoparticles, Proceedings of the National Academy of Sciences 101(39) (2004) 14036-14039.

[18] S.-J. Chen, Y.-F. Huang, C.-C. Huang, K.-H. Lee, Z.-H. Lin, H.-T. Chang, Colorimetric determination of urinary adenosine using aptamer-modified gold nanoparticles, Biosensors and Bioelectronics 23(11) (2008) 1749-1753.

[19] K. Sato, K. Hosokawa, M. Maeda, Rapid aggregation of gold nanoparticles induced by non-cross-linking DNA hybridization, Journal of the American Chemical Society 125(27) (2003) 8102-8103.

[20] E. Priyadarshini, N. Pradhan, Gold nanoparticles as efficient sensors in colorimetric detection of toxic metal ions: a review, Sensors and Actuators B: Chemical 238 (2017) 888-902.

[21] B. Van Weemen, A. Schuurs, Immunoassay using antigen—enzyme conjugates, FEBS letters 15(3) (1971) 232-236.

[22] S. Aydin, A short history, principles, and types of ELISA, and our laboratory experience with peptide/protein analyses using ELISA, Peptides 72 (2015) 4-15.

[23] E. Engvall, P. Perlmann, Enzyme-linked immunosorbent assay (ELISA) quantitative assay of immunoglobulin G, Immunochemistry 8(9) (1971) 871-874.

[24] F. Bishai, R. Galli, Enzyme-linked immunosorbent assay for detection of antibodies to influenza A and B and parainfluenza type 1 in sera of patients, Journal of clinical microbiology 8(6) (1978) 648-656.

[25] H.E. Carlsson, A.A. Lindberg, S. Hammarström, Titration of antibodies to salmonella O antigens by enzyme-linked immunosorbent assay, Infection and immunity 6(5) (1972) 703-708.

[26] J. Holmgren, A.-M. Svennerholm, Enzyme-linked immunosorbent assays for cholera serology, Infection and immunity 7(5) (1973) 759-763.

[27] P.O. Leinikki, I. Shekarchi, N. Tzan, D.L. Madden, J.L. Sever, Evaluation of enzyme-linked immunosorbent assay (ELISA) for mumps virus antibodies, Proceedings of the Society for Experimental Biology and Medicine 160(3) (1979) 363-367.

[28] P. Ukkonen, K. Penttinen, M.L. Granström, Mumps-specific immunoglobulin M and G antibodies in natural mumps infection as measured by enzyme-linked immunosorbent assay, Journal of medical virology 8(2) (1981) 131-142.

[29] R.L. Siegle, B.R. Jennings, P.L. Adams, L.P. King, Development of a model using polypeptide antibodies for scintigraphy of the pancreas, Investigative radiology 15(5) (1980) 457-461.

[30] P. Lindström, O. Wager, IgG autoantibody to human serum albumin studied by the ELISA-technique, Scandinavian journal of immunology 7(5) (1978) 419-425.

[31] K. Kato, Y. HAMAGUCHI, S. OKAWA, E. ISHIKAWA, K. KOBAYASHI, N. KATUNUMA, Use of rabbit antibody IgG bound onto plain and aminoalkylsilyl glass surface for the enzyme-linked sandwich immunoassay, The Journal of Biochemistry 82(1) (1977) 261-266.

[32] S. Tang, I. Hewlett, Nanoparticle-based immunoassays for sensitive and early detection of HIV-1 capsid (p24) antigen, Journal of Infectious Diseases 201(Supplement_1) (2010) S59-S64.

[33] D.R. Thévenot, K. Toth, R.A. Durst, G.S. Wilson, Electrochemical biosensors: recommended definitions and classification, Analytical Letters 34(5) (2001) 635-659.

[34] D. Grieshaber, R. MacKenzie, J. Voeroes, E. Reimhult, Electrochemical biosensors-sensor principles and architectures, Sensors 8(3) (2008) 1400-1458.

[35] A. Turner, I. Karube, G.S. Wilson, Biosensors: fundamentals and applications, Oxford university press1987.

[36] J. Wang, Analytical electrochemistry, John Wiley & Sons2006.

[37] P. D'Orazio, Biosensors in clinical chemistry, Clinica Chimica Acta 334(1-2) (2003) 41-69.

[38] D. Nilsson, T. Kugler, P.-O. Svensson, M. Berggren, An all-organic sensor–transistor based on a novel electrochemical transducer concept printed electrochemical sensors on paper, Sensors and Actuators B: Chemical 86(2-3) (2002) 193-197.

[39] G. Urban, G. Jobst, F. Keplinger, E. Aschauer, O. Tilado, R. Fasching, F. Kohl, Miniaturized multi-enzyme biosensors integrated with pH sensors on flexible polymer carriers for in vivo applications, Biosensors and Bioelectronics 7(10) (1992) 733-739.

[40] B.R. Eggins, Chemical sensors and biosensors, John Wiley & Sons2008.

[41] A. Chaubey, B. Malhotra, Mediated biosensors, Biosensors and Bioelectronics 17(6-7) (2002) 441-456.

[42] P.B. Luppa, L.J. Sokoll, D.W. Chan, Immunosensors—principles and applications to clinical chemistry, Clinica Chimica Acta 314(1-2) (2001) 1-26.

[43] C.R. Lowe, Biosensors, Trends in biotechnology 2(3) (1984) 59-65.

[44] B. Kasemo, Biological surface science, Surface science 500(1-3) (2002) 656-677.

[45] M. Zayats, Y. Huang, R. Gill, C.-a. Ma, I. Willner, Label-free and reagentless aptamer-based sensors for small molecules, Journal of the American Chemical Society 128(42) (2006) 13666-13667.

[46] A. Ogawa, M. Maeda, Aptazyme-based riboswitches as label-free and detector-free sensors for cofactors, Bioorganic & medicinal chemistry letters 17(11) (2007) 3156-3160.

[47] J.H. Lee, Z. Wang, J. Liu, Y. Lu, Highly sensitive and selective colorimetric sensors for uranyl (UO22+): Development and comparison of labeled and label-free DNAzyme-gold nanoparticle systems, Journal of the American Chemical Society 130(43) (2008) 14217-14226.

[48] W.K. Adeniyi, A.R. Wright, Novel fluorimetric assay of trace analysis of epinephrine in human serum, Spectrochimica acta. Part A, Molecular and biomolecular spectroscopy 74(5) (2009) 1001-4.

[49] H. Sun, Y. Zu, A highlight of recent advances in aptamer technology and its application, Molecules 20(7) (2015) 11959-11980.

[50] C. Boiziau, E. Dausse, L. Yurchenko, J.-J. Toulmé, DNA Aptamers Selected Against the HIV-1trans-Activation-responsive RNA Element Form RNA-DNA Kissing Complexes, Journal of Biological Chemistry 274(18) (1999) 12730-12737.

[51] T.W. Wiegand, P.B. Williams, S.C. Dreskin, M.-H. Jouvin, J.-P. Kinet, D. Tasset, High-affinity oligonucleotide ligands to human IgE inhibit binding to Fc epsilon receptor I, The journal of immunology 157(1) (1996) 221-230.

[52] A. Tahiri-Alaoui, L. Frigotto, N. Manville, J. Ibrahim, P. Romby, W. James, High affinity nucleic acid aptamers for streptavidin incorporated into bi-specific capture ligands, Nucleic acids research 30(10) (2002) e45-e45.

[53] A.D. Ellington, J.W. Szostak, Selection in vitro of single-stranded DNA molecules that fold into specific ligand-binding structures, Nature 355(6363) (1992) 850.

[54] J. Ciesiolka, J. Gorski, M. Yarus, Selection of an RNA domain that binds Zn2+, Rna 1(5) (1995) 538-550.

[55] W. Pan, R.C. Craven, Q. Qiu, C.B. Wilson, J.W. Wills, S. Golovine, J.-F. Wang, Isolation of virus-neutralizing RNAs from a large pool of random sequences, Proceedings of the National Academy of Sciences 92(25) (1995) 11509-11513.

[56] J.G. Bruno, J.L. Kiel, In vitro selection of DNA aptamers to anthrax spores with electrochemiluminescence detection, Biosensors and Bioelectronics 14(5) (1999) 457-464.

[57] M. Darmostuk, S. Rimpelova, H. Gbelcova, T. Ruml, Current approaches in SELEX: An update to aptamer selection technology, Biotechnology advances 33(6) (2015) 1141-1161.

[58] D. Aili, R. Selegard, L. Baltzer, K. Enander, B. Liedberg, Colorimetric protein sensing by controlled assembly of gold nanoparticles functionalized with synthetic receptors, Small (Weinheim an der Bergstrasse, Germany) 5(21) (2009) 2445-52.

[59] R.D. Grange, J.P. Thompson, D.G. Lambert, Radioimmunoassay, enzyme and non-enzyme-based immunoassays, British journal of anaesthesia 112(2) (2014) 213-6.

[60] M. Vidotti, R.F. Carvalhal, R.K. Mendes, D.C.M. Ferreira, L.T. Kubota, Biosensors based on gold nanostructures, Journal of the Brazilian Chemical Society 22 (2011) 3-20.

[61] W.R.G. Baeyens, S.G. Schulman, A.C. Calokerinos, Y. Zhao, A.M. García Campaña, K. Nakashima, D. De Keukeleire, Chemiluminescence-based detection: principles and analytical applications in flowing streams and in immunoassays, Journal of Pharmaceutical and Biomedical Analysis 17(6–7) (1998) 941-953.

[62] Y.C. Chen, W.Y. Lin, Enhancement of chemiluminescence of the KIO4-luminol system by gallic acid, acetaldehyde and Mn2+: application for the determination of catecholamines, Luminescence 25(1) (2010) 43-9.

[63] S. Zhao, Y. Huang, M. Shi, R. Liu, Y.M. Liu, Chemiluminescence resonance energy transfer-based detection for microchip electrophoresis, Anal Chem 82(5) (2010) 2036-41.

[64] M.T. Donato, N. Jimenez, J.V. Castell, M.J. Gomez-Lechon, Fluorescence-based assays for screening nine cytochrome P450 (P450) activities in intact cells expressing individual human P450 enzymes, Drug Metab Dispos 32(7) (2004) 699-706.

[65] L.J. Jones, S.T. Yue, C.Y. Cheung, V.L. Singer, RNA quantitation by fluorescence-based solution assay: RiboGreen reagent characterization, Analytical biochemistry 265(2) (1998) 368-74.

[66] G.-H. Chen, W.-Y. Chen, Y.-C. Yen, C.-W. Wang, H.-T. Chang, C.-F. Chen, Detection of mercury (II) ions using colorimetric gold nanoparticles on paper-based analytical devices, Analytical chemistry 86(14) (2014) 6843-6849.

[67] D.D. Liana, B. Raguse, J.J. Gooding, E. Chow, Recent advances in paper-based sensors, Sensors 12(9) (2012) 11505-11526.

[68] W. Zhao, M.M. Ali, S.D. Aguirre, M.A. Brook, Y. Li, Paper-based bioassays using gold nanoparticle colorimetric probes, Anal Chem 80(22) (2008) 8431-7.

[69] M.C. Daniel, D. Astruc, Gold nanoparticles: Assembly, supramolecular chemistry, quantum-size-related properties, and applications toward biology, catalysis, and nanotechnology, Chem Rev 104(1) (2004) 293-346.

[70] N.I. Kovtyukhova, T.E. Mallouk, Nanowires as Building Blocks for Self-Assembling Logic and Memory Circuits, Chemistry – A European Journal 8(19) (2002) 4354-4363.

[71] D.S. Grubisha, R.J. Lipert, H.-Y. Park, J. Driskell, M.D. Porter, Femtomolar Detection of Prostate-Specific Antigen: An Immunoassay Based on Surface-Enhanced Raman Scattering and Immunogold Labels, Analytical chemistry 75(21) (2003) 5936-5943.

[72] X.X. Han, Y. Kitahama, T. Itoh, C.X. Wang, B. Zhao, Y. Ozaki, Protein-Mediated Sandwich Strategy for Surface-Enhanced Raman Scattering: Application to Versatile Protein Detection, Analytical chemistry 81(9) (2009) 3350-3355.

[73] C.J. Murphy, T.K. Sau, A.M. Gole, C.J. Orendorff, J. Gao, L. Gou, S.E. Hunyadi, T. Li, Anisotropic metal nanoparticles: Synthesis, assembly, and optical applications, The journal of physical chemistry. B 109(29) (2005) 13857-70.

[74] G. Wang, R.J. Lipert, M. Jain, S. Kaur, S. Chakraboty, M.P. Torres, S.K. Batra, R.E. Brand, M.D. Porter, Detection of the Potential Pancreatic Cancer Marker MUC4 in Serum Using Surface-Enhanced Raman Scattering, Analytical chemistry 83(7) (2011) 2554-2561.

[75] R. Elghanian, J.J. Storhoff, R.C. Mucic, R.L. Letsinger, C.A. Mirkin, Selective Colorimetric Detection of Polynucleotides Based on the Distance-Dependent Optical Properties of Gold Nanoparticles, Science 277(5329) (1997) 1078-1081.

[76] M. Gluodenis, C.A. Foss, The effect of mutual orientation on the spectra of metal nanoparticle rod− rod and rod− sphere pairs, The Journal of Physical Chemistry B 106(37) (2002) 9484-9489.

[77] P. Hanarp, M. Käll, D.S. Sutherland, Optical Properties of Short Range Ordered Arrays of Nanometer Gold Disks Prepared by Colloidal Lithography, The Journal of Physical Chemistry B 107(24) (2003) 5768-5772.

[78] S. Link, M.A. El-Sayed, Spectral Properties and Relaxation Dynamics of Surface Plasmon Electronic Oscillations in Gold and Silver Nanodots and Nanorods, The Journal of Physical Chemistry B 103(40) (1999) 8410-8426.

[79] S. Schultz, D.R. Smith, J.J. Mock, D.A. Schultz, Single-target molecule detection with nonbleaching multicolor optical immunolabels, Proceedings of the National Academy of Sciences 97(3) (2000) 996-1001.

[80] K. Ai, Y. Liu, L. Lu, Hydrogen-bonding recognition-induced color change of gold nanoparticles for visual detection of melamine in raw milk and infant formula, Journal of the American Chemical Society 131(27) (2009) 9496-9497.

[81] S. Krishnan, V. Mani, D. Wasalathanthri, C.V. Kumar, J.F. Rusling, Attomolar detection of a cancer biomarker protein in serum by surface plasmon resonance using superparamagnetic particle labels, Angewandte Chemie (International ed. in English) 50(5) (2011) 1175-8.

[82] X. Xie, W. Xu, X. Liu, Improving colorimetric assays through protein enzyme-assisted gold nanoparticle amplification, Accounts of Chemical Research 45(9) (2012) 1511-1520.

[83] A.W. Clark, J.M. Cooper, Plasmon shaping by using protein nanoarrays and molecular lithography to engineer structural color, Angewandte Chemie 124(15) (2012) 3622-3626.

[84] C.A. Mirkin, R.L. Letsinger, R.C. Mucic, J.J. Storhoff, A DNA-based method for rationally assembling nanoparticles into macroscopic materials, Nature 382(6592) (1996) 607.

[85] T. Mori, M. Maeda, Stability change of DNA-carrying colloidal particle induced by hybridization with target DNA, Polymer journal 34(8) (2002) 624-628.

[86] J. Liu, Y. Lu, Accelerated color change of gold nanoparticles assembled by DNAzymes for simple and fast colorimetric Pb2+ detection, Journal of the American Chemical Society 126(39) (2004) 12298-12305.

[87] X. Xue, F. Wang, X. Liu, One-step, room temperature, colorimetric detection of mercury (Hg2+) using DNA/nanoparticle conjugates, Journal of the American Chemical Society 130(11) (2008) 3244-3245.

[88] S. Kim, J.W. Park, D. Kim, D. Kim, I.H. Lee, S. Jon, Bioinspired Colorimetric Detection of Calcium (II) Ions in Serum Using Calsequestrin-Functionalized Gold Nanoparticles, Angewandte Chemie 121(23) (2009) 4202-4205.

[89] Z. Mei, H. Chu, W. Chen, F. Xue, J. Liu, H. Xu, R. Zhang, L. Zheng, Ultrasensitive one-step rapid visual detection of bisphenol A in water samples by label-free aptasensor, Biosensors and Bioelectronics 39(1) (2013) 26-30.

[90] N. Zhou, J. Wang, J. Zhang, C. Li, Y. Tian, J. Wang, Selection and identification of streptomycin-specific single-stranded DNA aptamers and the application in the detection of streptomycin in honey, Talanta 108 (2013) 109-116.

[91] Y.S. Kim, J.H. Kim, I.A. Kim, S.J. Lee, J. Jurng, M.B. Gu, A novel colorimetric aptasensor using gold nanoparticle for a highly sensitive and specific detection of oxytetracycline, Biosensors and Bioelectronics 26(4) (2010) 1644-1649.

[92] K.-M. Song, E. Jeong, W. Jeon, M. Cho, C. Ban, Aptasensor for ampicillin using gold nanoparticle based dual fluorescence–colorimetric methods, Analytical and bioanalytical chemistry 402(6) (2012) 2153-2161.

[93] J. Abelson, Directed evolution of nucleic acids by independent replication and selection, Science 249(4968) (1990) 488+.

[94] S.K. Ghosh, T. Pal, Interparticle coupling effect on the surface plasmon resonance of gold nanoparticles: from theory to applications, Chem Rev 107(11) (2007) 4797-4862.

[95] C.J. Murphy, A.M. Gole, J.W. Stone, P.N. Sisco, A.M. Alkilany, E.C. Goldsmith, S.C. Baxter, Gold nanoparticles in biology: beyond toxicity to cellular imaging, Accounts of Chemical Research 41(12) (2008) 1721-1730.

[96] F.E.R. Simons, First-aid treatment of anaphylaxis to food: Focus on epinephrine, Journal of Allergy and Clinical Immunology 113(5) (2004) 837-844.

[97] T. Härle, K. Kronberg, H. Nef, H. Möllmann, A. Elsässer, Inverted Takotsubo cardiomyopathy following accidental intravenous administration of epinephrine in a young woman, Clinical Research in Cardiology 100(5) (2011) 471-473.

[98] A. Sheikh, Y.A. Shehata, S.G.A. Brown, F.E.R. Simons, Adrenaline (epinephrine) for the treatment of anaphylaxis with and without shock, Cochrane Database of Systematic Reviews (4) (2008).

[99] E.D. Bergmann, Z. Goldschmidt, Some epinephrine analogs, Journal of Medicinal Chemistry 11(6) (1968) 1121-1125.

[100] Alpat, #x15e, enol, #xd6, K. zdemir, #x131, #x131, #x131, #xe7, S. Alpat, Voltammetric Determination of Epinephrine in Pharmaceutical Sample with a Tyrosinase Nanobiosensor, Journal of Sensors 2016 (2016) 9.

[101] X. Lu, Y. Li, J. Du, X. Zhou, Z. Xue, X. Liu, Z. Wang, A novel nanocomposites sensor for epinephrine detection in the presence of uric acids and ascorbic acids, Electrochimica Acta 56(21) (2011) 7261-7266.

[102] F.C. Moraes, D.L. Golinelli, L.H. Mascaro, S.A. Machado, Determination of epinephrine in urine using multi-walled carbon nanotube modified with cobalt phthalocyanine in a paraffin composite electrode, Sensors and Actuators B: Chemical 148(2) (2010) 492-497.

[103] Z. Yang, G. Hu, X. Chen, J. Zhao, G. Zhao, The nano-Au self-assembled glassy carbon electrode for selective determination of epinephrine in the presence of ascorbic acid, Colloids and Surfaces B: Biointerfaces 54(2) (2007) 230-235.

[104] V. Carrera, E. Sabater, E. Vilanova, M.A. Sogorb, A simple and rapid HPLC–MS method for the simultaneous determination of epinephrine, norepinephrine, dopamine and 5-hydroxytryptamine: Application to the secretion of bovine chromaffin cell cultures, Journal of Chromatography B 847(2) (2007) 88-94.

[105] M.A. Fotopoulou, P.C. Ioannou, Post-column terbium complexation and sensitized fluorescence detection for the determination of norepinephrine, epinephrine and dopamine using high-performance liquid chromatography, Analytica Chimica Acta 462(2) (2002) 179-185.

[106] M. Sorouraddin, J. Manzoori, E. Kargarzadeh, A.H. Shabani, Spectrophotometric determination of some catecholamine drugs using sodium bismuthate, Journal of Pharmaceutical and Biomedical Analysis 18(4) (1998) 877-881.

[107] S. Wei, G. Song, J.-M. Lin, Separation and determination of norepinephrine, epinephrine and isoprinaline enantiomers by capillary electrophoresis in pharmaceutical formulation and human serum, Journal of Chromatography A 1098(1) (2005) 166-171.

[108] J. Du, L. Shen, J. Lu, Flow injection chemiluminescence determination of epinephrine using epinephrine-imprinted polymer as recognition material, Analytica Chimica Acta 489(2) (2003) 183-189.

[109] X. Zheng, Z. Guo, Z. Zhang, Flow-injection electrogenerated chemiluminescence determination of epinephrine using luminol, Analytica Chimica Acta 441(1) (2001) 81-86.

[110] J. Yang, G. Zhang, X. Wu, F. Huang, C. Lin, X. Cao, L. Sun, Y. Ding, Fluorimetric determination of epinephrine with o-phenylenediamine, Analytica Chimica Acta 363(1) (1998) 105-110.

[111] Y.-F. Huang, H.-T. Chang, W. Tan, Cancer cell targeting using multiple aptamers conjugated on nanorods, Analytical chemistry 80(3) (2008) 567-572.

[112] H.R. Sim, A.W. Wark, H.J. Lee, Attomolar detection of protein biomarkers using biofunctionalized gold nanorods with surface plasmon resonance, Analyst 135(10) (2010) 2528-2532.

[113] S.J. Zhen, C.Z. Huang, J. Wang, Y.F. Li, End-to-End Assembly of Gold Nanorods on the Basis of Aptamer− Protein Recognition, The Journal of Physical Chemistry C 113(52) (2009) 21543-21547.

[114] S. Niu, Z. Lv, J. Liu, W. Bai, S. Yang, A. Chen, Colorimetric aptasensor using unmodified gold nanoparticles for homogeneous multiplex detection, PloS one 9(10) (2014) e109263.

[115] M.M. Maye, L. Han, N.N. Kariuki, N.K. Ly, W.-B. Chan, J. Luo, C.-J. Zhong, Gold and alloy nanoparticles in solution and thin film assembly: spectrophotometric determination of molar absorptivity, Analytica Chimica Acta 496(1) (2003) 17-27.

[116] V. Behaj, J.I. Cohen, R. Engel, Polycationic modified paper for chromatography, Analytical letters 35(10) (2002) 1715-1720.

[117] D.A. Bruzewicz, M. Reches, G.M. Whitesides, Low-cost printing of poly (dimethylsiloxane) barriers to define microchannels in paper, Analytical chemistry 80(9) (2008) 3387-3392.

[118] E. Metcalf, M. Morgan, P. Dean, Chromatographic assay of steroids on immuno-affinity paper strips; a rapid method for the quantitation of digoxin and oestriol-16α-glucuronide concentrations, Journal of Chromatography A 235(2) (1982) 501-506.

[119] A.J. Nozik, R. Memming, Physical chemistry of semiconductor− liquid interfaces, The Journal of Physical Chemistry 100(31) (1996) 13061-13078.

[120] H. Patel, A. Kharat, COMPARATIVE STUDY OF FREE ENZYME & IMMOBILIZED ENZYME ON BSA DIGESTION.

[121] J. Wang, A. Munir, Z. Li, H.S. Zhou, Aptamer–Au NPs conjugates-enhanced SPR sensing for the ultrasensitive sandwich immunoassay, Biosensors and Bioelectronics 25(1) (2009) 124-129.

[122] Y. Zheng, Y. Wang, X. Yang, Aptamer-based colorimetric biosensing of dopamine using unmodified gold nanoparticles, Sensors and Actuators B: Chemical 156(1) (2011) 95-99.

[123] Y. Xue, X. Li, H. Li, W. Zhang, Quantifying thiol-gold interactions towards the efficient strength control, Nature communications 5 (2014) 4348.

[124] H. Häkkinen, The gold-sulfur interface at the nanoscale, Nature chemistry 4(6) (2012) 443-455.

[125] V.S.R. Aaryasomayajula, T. Severs, K. Ghosh, R. DeLong, X. Zhang, S. Talapatra, A.K. Wanekaya, Assembly of a dual aptamer gold nanoparticle conjugate ensemble in the specific detection of thrombin when coupled with dynamic light scattering spectroscopy, Journal of Nanomedicine & Nanotechnology 5(4) (2014) 1.

[126] H. Li, L. Rothberg, Colorimetric detection of DNA sequences based on electrostatic interactions with unmodified gold nanoparticles, Proceedings of the National Academy of Sciences of the United States of America 101(39) (2004) 14036-14039.

[127] S. Basu, S.K. Ghosh, S. Kundu, S. Panigrahi, S. Praharaj, S. Pande, S. Jana, T. Pal, Biomolecule induced nanoparticle aggregation: effect of particle size on interparticle coupling, Journal of colloid and interface science 313(2) (2007) 724-734.

[128] A.N. Afrooz, S.T. Sivalapalan, C.J. Murphy, S.M. Hussain, J.J. Schlager, N.B. Saleh, Spheres vs. rods: The shape of gold nanoparticles influences aggregation and deposition behavior, Chemosphere 91(1) (2013) 93-98.

[129] A.V. Kyrylyuk, A.P. Philipse, Effect of particle shape on the random packing density of amorphous solids, physica status solidi (a) 208(10) (2011) 2299-2302.

[130] J.F. Rudge, M.B. Holness, G.C. Smith, Quantitative textural analysis of packings of elongate crystals, Contributions to Mineralogy and Petrology 156(4) (2008) 413-429.

[131] G.-H. Chen, W.-Y. Chen, Y.-C. Yen, C.-W. Wang, H.-T. Chang, C.-F. Chen, Detection of Mercury(II) Ions Using Colorimetric Gold Nanoparticles on Paper-Based Analytical Devices, Analytical chemistry 86(14) (2014) 6843-6849.

[132] I.S. Wittstein, D.R. Thiemann, J.A. Lima, K.L. Baughman, S.P. Schulman, G. Gerstenblith, K.C. Wu, J.J. Rade, T.J. Bivalacqua, H.C. Champion, Neurohumoral features of myocardial stunning due to sudden emotional stress, New England Journal of Medicine 352(6) (2005) 539-548.

[133] J. Liu, D. Mazumdar, Y. Lu, A Simple and Sensitive “Dipstick” Test in Serum Based on Lateral Flow Separation of Aptamer-Linked Nanostructures, Angewandte Chemie 118(47) (2006) 8123-8127.

[134] P. Lin, F. Yan, H.L. Chan, Ion-sensitive properties of organic electrochemical transistors, ACS applied materials & interfaces 2(6) (2010) 1637-1641.

[135] L. Kergoat, B. Piro, D.T. Simon, M.C. Pham, V. Noël, M. Berggren, Detection of glutamate and acetylcholine with organic electrochemical transistors based on conducting polymer/platinum nanoparticle composites, Advanced Materials 26(32) (2014) 5658-5664.

[136] H. Tang, P. Lin, H.L. Chan, F. Yan, Highly sensitive dopamine biosensors based on organic electrochemical transistors, Biosensors and Bioelectronics 26(11) (2011) 4559-4563.

[137] I. Kubo, T. Eguchi, Study on Electrochemical Insulin Sensing Utilizing a DNA Aptamer-Immobilized Gold Electrode, Materials 8(8) (2015) 4710-4719.

[138] P. Lin, X. Luo, I. Hsing, F. Yan, Organic electrochemical transistors integrated in flexible microfluidic systems and used for label-free DNA sensing, Advanced Materials 23(35) (2011) 4035-4040.

[139] R.-X. He, M. Zhang, F. Tan, P.H. Leung, X.-Z. Zhao, H.L. Chan, M. Yang, F. Yan, Detection of bacteria with organic electrochemical transistors, Journal of Materials Chemistry 22(41) (2012) 22072-22076.

[140] Z.-T. Zhu, J.T. Mabeck, C. Zhu, N.C. Cady, C.A. Batt, G.G. Malliaras, A simple poly (3, 4-ethylene dioxythiophene)/poly (styrene sulfonic acid) transistor for glucose sensing at neutral pH, Chemical communications (13) (2004) 1556-1557.

[141] S.Y. Yang, J.A. DeFranco, Y.A. Sylvester, T.J. Gobert, D.J. Macaya, R.M. Owens, G.G. Malliaras, Integration of a surface-directed microfluidic system with an organic

electrochemical transistor array for multi-analyte biosensors, Lab on a Chip 9(5) (2009) 704-708.

[142] H. Tang, F. Yan, P. Lin, J. Xu, H.L. Chan, Highly sensitive glucose biosensors based on organic electrochemical transistors using platinum gate electrodes modified with enzyme and nanomaterials, Advanced Functional Materials 21(12) (2011) 2264-2272.

[143] N. Aliakbarinodehi, P. Jolly, N. Bhalla, A. Miodek, G. De Micheli, P. Estrela, S. Carrara, Aptamer-based Field-Effect Biosensor for Tenofovir Detection, Scientific reports 7 (2017) 44409.

[144] F. Felderer, P. Fromherz, Transistor needle chip for recording in brain tissue, Applied Physics A 104(1) (2011) 1.

[145] D. Khodagholy, J. Rivnay, M. Sessolo, M. Gurfinkel, P. Leleux, L.H. Jimison, E. Stavrinidou, T. Herve, S. Sanaur, R.M. Owens, High transconductance organic electrochemical transistors, Nature communications 4 (2013) 2133.

[146] B.R. Baker, R.Y. Lai, M.S. Wood, E.H. Doctor, A.J. Heeger, K.W. Plaxco, An electronic, aptamer-based small-molecule sensor for the rapid, label-free detection of cocaine in adulterated samples and biological fluids, Journal of the American Chemical Society 128(10) (2006) 3138-3139.

[147] P. Lin, F. Yan, Organic thin-film transistors for chemical and biological sensing, Advanced Materials 24(1) (2012) 34-51.

[148] W. Ye, M. Yang, A Functionalized Nanoporous Alumina Membrane Electrochemical Sensor for DNA Detection with Gold Nanoparticle Amplification, Advances in Bioceramics and Biotechnologies II: Ceramic Transactions 247 (2014) 191.

[149] N. Saraf, A. Bosak, A. Willenberg, S. Das, B.J. Willenberg, S. Seal, Colorimetric detection of epinephrine using an optimized paper-based aptasensor, RSC Advances 7(77) (2017) 49133-49143.

[150] J.A. Hansen, J. Wang, A.-N. Kawde, Y. Xiang, K.V. Gothelf, G. Collins, Quantum-dot/aptamer-based ultrasensitive multi-analyte electrochemical biosensor, Journal of the American Chemical Society 128(7) (2006) 2228-2229.

[151] N. Zhou, J. Zhang, Y. Tian, Aptamer-based spectrophotometric detection of kanamycin in milk, Analytical Methods 6(5) (2014) 1569-1574.

[152] T.M. Lerga, C.K. O'Sullivan, Rapid determination of total hardness in water using fluorescent molecular aptamer beacon, Analytica Chimica Acta 610(1) (2008) 105-111.

[153] S. Song, L. Wang, J. Li, C. Fan, J. Zhao, Aptamer-based biosensors, TrAC Trends in Analytical Chemistry 27(2) (2008) 108-117.

[154] S.D. Mendonsa, M.T. Bowser, In vitro evolution of functional DNA using capillary electrophoresis, Journal of the American Chemical Society 126(1) (2004) 20-21.

[155] R.T. Turgeon, B.R. Fonslow, M. Jing, M.T. Bowser, Measuring aptamer equilibria using gradient micro free flow electrophoresis, Analytical chemistry 82(9) (2010) 3636-3641.

[156] R. Rizza, M. Haymond, P. Cryer, J. Gerich, Differential effects of epinephrine on glucose production and disposal in man, American Journal of Physiology-Endocrinology And Metabolism 237(4) (1979) E356.

[157] H.S. Thompson, J.H. Mensher, Adrenergic mydriasis in Horner's syndrome: Hydroxyamphetamine test for diagnosis of postganglionic defects, American journal of ophthalmology 72(2) (1971) 472-480.

[158] Ş. Alpat, K. Özdemir, S. Kılınç Alpat, Voltammetric Determination of Epinephrine in Pharmaceutical Sample with a Tyrosinase Nanobiosensor, Journal of Sensors 2016 (2016).

[159] M. Worthen, B. Placik, B. Argano, D. MacCanon, A. Luisada, On the mechanism of epinephrine-induced pulmonary edema, Japanese heart journal 10(2) (1969) 133-141.

[160] Y.J. Akashi, D.S. Goldstein, G. Barbaro, T. Ueyama, Takotsubo cardiomyopathy, Circulation 118(25) (2008) 2754-2762.

[161] D.R. Ferry, R.L. Henry, M.J. Kern, Epinephrine-induced myocardial infarction in a patient with angiographically normal coronary arteries, American heart journal 111(6) (1986) 1193-1195.

[162] M. Ajioka, S. Sugiyama, K. Ogawa, T. Satake, T. Ozawa, Mechanism of cardiac arrhythmias induced by epinephrine in dogs with hypokalemia, Journal of the American College of Cardiology 8(6) (1986) 1373-1379.

[163] X. Xu, H. Zhang, H. Shi, C. Ma, B. Cong, W. Kang, Determination of three major catecholamines in human urine by capillary zone electrophoresis with chemiluminescence detection, Analytical biochemistry 427(1) (2012) 10-17.

[164] J. Michałowski, P. Hałaburda, Flow-injection chemiluminescence determination of epinephrine in pharmaceutical preparations using raw apple juice as enzyme source, Talanta 55(6) (2001) 1165-1171.

[165] C.H. Mak, C. Liao, Y. Fu, M. Zhang, C.Y. Tang, Y.H. Tsang, H.L. Chan, F. Yan, Highly-sensitive epinephrine sensors based on organic electrochemical transistors with carbon nanomaterial modified gate electrodes, Journal of Materials Chemistry C 3(25) (2015) 6532-6538.

[166] M. Zhou, L.-P. Guo, Y. Hou, X.-J. Peng, Immobilization of Nafion-ordered mesoporous carbon on a glassy carbon electrode: Application to the detection of epinephrine, Electrochimica Acta 53(12) (2008) 4176-4184.

[167] C. Guan, J. Ouyang, Q. Li, B. Liu, W. Baeyens, Simultaneous determination of catecholamines by ion chromatography with direct conductivity detection, Talanta 50(6) (2000) 1197-1203.

[168] S. Salmanpour, T. Tavana, A. Pahlavan, M.A. Khalilzadeh, A.A. Ensafi, H. Karimi-Maleh, H. Beitollahi, E. Kowsari, D. Zareyee, Voltammetric determination of norepinephrine in the presence of acetaminophen using a novel ionic liquid/multiwall carbon nanotubes paste electrode, Materials Science and Engineering: C 32(7) (2012) 1912-1918.

[169] Y. Xia, J. Ouyang, PEDOT: PSS films with significantly enhanced conductivities induced by preferential solvation with cosolvents and their application in polymer photovoltaic cells, Journal of Materials Chemistry 21(13) (2011) 4927-4936.

[170] D.A. Bernards, G.G. Malliaras, Steady-State and Transient Behavior of Organic Electrochemical Transistors, Advanced Functional Materials 17(17) (2007) 3538-3544.

[171] D. Khodagholy, J. Rivnay, M. Sessolo, M. Gurfinkel, P. Leleux, L.H. Jimison, E. Stavrinidou, T. Herve, S. Sanaur, R.M. Owens, High transconductance organic electrochemical transistors, Nature communications 4 (2013).

[172] D.A. Bernards, D.J. Macaya, M. Nikolou, J.A. DeFranco, S. Takamatsu, G.G. Malliaras, Enzymatic sensing with organic electrochemical transistors, Journal of Materials Chemistry 18(1) (2008) 116-120.

[173] A.K. Cheng, B. Ge, H.-Z. Yu, Aptamer-based biosensors for label-free voltammetric detection of lysozyme, Analytical chemistry 79(14) (2007) 5158-5164.

[174] L. Zhang, G. Wang, D. Wu, C. Xiong, L. Zheng, Y. Ding, H. Lu, G. Zhang, L. Qiu, Highly selective and sensitive sensor based on an organic electrochemical transistor for the detection of ascorbic acid, Biosensors and Bioelectronics 100 (2018) 235-241.

[175] C.-W. Yen, H. de Puig, J.O. Tam, J. Gómez-Márquez, I. Bosch, K. Hamad-Schifferli, L. Gehrke, Multicolored silver nanoparticles for multiplexed disease diagnostics: distinguishing dengue, yellow fever, and Ebola viruses, Lab on a Chip 15(7) (2015) 1638-1641.

[176] S. Zhang, P. Kumar, A.S. Nouas, L. Fontaine, H. Tang, F. Cicoira, Solvent-induced changes in PEDOT: PSS films for organic electrochemical transistors, APL materials 3(1) (2015) 014911.

[177] Y. Ohno, K. Maehashi, K. Matsumoto, Label-free biosensors based on aptamer-modified graphene field-effect transistors, Journal of the American Chemical Society 132(51) (2010) 18012-18013.

[178] W. Tao, P. Lin, J. Hu, S. Ke, J. Song, X. Zeng, A sensitive DNA sensor based on an organic electrochemical transistor using a peptide nucleic acid-modified nanoporous gold gate electrode, RSC Advances 7(82) (2017) 52118-52124.

[179] Pan American Health Organization / World Health Organization. Zika - Epidemiological Report. United States of America. June 2017. Washington, D.C.: PAHO/WHO; 2017.

[180] European Centre for Disease Prevention and Control. Rapid risk assessment: Zika virus epidemic in the Americas: potential association with microcephaly and Guillain-Barré syndrome – 10 December 2015. Stockholm: ECDC; 2015.

[181] S. Ramos da Silva, S.J. Gao, Zika virus: an update on epidemiology, pathology, molecular biology, and animal model, Journal of medical virology 88(8) (2016) 1291-1296.

[182] WHO statement on the first meeting of the International Health Regulations (2005) (IHR 2005) Emergency Committee on Zika virus and observed increase in neurological disorders and neonatal malformations, World Health Organization, 2016.

[183] J. Lessler, L.H. Chaisson, L.M. Kucirka, Q. Bi, K. Grantz, H. Salje, A.C. Carcelen, C.T. Ott, J.S. Sheffield, N.M. Ferguson, Assessing the global threat from Zika virus, Science 353(6300) (2016) aaf8160.

[184] V. van der Linden, Description of 13 infants born during October 2015–January 2016 with congenital Zika virus infection without microcephaly at birth—Brazil, MMWR. Morbidity and mortality weekly report 65 (2016).

[185] B. Tian, Z. Qiu, J. Ma, T.Z.G. de la Torre, C. Johansson, P. Svedlindh, M. Strömberg, Attomolar Zika virus oligonucleotide detection based on loop-mediated isothermal amplification and AC susceptometry, Biosensors and Bioelectronics 86 (2016) 420-425.

[186] J. Song, M.G. Mauk, B.A. Hackett, S. Cherry, H.H. Bau, C. Liu, Instrument-free point-of-care molecular detection of Zika virus, Analytical chemistry 88(14) (2016) 7289-7294.

[187] X. Wang, F. Yin, Y. Bi, G. Cheng, J. Li, L. Hou, Y. Li, B. Yang, W. Liu, L. Yang, Rapid and sensitive detection of Zika virus by reverse transcription loop-mediated isothermal amplification, Journal of virological methods 238 (2016) 86-93.

[188] D. Lee, Y. Shin, S. Chung, K.S. Hwang, D.S. Yoon, J.H. Lee, Simple and highly sensitive molecular diagnosis of Zika virus by lateral flow assays, Analytical chemistry 88(24) (2016) 12272-12278.

[189] A. Priye, S.W. Bird, Y.K. Light, C.S. Ball, O.A. Negrete, R.J. Meagher, A smartphone-based diagnostic platform for rapid detection of Zika, chikungunya, and dengue viruses, Scientific reports 7 (2017) 44778.

[190] K. Chan, S.C. Weaver, P.-Y. Wong, S. Lie, E. Wang, M. Guerbois, S.P. Vayugundla, S. Wong, Rapid, affordable and portable medium-throughput molecular device for Zika virus, Scientific reports 6 (2016) 38223.

[191] S.W.B. Aashish Priye, Yooli K. Light, Cameron S. Ball, Oscar A. Negrete, Robert J. Meaghar, A smartphone-based diagnostic platform for rapid detection of Zika, chikungunya, and dengue viruses, Scientific reports 7 (2017).

[192] S.C.W. Kamfai Chan, Pui-Yan Wong, Sherly Lie, Eryu Wang, Mathilde Guerbois, Siva Praneeth Vayugundla, Season Wong, Rapid, Affordable and Portable Medium-Throughput Molecular Device for Zika Virus, Scientific reports 6 (2016).

[193] G.A. Pardee K, Takahashi MK, Lambert G, Lee JW, Ferrante T, Ma D, Donghia N, Fan M, Daringer NM, Bosch I, Dudley DM, O'Connor DH, Collins JJ, Rapid, Low-Cost Detection of Zika Virus Using Programmable Biomolecular Components, Cell 165(5) (2016) 1255-1266.

[194] M.G.M. Jinzhao Song, Brent A. Hackett, Sara Cherry, Haim H. Mau, Changchun Liu, Instrument-Free Point-of-Care Molecular Detection of Zika Virus, Analytical chemistry 88(14) (2016) 7289-7294.

[195] O.A. Ganguli A, Yu H, Damhorst GL, Chen W, Sun F, Bhuiya A, Cunningham BT, Bashir R, Hands-free smartphone-based diagnostics for simultaneous detection of Zika, Chikungunya, and Dengue at point-of-care, Biomedical Microdevices 19(73) (2017).

[196] L.B. Frederic Bedin, Elodie Voilin, Gerald Theillet, Agnes Rubens, Christine Rozand, Paper-based point-of-care testing for cost-effective diagnosis of acute flavivirus infections, Medical Virology 89(9) (2017).

[197] H.Z. Kyung Hyun Lee, Aptamer-Based ELISA Assay for Highly Specific and Sensitive Detection of Zika NS1 Protein, Analytical chemistry 89(23) 12743-12748.

[198] A.M. Nicolini, K.E. McCracken, J.-Y. Yoon, Future developments in biosensors for field-ready Zika virus diagnostics, Journal of biological engineering 11(1) (2017) 7.

[199] S.Y. Toh, M. Citartan, S.C. Gopinath, T.-H. Tang, Aptamers as a replacement for antibodies in enzyme-linked immunosorbent assay, Biosensors and Bioelectronics 64 (2015) 392-403.

[200] M. Baker, Reproducibility crisis: Blame it on the antibodies, Nature News 521(7552) (2015) 274.

[201] M. Famulok, G. Mayer, Aptamers and SELEX in chemistry & biology, Chemistry & biology 21(9) (2014) 1055-1058.

[202] S.L. Kyung-Mi Song, Changill Ban, Aptamers and Their Biological Applications, Sensors 12(1) (2012) 612-631.

[203] D. Mark, S. Haeberle, G. Roth, F. Von Stetten, R. Zengerle, Microfluidic lab-on-a-chip platforms: requirements, characteristics and applications, Microfluidics Based Microsystems, Springer2010, pp. 305-376.

[204] K.i. Ohno, K. Tachikawa, A. Manz, Microfluidics: applications for analytical purposes in chemistry and biochemistry, Electrophoresis 29(22) (2008) 4443-4453.

[205] S. Souf, Recent advances in diagnostic testing for viral infections, Bioscience Horizons: The International Journal of Student Research 9 (2016).

[206] M. Lake, C. Narciso, K. Cowdrick, T. Storey, S. Zhang, J. Zartman, D. Hoelzle, Microfluidic device design, fabrication, and testing protocols, Protoc. Exch 10 (2015).

[207] I. Hoek, F. Tho, W.M. Arnold, Sodium hydroxide treatment of PDMS based microfluidic devices, Lab on a Chip 10(17) (2010) 2283-2285.

[208] X. Ren, M. Bachman, C. Sims, G. Li, N. Allbritton, Electroosmotic properties of microfluidic channels composed of poly (dimethylsiloxane), Journal of Chromatography B: Biomedical Sciences and Applications 762(2) (2001) 117-125.

[209] S. Thorslund, P. Lindberg, P.E. Andrén, F. Nikolajeff, J. Bergquist, Electrokinetic-driven microfluidic system in poly (dimethylsiloxane) for mass spectrometry detection integrating sample injection, capillary electrophoresis, and electrospray emitter on-chip, Electrophoresis 26(24) (2005) 4674-4683.

[210] U. Weinert, T. Günther, J. Raff, K. Pollmann, Self assembling proteins as matrix for the construction of optical devices, WIT Transactions on Modelling and Simulation 51 (2011) 569-575.

[211] T.R. Thatiparti, N. Averell, D. Overstreet, H.A. Von Recum, Multiplexing interactions to control antibiotic release from cyclodextrin hydrogels, Macromolecular bioscience 11(11) (2011) 1544-1552.

[212] D. Li, W.Y. Teoh, J.J. Gooding, C. Selomulya, R. Amal, Functionalization strategies for protease immobilization on magnetic nanoparticles, Advanced Functional Materials 20(11) (2010) 1767-1777.

[213] J.W. Soares, D.M. Steeves, J. Singh, J. Im, J.E. Whitten, Effect of surface modification on the optical properties of nanocrystalline zinc oxide materials, Oxide-based Materials and Devices, International Society for Optics and Photonics, 2010, p. 76031L.

[214] G. Shen, M.F.G. Anand, R. Levicky, X-ray photoelectron spectroscopy and infrared spectroscopy study of maleimide-activated supports for immobilization of oligodeoxyribonucleotides, Nucleic acids research 32(20) (2004) 5973-5980.

[215] Y. Han, L. Han, Y. Yao, Y. Li, X. Liu, Key factors in FTIR spectroscopic analysis of DNA: the sampling technique, pretreatment temperature and sample concentration, Analytical Methods 10(21) (2018) 2436-2443.

[216] K.H. Lee, H. Zeng, Aptamer-Based ELISA Assay for Highly Specific and Sensitive Detection of Zika NS1 Protein, Analytical chemistry 89(23) (2017) 12743-12748.

[217] J. Cecchetto, F.C. Fernandes, R. Lopes, P.R. Bueno, The capacitive sensing of NS1 Flavivirus biomarker, Biosensors and Bioelectronics 87 (2017) 949-956.

[218] D. Acharya, P. Bastola, L. Le, A.M. Paul, E. Fernandez, M.S. Diamond, W. Miao, F. Bai, An ultrasensitive electrogenerated chemiluminescence-based immunoassay for specific detection of Zika virus, Scientific reports 6 (2016) 32227.

[219] Novateinbio, Zika virus NS1 DIY ELISA Kit.

[220] Biofronttechnologies, Zika Virus NS1 ELISA.